

NASA Technical Paper 1694

NASA
TP
1694
c.1

LOAN COPY: 1
AFWL TECHN
KIRTLAND AFB



Coordinated Aircraft and Ship Surveys for Determining Impact of River Inputs on Great Lakes Waters - Remote Sensing Results

Charles A. Raquet, Jack A. Salzman,
Thom A. Coney, Roger A. Svehla,
Donald F. Shook, and Richard T. Gedney

JULY 1980

NASA





NASA Technical Paper 1694

Coordinated Aircraft and Ship Surveys for Determining Impact of River Inputs on Great Lakes Waters - Remote Sensing Results

Charles A. Raquet, Jack A. Salzman,
Thom A. Coney, Roger A. Svehla,
Donald F. Shook, and Richard T. Gedney
Lewis Research Center
Cleveland, Ohio



National Aeronautics
and Space Administration

**Scientific and Technical
Information Office**

1980

CONTENTS

	Page
SUMMARY	1
INTRODUCTION	1
EXPERIMENT PROCEDURE	2
REMOTE SENSING DATA AND ANALYSIS	3
Recording of Data	3
Multispectral Scanners	3
Scanner/Aircraft Systems	4
Processing of Data	5
Single-Channel Images	5
Analysis of Digital Data	6
RESULTS AND DISCUSSION	8
Maumee River Results	8
History of Events	8
Data Analysis and Discussion	10
Summary of Results	28
Genesee River Results	28
History of Events	29
Data Analysis and Discussion	30
Summary of Results	40
Memonomee River Results	40
History of Events	40
Data Analysis and Discussion	41
Summary of Results	42
Grand River Results	52
History of Events	52
Data Analysis and Discussion	54
Summary of Results	66
Nemadji River Results	66
History of Events	67
Data Analysis and Discussion	68
Summary of Results	70
OVERALL SUMMARY OF RESULTS	86
General Results	86
Correlations and Contour Maps	86
River Discharge, Resuspension, and Shore Erosion	87
Transport and Dispersion of River Inputs	88
Comments on Near Real-Time Data Transmission	88
Extrapolation of Results	89
REFERENCES	89

SUMMARY

The remote sensing results of a coordinated program of aircraft and ship surveys for determining the effect of river effluents on Great Lakes waters are presented. The program was performed in support of U.S. Task D of the Pollution from Land-Use Activities Reference Group (PLUARG) of the International Joint Commission. Aircraft multispectral scanner data were acquired throughout the spring and early summer of 1976 at five locations, the West Basin of Lake Erie, Genesee River-Lake Ontario, Menomonee River-Lake Michigan, Grand River-Lake Michigan, and Nemadji River-Lake Superior. Forty-seven images of the various study sites are presented. Twenty of these overflights were coincident with ship surveys. Correlations of the multispectral scanner and in-the-water data (collected by organizations conducting comprehensive ship surveys at each of the sites) were made, and 40 contour maps showing large scale distributions of water-quality parameters are presented. The map products show the distributions of total suspended solids, turbidity, Secchi depth, nutrients, salts, and dissolved oxygen.

The overall results of the aircraft survey program demonstrate that there are sufficient opportunities with cloud-free sky conditions over the Great Lakes that a dedicated remote-sensing system can support the objectives of large-scale lake surveys. Landsat imagery and aircraft multispectral data analysis are used to determine the transport and dispersion of materials from the river discharges, especially during spring runoff events, and to evaluate the relative effects of river input, resuspension, and shore erosion on the total suspended solid distributions in lakes. Twenty-five Landsat satellite images of the study sites were included to assist in these efforts. Examples of the use of remote sensing data for quantitative estimates of total particulate loading, determination of sediment-water spectral classes, assessment of transport across international boundaries, and numerical current-modeling support are included. The importance of coordination of aircraft and ship lake surveys is discussed, including the use of telefacsimile for rapid transmission of imagery.

The studies revealed that the dispersion of particulates and associated pollutants is very dependent on local factors, including particulate composition, river discharge rates, the degree of resuspension, lake

and river currents, the existence or nonexistence of breakwalls, and ice formations. As a result the impact of each river on its receiving lake varies considerably. The implementation of controls on pollution from land use activities should therefore take into account these local factors as well as the amounts of pollutants generated from various sources.

INTRODUCTION

The assessment of the effects of river inputs on receiving waters is an important part of evaluating possible detrimental effects of land-use activities. Task D of the Pollution from Land Use Activities Reference Group (PLUARG) of the International Joint Commission Great Lakes Water Quality Board was formulated to study the effects of river effluents on the Great Lakes. A detailed account of the United States Task D objectives of PLUARG may be found in reference 1. The specific objectives for Activity 3 of Task D are

A. "To assess the significance of specific contaminants gaining access to boundary waters as a result of land use activities.

B. "To establish areas which may be adversely affected as a result of such inputs including a determination of the extent of dispersion of sediments offshore and the extent of impairment of water quality in boundary waters.

C. "To determine the degree of contamination of fish and other aquatic resources in areas exposed to higher-than-average loadings of specific contaminants."

The overall strategy of the U.S. Task D program for meeting these objectives involved the monitoring of representative rivers and their respective receiving lakes during peak runoff conditions. As a first step in this program, the U.S. Task D Technical Advisory Committee conducted a pilot study in the spring of 1975 which focused on the Maumee River-Lake Erie West Basin system. This study served as a prototype for the expanded program conducted in 1976 and described in this report.

The principal objective of the 1975 pilot study was to identify and determine the dispersion and fate of the Maumee River pollutants during the spring runoff maximum. A combination of conventional ship surveys and aircraft remote-sensing flights was used to address this objective. The direct shipboard

water quality measurements were made by the Ohio State University Center for Lake Erie Area Research. Remote-sensing multispectral scanner data were recorded by the NASA Lewis Research Center. Results of the pilot study were documented in separate research reports by the participating organizations (refs. 2 and 3). The study demonstrated the special advantages of a combined ship-survey and remote-sensing system for meeting the PLUARG objectives of river plume monitoring.

The five sites selected for the 1976 study are shown in figure 1. These sites represent a range of Great Lakes watersheds with respect to the degree of urbanization, soil types, and drainage characteristics. Consequently, the effects on the respective receiving waters of these watersheds from the major rivers reflect a wide range of land use activities. As in the pilot study, a combination of ship survey and remote sensing techniques were used in the 1976 program. The study objectives were to

- (1) Survey the quality of water offshore of a river mouth following a runoff event during the spring thaw. Contaminants to be considered include suspended sediments, nutrients, toxic substances, and other parameters useful for specifying water quality.

- (2) Identify general distribution patterns and transport mechanisms of contaminants contributed by the river, particularly those contaminants thought to be derived from land drainage.

- (3) Determine whether resuspension of sedimented materials is likely to be significant relative to the tributary input of suspended material in the near-shore area of the river under study.

- (4) Assess the general impact of wind-induced resuspension of sedimented material on the water quality of the area under study.

- (5) Assess the general impact of the tributary loading on the lake under runoff event conditions.

Figure 1 lists the five organizations performing the ship survey work. NASA Lewis performed the aircraft overflights. This report summarizes the results of the NASA Lewis 1976 remote-sensing work for PLUARG. Separate reports by the five other organizations present the findings of the ship surveys. Since the overall survey program included the combined application of in-the-water sampling and remote sensing techniques, a significant portion of this report will demonstrate the complementary nature of the two techniques.

EXPERIMENT PROCEDURE

The objective of the studies at the five sites was to coordinate an aircraft flight and a ship-sampling cruise during a major event (peak river runoff or resuspension event). Figure 2 summarizes the factors and sources of information involved in this task. The weather was the controlling factor, affecting the timing of major runoff events and determining whether useful aircraft or ship operations could take place.

The time of peak runoff varies significantly from year to year for a given river. To assist in scheduling aircraft and ship operations, the U.S. Geological Service gaging stations on the five rivers were monitored by the ship survey teams. Information concerning the occurrence of major flow events was then telephoned



Figure 1 - Study sites and organizations having ship-survey responsibilities.

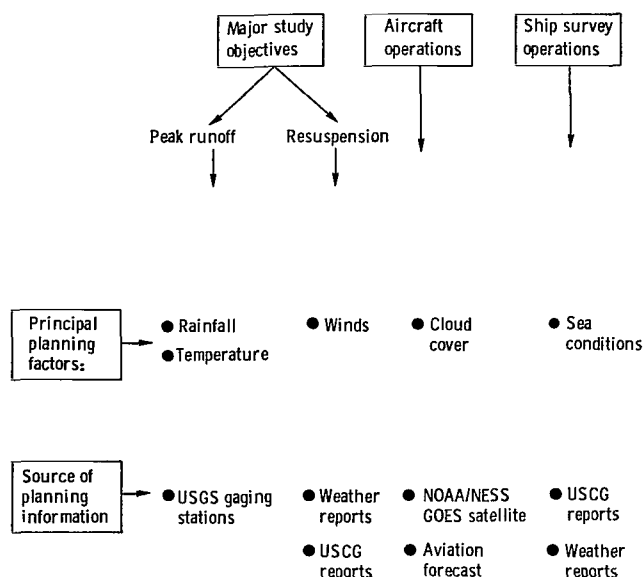


Figure 2. - Principal planning factors and sources of planning information.

to NASA in Cleveland. Another very useful flight planning aid was the NOAA/NESS GOES satellite pictures received every half hour on an image recorder via special telephone lines. These pictures, revealing the presence or absence of cloud cover at the study sites, were essential for planning flight operations located as far as 1000 km (600 mi) away from the NASA Cleveland base.

To assist the ship survey teams in selecting their sampling sites in a more productive manner, telephone-connected facsimile receivers were installed at the operations bases of the five survey vessels. In this way images from certain overflights were transmitted to provide information useful for next-day ship surveys. Transparent map overlays were provided to the ship personnel to facilitate extraction of planning information from the geometrically scaled aircraft imagery. Direct aircraft-to-ship transmission of image data would have been the most useful for aiding in the selection of ship sampling sites. However, the equipment required to perform real-time transmission and on-board recording was not available for this study.

Table I summarizes the aircraft and ship activity during the entire study period. Remote sensing data collected during aircraft flights over the study areas consisted of multispectral scanner data. In-the-water measurements made by the ship survey organizations included those shown in table II. As table I indicates, the number of data producing flights and ship surveys exceeded the planning goals. A large number of Landsat satellite images are presented and discussed in later sections. However, these were selected

after the flights based on the degree of cloud cover and relevance to the study. The Landsat schedule was not a major factor in planning the aircraft overflights and ship surveys.

Efforts at coordinating aircraft and ship measurements resulted in the achievement of 20 simultaneous (that is, same day) missions. It should be noted that the lower numbers of simultaneous missions at the Genesee, Menomonee, and Grand River sites were due partially to the concentration of aircraft operations during the spring runoff periods, whereas the ship operations extended substantially into the summer and fall. Many other factors limited the number of simultaneous aircraft and ship surveys. These included cloud cover, which prevented or compromised the data of aircraft flights, high seas or ice conditions which prevented ship surveys, scheduling conflicts with other survey programs, and coordination breakdowns.

As documented in later sections, multiple days of remote sensing data from aircraft and satellites, when added to the multiple days of ship-survey data, provide a more complete picture of the river effects at the five study sites than any reported to date. Complete lists of the dates of remote sensing operations at each of the study sites are presented in the individual river summaries.

REMOTE SENSING DATA AND ANALYSIS

Recording of Data

Multispectral Scanners

All of the remote-sensing data presented in this report are multispectral scanner data. Figure 3 is a schematic illustrating the basic scanner system. Scanning of the scene below is achieved by means of a rotating mirror which directs electromagnetic radiation from one narrow line on the Earth below (scan line) to a number of detectors. (The term radiation as used in this report refers to reflected solar illumination in the visible and near-infrared portion of the spectrum.) These convert the radiation to electrical signals, which are recorded on multiple tape recorder tracks or channels. The mirror rotation speed is adjusted so that, for a given aircraft ground speed and altitude, the forward movement of the aircraft during one mirror revolution exactly equals the resolution of a scan line on the ground. The electrical signal corresponding to one scan line is digitized into a sequence of numbers such that each number corresponds to the radiation intensity coming from one picture element (pixel) on the scan line. Thus, the

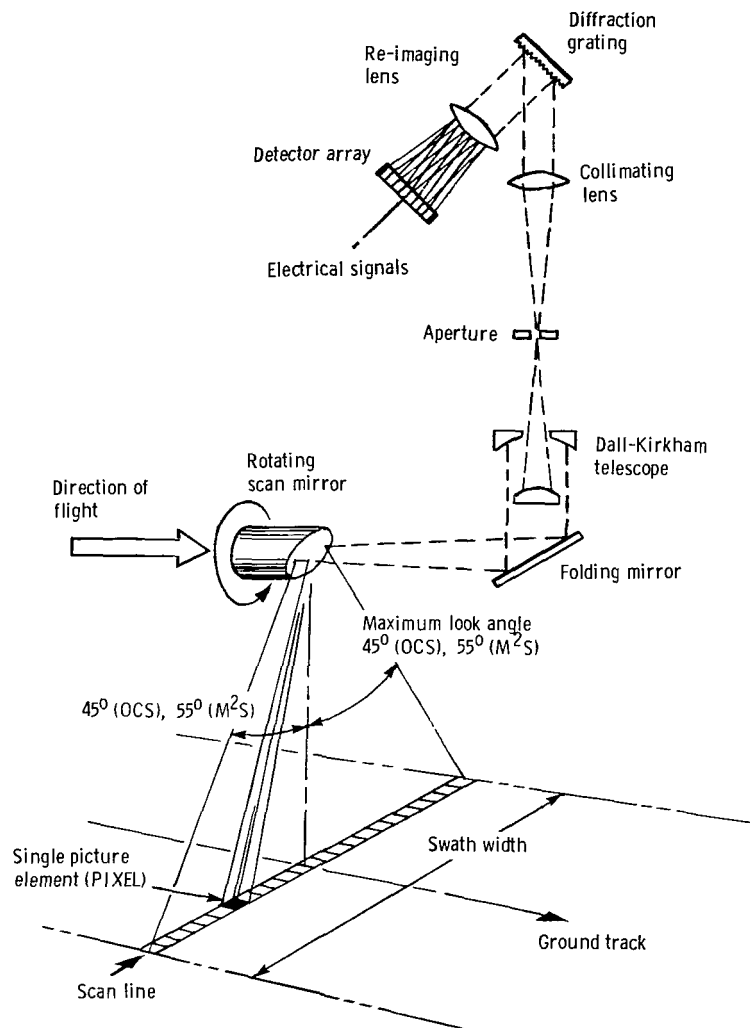


Figure 3. - Schematic diagram of multispectral scanner system.

scanner maps out the radiation intensity of the scene below and stores the information as a sequence of radiation intensity numbers.

Each of the several detector systems in a multispectral scanner is designed to record radiation in a specific wavelength region of the electromagnetic spectrum. Each simultaneously records radiation in the visible, near-infrared, or thermal-infrared portions of the spectrum. In this way the multiple-scanner channels record the spectral signature of each ground pixel.

Scanner/Aircraft Systems

Two scanners were used in this study: the 10-channel ocean color scanner (OCS) developed at NASA Goddard Space Flight Center and the 11 channel Bendix M²S (modular multiband scanner). The basic specifications of the OCS and M²S scanners are given in table III. The OCS scanner was mounted in either the NASA F-106 aircraft or a leased Lear Jet. Flown at an altitude of 12.5 kilometers (41 000 ft), the OCS recorded data over a

24.5-kilometer (13.2-nmi) swath width. The M²S was mounted in the NASA C-47 aircraft and recorded data at an altitude of 3.05 kilometers (10 000 ft). At this lower altitude the swath width was 7.26 kilometers (3.92 nmi). The OCS/F-106 or OCS/Lear combinations were used for most of the overflights because of their ability to cover large areas at the higher altitude and because of the greater aircraft speed, which provided a quicker response than the M²S/C-47 combination.

At three of the study sites (Genesee, Grand, and Menomonee Rivers) a single flight line usually proved to be sufficient to cover the target area. Multiple, overlapping flight lines were required for the larger sites (Maumee and Nemadji Rivers). All flight lines were designed to minimize the effects of direct solar reflections from the water surface and were flown with the aid of inertial navigation equipment.

Processing of Data

Processing of the scanner data is summarized in figure 4. The data fall into two basic categories: (1) images produced from a single channel of scanner data; and (2) quantitative data products produced from analysis of the digital data from one or more scanner channels. These two types of data are discussed separately.

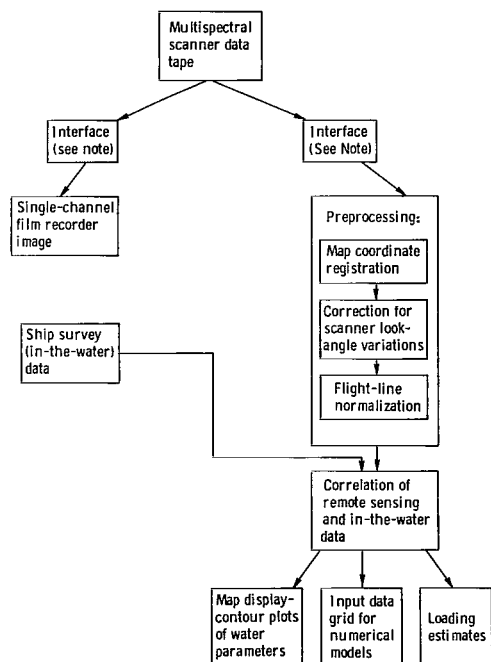


Figure 4. - Multispectral scanner data processing flow diagram. Note: OCS data recorded in analog format, and M²S in digital format. Interfaces represent A/D or D/A conversion as appropriate, and provision for rectification and drift-and-roll correction, as required.

Single-Channel Images

Single-channel images were created from one channel of scanner data using a film recorder. The film recorder converted the measured brightness of a scene and the scan rate to a variation in the z-axis intensity and the horizontal sweep of a cathode-ray tube. This in turn exposed dry process paper and/or a film negative. Because of careful scaling and corrections for aircraft drift and roll, the images are geometrically accurate. The shades of gray (gray scale) correspond to the backscattered light intensity levels recorded in the particular channel. The film recorder was adjusted so that in the image the region of highest radiation levels appeared white and the lowest (or background) appeared black. Intermediate gray tones corresponded to intermediate radiation levels.

The amount of light reaching the scanner from the water below is related to the concentration of suspended material in the water. However, the detailed spectral distribution of light seen by the scanner is a function not only of the distribution and composition of particulate and dissolved matter in the water, but also of the reflection occurring at the surface (which is a function of wave height and shape), the transmission characteristics of the intervening atmosphere, and the auxiliary illumination from the sky and clouds. Despite the complexity of the process, it has been demonstrated (refs. 4 to 6) that the magnitude of the radiation coming from the water may be used as a measure of the concentration of suspended solids near the water surface. The physical basis for this may be understood in terms of the light scattering and absorbing properties of suspended particles in water.

Single-channel scanner images can be used to qualitatively indicate the location and distribution of suspended solid matter, with the longer wavelength channels generally most useful for this purpose. Seventy-five single-channel scanner images are presented in the individual river summaries. Although these images are very useful, caution must be exercised in their interpretation. For example, it is difficult to make accurate quantitative comparisons of images of data taken at different times or locations. Two sediment plumes may appear equally bright on different images and yet contain different concentrations of suspended solids, because of differences in lighting, sea, or atmospheric conditions at the time the data were recorded. Variations in the film recorder levels, in the photographic processing steps, and in materials can affect the image gray scale. Also differences in the spectral reflection and absorption properties of the suspended solids must be considered. For example, the sediment composed predominately of red clay such as found in western

Lake Superior can appear different from one composed of gray-brown silt from the Maumee Basin of Lake Erie. Therefore, all the images of a given river were processed as a group, generally at the same or similar gray scale levels. Thus qualitative comparisons of images of the same river may be made subject to the above cautions. However, comparison of images of different rivers should not be attempted.

It must be remembered that single-channel images produced in the red or near infrared portion of the spectrum are measures of sediment concentrations at or near the surface. This is especially true in the more turbid areas where the penetration of longer wavelength light into water extends only a few centimeters.

It should also be noted that in the longer-wavelength channels the reflectance of vegetation-covered land areas is high compared with that of water. In making the single channel images, the film recorder levels were adjusted to emphasize differences in reflectance within the lake portion of the scene. Consequently, in several of the images, the land area appears very light (saturated) and few, if any, land features are discernible.

Analysis of Digital Data

The combination of digital processing of multispectral-scanner data with in-the-water measurements at sampling points provides quantitative water-quality parameters over large areas. Three necessary steps are indicated in figure 4: (1) preprocessing of digital data; (2) correlation of digital data with in-the-water measurements (so-called "surface truth"); and (3) use of correlations to produce map products, contour plots, loading estimates, input grids for numerical models, and other large-scale products.

Preprocessing. — The preprocessing of digital scanner data includes (1) map coordinate registration, (2) correction for scan-angle variations, and (3) flight-line normalization. Map coordinate registration refers to processing required to assign geographical grid coordinates to each element of data on the digital tape. (Or conversely, registration enables the extraction of the digital data corresponding to specified grid coordinates.) The registration process includes those steps required for preserving accurate geometric relationships—corrections for aircraft drift and roll, pixel rectification along the scan direction perpendicular to the flight line, and scaling along the flight line.

Corrections for effects due to scan angle variations are essential for scanners such as the ones used in this program in which the maximum scan angles are large—45° in the OCS and 55° in the M²S. As the

scan angle increases, the distance from the scanner to the water-surface element being viewed increases and increasingly greater amounts of sun and sky radiation scattered by the atmosphere reach the scanner and contribute to the total radiation seen by it. At the same time, the longer path length results in increased atmospheric attenuation of the radiation originating from the water. Furthermore, the radiation reflected from the water surface has an anisotropy that acts to increase the radiation seen by the scanner as the scan angle increases. The process of normalizing the radiance at nonzero scan angles to that at nadir (straight down) is the scan-angle correction. In this study this correction is made empirically using an algorithm based on an atmospheric scattering model. The correction differs from channel to channel primarily because of the strong spectral dependence of atmospheric scattering processes.

In missions in which multiple flight lines were flown, it was necessary to renormalize overall digital data levels between adjacent flight lines. These small normalization corrections were necessary because of variations from flight line to flight line in scene illumination and in aircraft attitude due to wind fluctuations. The magnitude of the corrections were determined by detailed comparison of the overlap region between adjacent flight lines.

In summary, careful preprocessing of the digital data was performed to make possible quantitative comparison of radiance data from different flight lines or different elements of the same flight line.

Correlations. — All analyses in this report were based on in-the-water data collected by the five survey ships. The correlation process produces a quantitative mathematical expression relating scanner spectral radiance measurements to the measurements made by the survey ships.

Using the ship sampling locations (latitude and longitude) provided by the survey teams, the magnitudes of the radiation in each channel from these locations were extracted from the preprocessed scanner data tapes. The radiance value established for each location was an average value taken over a square array (usually 100 total) of individual pixel values centered at the sampling point. The set of radiance values and the corresponding set of in-the-water measurements from one location form one so-called data pair.

Correlations between remotely sensed and in-the-water data were made using standard regression analysis algorithms. The simplest correlation forms were tested first. Initially, linear correlations between the intensities in each of the scanner channels and various water parameters were attempted. Using statistical measures of goodness of fit such as the standard error of the estimate and the correlation

coefficient, the channel best fitting each particular water parameter was determined. If a linear relation to a single channel was not adequate to describe the data, then higher order polynomials, nonlinear forms, and multiple channel relationships were explored and accepted when successful. A typical correlation relating OCS channel 8 (714 nm) to total suspended solids is shown in figure 32.

Several general comments may be made concerning the correlations produced in this study. The physical basis for some of the correlations can be understood by considering the direct interaction of light with a particular water pollutant. For example, suspended solids in water scatter and absorb light. The various types and concentrations of suspended particles produce measurable variations in the magnitude and spectral distribution of the back-scattered radiation. *Direct* correlations of this type are to be distinguished from *indirect* correlations. The correlations involving dissolved chlorides, for example, fall into this latter category. No mechanisms exist whereby the dissolved chlorides in the water could interact with light to the extent that the effects could be measured by a passive scanner. Yet it can be demonstrated for some data that a correlation exists between the intensity in one of the scanner channels and the chloride concentration. This can be qualitatively understood by assuming that either the chlorides and suspended solids originate from the same source and are distributed in essentially the same flow pattern, or that the chlorides are adsorbed in some way by the suspended solids. In any event the correlation of chloride with radiance data is possible because of its association with suspended solids which do interact with light; the suspended solids whose effects on light can be directly measured act as a tracer for the dissolved chlorides.

In addition to indirect correlations of radiance data with chlorides, correlations with several other chemical parameters such as total phosphorous and total organic nitrogen are reported. All chemical correlations are regarded as indirect in the sense defined above. The existence or nonexistence of such correlations at a particular site depends on many variables including flow levels, background levels, availability of in-the-water measurements, water depth, the conservative or reactive nature of the parameter, and the existence and state of mixing of more than one sediment-water spectral class.

Success in developing a correlation depends on two factors: (1) the ability of the ship to precisely determine its location when sampling and (2) the relevance of sampling sites with respect to the phenomena being studied. If the survey vessel is not equipped with an adequate location finding device, the position of

the ship may be substantially in error, depending on crew navigational skills and the nearness of land reference marks. Consequently, remote-sensing radiance data extracted at a location removed from the sampling site are input to the correlation algorithm. The errors introduced into the correlation process by this displacement are not important if the water is uniform over the distance from actual to presumed ship location. However, the errors may be substantial if the sampling site is in a region of widely fluctuating water compositions near plume edges.

The most accurate and useful correlations are produced when the ship sampling sites are selected based on the lake conditions on the day of the survey. For this reason it is desirable to transmit scanner imagery to the ship in near real time. Ideally, sites should be selected at locations representing a broad range of representative water conditions, including both extremes of high and low (background) particulate concentrations. Also, points should be ideally selected as much as is possible in relatively uniform regions of water. In the present study, the ship data collection missions were designed by the survey teams to meet several objectives, only one of which was to coordinate with simultaneous aircraft surveys. As a result, the ship data were usually taken at preselected sampling grids, which fortuitously met the foregoing remote sensing criteria.

Another important factor influencing correlation development is the degree of simultaneity of aircraft and ship survey data. In this report correlation analyses were attempted only with data pairs collected on the same day. Consequently, the maximum time difference between the aircraft overflight of a point and the actual in-the-water measurement at that point was as much as 7 to 8 hours, although most of the data were coincident within 2 to 3 hours. Since changing winds and lake currents can alter flow patterns in a matter of hours, nonsimultaneity of data collection undoubtedly affected the correlation efforts to some degree.

Products. — After the upwelling radiation intensity data had been registered and a mathematical relationship between intensities in one or more channels and water parameter concentration or classes had been developed, a variety of useful output products were produced. These included map displays of parameter concentrations, input data for numerical models, and estimates of total loading.

In most cases the mathematical relationship developed was a correlation between intensity in one or two channels and a particular parameter, as discussed earlier. Other relationships are demonstrated that result in a classification of water types (Examples are discussed in later sections). Geometrically accurate map displays of concentra-

tion levels or water types were produced in several formats. In most cases computer-generated contour plots were used to depict concentration levels. In one case different shadings were used to graphically portray suspended-solids concentration levels. Figures 31 and 33 are examples of map products.

Like the single-channel images, the map products illustrate the remote-sensing advantages of large areal coverage and synoptic perspective. But, because they are based on quantitative in-the-water measurements, the maps have much greater application. One can make reliable quantitative comparisons of concentration levels at various locations on the same map as well as of levels at one location on different maps.

In some cases the analysis procedures used to make concentration maps were also used to generate a grid of input data for modeling calculations. For example, suspended-solid values on a 1-kilometer-square grid over the entire Erie West Basin were calculated and used in numerical models for calculating particulate dispersion. These models can predict the transport of solids and therefore represent a means of extrapolating the solids movement forward in time. Scanner data from a succession of days support the modeling programs by providing verification information. Remote-sensing and current-modeling techniques thus complement each other and together represent a way of quantitatively studying the movement of pollutants through the lake.

If information about the distribution of pollutants at all depths is available or if a reasonable assumption about a distribution can be made, the surface values of concentration can be used to estimate total loading in a given body of water. Examples of this calculation, using an assumed constant vertical profile, are presented in the following sections. Loading estimates made for various volumes of water on a number of different days permit quantitative estimates of the movement of materials to be made. The loading estimates also permit quantitative comparison of runoff, resuspension, and shore erosion effects.

RESULTS AND DISCUSSION

The remote-sensing data results for the five rivers – Maumee, Genesee, Menomonee, Grand, and Necedah – are presented. Although certain of the results pertain to all of the study sites, the data and analyses vary from site to site, reflecting the differing characteristics of the respective drainage basins and lakes and also the diversity in the available ship-survey data. Using the single-channel imagery in conjunction with river flow and wind data, a narrative

summary of the river's effect on the lake throughout the study period is presented. Following these qualitative interpretations, the quantitative results of the digital data analysis are discussed. These analyses illustrate the detailed information about nonpoint-source pollution on lakes that can be extracted from a combination of remote-sensing and ship-survey data.

In addition to the aircraft scanner images, 25 Landsat satellite images of the study sites are presented. These are photographic enlargements of the standard 9- by 9-inch black and white positive prints of the Landsat multispectral scanner band 5 (MSS-5, 600 to 700 nm). The satellite pictures selected were those that best supplemented the aircraft single-channel imagery in revealing the distribution and movement of materials in the various lakes. Some of the same comments made in the previous section concerning the interpretation of single-channel images also apply to these satellite pictures.

Maumee River Results

The chronological single-channel imagery, multiple examples of quantitative analysis of digital data, and numerous ship-survey missions combine to provide a relatively complete and detailed analysis of the effects of major tributary input on the water quality of the Erie West Basin during the spring of 1976. Remote sensing techniques are shown to complement shipboard sampling techniques.

The aircraft remote sensing data presented in this summary were recorded on 16 overflights of the West Basin of Lake Erie from February 18 to June 5, 1976. Figure 5 is a reference map of the Maumee River study area. Also presented are five representative Landsat satellite images of the basin. Table IV summarizes the aircraft and ship survey activities and information obtained by the Ohio State University Center of Lake Erie Area Research (OUS-CLEAR) in the West Basin. The Maumee and Detroit River flow rates are also presented in figures 6 and 7. The wind history at the Toledo, Ohio, airport is indicated in table V.

History of Events

On February 11 the Maumee flow began to rise as increasing temperatures released frozen ground water. By February 13 the flow rate had reached 850 m³/sec. Figure 8 is a Landsat image showing the Erie West Basin to be 80 to 90 percent ice covered on that date. The predominantly west to southwest winds of the preceding three days had apparently driven the ice toward the north shore, thus producing a region of open water in the vicinity of the Maumee River.

By February 18 the flow rate had reached 1920 m³/sec. nearly equaling the spring maximum flow rate of 2040 m³/sec. Although hampered by ice, water samples were obtained in Maumee Bay. Weather conditions did not permit an overflight until February 23 (see fig. 9). The river flow rate at that time was still high at 1980 m³/sec. Westerly winds had driven the ice to the east, leaving the western half of the basin ice free. It is significant to note that there is little, if any, apparent resuspension in the West Basin despite a two-day average wind speed of 5.4 m/sec. This image illustrates clearly the behavior of a Maumee River runoff plume in the presence of ice cover and westerly winds. The plume is observed to move eastward along the south shore driven by the winds. It reaches the ice cover where its easterly movement is apparently blocked, since no heavily sedimented water appears east of the ice.

The first ship-and-aircraft coordinated mission took place on February 25 (fig. 10). The river flow, while still high, had decreased from the spring maximum to a rate of 1530 m³/sec. The wind on the four consecutive days before the flight was from the southwest at an average speed of 5.4 m/sec. Although clouds partially obscured the mouth of the river as well as Locust Point, the plume can be seen to be moving in a northeast direction, as is a large region of resuspension on the south shore near Magee Marsh. A plume from the River Raisin is also moving northeast along the Michigan shore toward Stony Point. By March 1 the Maumee River flows had subsided to 250 m³/sec, but shortly thereafter began to rise. A second peak flow occurred on March 6 at 1470 m³/sec. On March 8 when the flow rate was 930 m³/sec, the second ship-and-aircraft coordinated mission took place. Two ships performed extensive sampling throughout the basin.

For three days preceding this date the wind was from the west averaging 8.0 m/sec. Figure 11 shows the apparent consequence—a very heavily sedimented plume driven east along the south shore. Based on the persistent strong winds and the shallow conditions along the south shore, it is likely that the heavily laden water, even that within the Maumee Bay itself, is due to resuspension of bottom sediment and that it is this resuspension that is moving in an easterly direction. Quantitative analysis of these data, discussed in a later section, supports this conclusion. The resuspended material was most likely to have been deposited during the earlier period of maximum Maumee runoff. A third flight was made on March 11 concurrently with a Landsat overpass (no ship data were taken). Figures 12 and 13 show the aircraft and satellite images. The river flow rate was about 400 m³/sec. The winds averaged 3.6 m/sec and were random in direction. The Maumee River plume

along with some resuspension seems to be mixing and generally moving in an easterly direction near the south shore. Also evident is the first occurrence of a significant Detroit River plume. The Detroit River flow rate is a typical 5940 m³/sec. The source of the heavily sedimented water in the Detroit River is the resuspended material in Lake St. Clair. The Detroit River plume appeared frequently throughout the study period.

The Maumee flow rate continued to decline from its secondary event peak of 1470 m³/sec to a rate of 230 m³/sec on March 15. An overflight was made on this date (fig. 14). The presence of variable haze (as noted in the aircraft log) and several contrails make it difficult to interpret the data.

On March 22 the first of three overflights within one four-day period took place. Figures 15 to 17 show the images from the March 22, 23, and 25 overflights. The Maumee and Detroit River flow rates averaged a low 140 and 5720 m³/sec, respectively. The winds rose steadily from 1.8 m/sec on the 22nd to 6.3 m/sec on the 24th, and dropped to 5.4 m/sec on the 25th. On all four days the winds were from the southwest. With little river input occurring and with steadily increasing winds the conditions were right to observe the buildup and movement of resuspended sediment.

Figure 15 shows the state of the water in the Western Basin for very low river input and calm wind conditions. Some resuspension is seen in the vicinity of the islands and along the west shore. There is little, if any, plume evident from either river. In fact, it is probable that the sediment laden water in Maumee Bay is resuspended sediment rather than sediment laden river water. In spite of an increase in wind speed to 4.0 m/sec, there is little change in the level of resuspension in either the island area or along the west shore (fig. 16). However, figure 17 shows a significant increase in the level of resuspension in both areas as might be anticipated with increasing southwest winds.

Figure 18 shows the movement of the basin water as inferred from the relative location of various sediment patterns shown on the imagery and from the wind history. It shows the west shore sediment moving in a northerly direction along the shore until met by the Detroit River, where it is turned back into the basin. The suspended solids north of the Portage River are moving toward the south shore where they separate with some heading to the northeast through the islands and some heading west near the south shore. Thus, this three-image sequence indicates the development of sedimented water masses and their general movement patterns under conditions of low river input and winds of constant direction but steadily increasing speed.

At this point in the spring 1976 history of the West Basin, it is important to note that the two major Maumee River flow events have essentially been completed. While some concentrations of suspended solids are observed in Maumee Bay and along the south shore, the major concentrations are seen along the west shore and especially in the island region. Wind effects stirring up bottom sediments from past flow events (not from new contributions from the rivers) appear to be the principal cause of heavy sediment concentrations in the basin. Analysis of the next three images supports this observation.

Figures 19 to 21 correspond to overflights on April 3 and 5 and a Landsat overpass on April 7. During this period the river inputs were again very low. However, unlike the previous March sequence, the average wind speed was constant, and the direction quite variable. The result was a relatively constant level of resuspension and inferred water movement as shown in figure 22. The Detroit River water moves almost due south, meeting a midbasin flow moving generally northeast. The flow south and east of Pelee Island is toward Kelleys Island, meeting the easterly flow through the south passage. There is also some indication of a westerly flow very near the south shore.

Figures 23 and 24 illustrate the resuspension patterns existing on April 12 and 13. The river flow rates were still very low. The wind was constant in speed and direction for the two days, blowing from the west at 2.7 m/sec. The significant amount of resuspension evident is probably due to the 6.3 m/sec north wind prevailing on April 11. The same wind is probably responsible for the large clear water area in the west-central part of the basin.

The image presented in figure 25 is the last to show any significant resuspension of bottom sediment. The overflight occurred on April 29. The river inputs were again very low while the winds were from the northeast averaging about 4 m/sec for four consecutive days. The only apparent area of resuspension is that in the vicinity of the islands. The plume near the mouth of the Detroit River probably originated in Lake St. Clair.

The remaining images (figs. 26 to 30) were generated from aircraft data obtained on May 12, June 5, and June 7 and by Landsat on May 22 and July 6. River flow rates were low; none of the images indicate river plumes containing significant concentrations of suspended particulate; and there is little or no resuspension apparent on any of the days despite modest wind conditions.

Based on an examination of the single-channel aircraft and satellite imagery and of the wind records, the following picture emerges of the history and ultimate fate of the spring Maumee River runoff.

The large amounts of material entering the Basin during the major runoff peak appear to move slowly eastward through the shallow basin over a period of about 3 months by repeated cycles of settling, resuspension, and eastward drift. During this period wind-induced resuspension is a dominant characteristic of West Basin water. By mid-May most of the material has left the West Basin, moving on to the Central Basin or settling out in the deeper waters of the Basin.

Data Analysis and Discussion

Contour maps of water parameters.—Five representative days were chosen for quantitative analysis, March 8 and 23, April 12 and 13, and May 12. The aircraft data obtained on these dates were digitized, preprocessed, and correlated with same-day ship data using the techniques described previously. Table VI presents the primary correlations relating total-suspended-solids concentration to the upwelling radiance for each of the five sets of data. In each set the data of OCS channel 8 (714 nm) produced the best correlation (smallest standard error).

The ship data of March 8 were among the most extensive of the study and covered the widest range in suspended-solids concentrations. The correlation for this date was based on 16 sampling sites having suspended solids concentrations ranging up to 200 mg/l. Included in table VI are the secondary correlations relating various other measured parameters to total-suspended solids for March 8. These include total phosphorus, dissolved oxygen, Secchi depth, and turbidity. Because of these relationships, a display of total suspended solids concentrations in the West Basin is also representative of the distribution and concentration of the other parameters (see table VII).

Figure 31 is a sediment map of the West Basin on March 8. The map was made from computer-drawn contour plots of suspended solids concentrations obtained using the above correlation. The various concentration levels have been coded as an example of one of several ways the quantitative data results can be presented.

Correlations of radiance measured in channel 8 with total suspended solids were also obtained for the April 12 and 13 data (see table VI). Since the form of these correlations is similar to that obtained using the March 8 data, it was possible to produce a *general* correlation based on the data from all three days. The motivation to develop this general correlation came from the assumption that it could be applied to scanner data taken on other days when the number of sampling sites or the range of data collected at the

sampling sites was small. The generalized correlation could thus be used as a basis for obtaining a reliable second-order correlation on March 23 when only two sites were sampled. Similarly, the generalized correlation enabled reliable, remotely measured suspended-solids data to be extracted from the May 12 scanner data over higher concentration regions, even though the ship measurements were made only at sites having a concentration of 9.5 mg/l or less.

The general correlation was obtained by normalizing the April 12 and 13 data to the March 8 data and performing a statistical analysis of the composite data. Figure 32 shows both the normalized data and the statistical correlation. The correlation coefficient and the standard deviation of the suspended-solids concentration are 0.99 and 5.3 mg/l, respectively. This correlation was then used to produce contour plots of total suspended-solids concentration for the March 23, April 12, April 13, and May 12 data (figs. 33 to 36). Each of the contour plots can be directly compared with its single-channel image counterparts (shown in figs. 11, 16, 23, 24, and 27). Comments on their content will be made in the following sections.

West Basin loading distributions. —To evaluate the relative effects the various sediment sources on the water of the West Basin, it is necessary to be able to differentiate one source from another. In the preceding interpretation of the scanner data, sources were identified by noting the locations and flow histories and lake bottom depth contours that could lead to resuspension of bottom sediments and by noting the types of shorelines that might be susceptible to shore erosion. Applying inductive reasoning to the data of March 8 in figure 11 could lead the user to conclude that the sediment in Maumee Bay is due to river input, that the large area of high sedimentation along the south shore and around the islands is due to resuspended bottom sediments (since the high levels of sediment in fig. 11 are not continuous from the Maumee River to the islands and there are no other sources of a size sufficient to contribute the volume indicated), and that there is relatively little shore erosion.

It should be noted that it is difficult to differentiate resuspended sediment from that produced by shore erosion. Therefore, part of the south shore resuspension plume may in fact be due to shore erosion. It is unlikely to be a large part, however, because shore erosion in this area is known to be relatively small (ref. 7).

Quantitative analysis of remote sensing data can be used to improve the assessment of loading mechanisms. The contour plot for March 8 shown in figure 31 shows the sediment concentration levels to be lower (~ 175 mg/l) in the Maumee River than on the south shore (~ 200 mg/l). It also emphasizes the

discontinuity in concentration around Cedar Point. These support the contention that the material along the south shore is due to resuspension rather than river input.

In some cases an analysis of spectral signatures can aid in the evaluation of loading type by locating regions of similar sediment types and thus identifying their origin. For example, a plot of the total suspended-solids concentration versus the radiance measured in channel 3 (508 nm) for the March 8 data showed three distinctly different correlations, indicating three different water classes (see fig. 37). One class is associated with the Detroit River, a second with the relatively clean mid-West Basin water, and a third with the Maumee River. The West Basin was classified by computer according to water class by first determining the total suspended-solids concentration using the suspended solids-channels 8 correlation, which is independent of water class. It was then noted on which of the three lines in figure 37 the point determined by the suspended-solids concentration and the radiance measured in channel 3 was located. Points falling between the lines were classified with the class of the nearest line.

The result of the classification is shown in figure 38. The areas that have been labelled as Maumee water class are consistent with Maumee River plume dispersal patterns noted previously. In particular, movement east along the south shore and also north along the west shore are indicated. The area does not necessarily represent the location of the Maumee River plume alone but in all likelihood the location of a combination of plume and resuspension of material originally deposited by earlier Maumee outflow. The location of the Detroit class water at the river and northwest of Pelee Island is reasonable, given the generally west winds of March 5 to 7. The mid-West Basin water class may represent a mixture of Detroit and Maumee River classes or an inflow from the Central Basin.

West Basin sediment transport modeling. —The following observations are based on the qualitative overview of the events in the West Basin provided by the single-channel imagery in figures 8 to 30:

- (1) There is a general movement of sediment from the Maumee River along the south shore passing through the islands. By early summer most of the particulate from the spring runoff of the Maumee River has been transported to the Central Basin of Lake Erie. Only that deposited in the deeper part of the West Basin, where it cannot be readily resuspended, remains.

- (2) The west shore sediment generally moves into the middle of the West Basin where considerable settling takes place.

- (3) The suspended solids from the Detroit River

originate in Lake St. Clair. In general, this plume moves east along the Canadian shore and only occasionally into the mid-West Basin. In either case there is considerable plume dispersion and most likely considerable settling within the West Basin.

(4) The amount of suspended particulate crossing the international boundary (shown in fig. 7) appears to be relatively small.

(5) Chemical pollutants for which total suspended solids are a tracer in general disperse in the same patterns as the suspended solids.

Two examples are given illustrating how the digital data are used to describe West Basin sediment transport. The first, discussed previously, makes use of the spectral differences in the data to identify areas of similar water class. If the source of a particular water class can be specified (e.g., a river, an area of resuspension, or an area of shore erosion), then the location of those water types throughout the basin can also be specified.

The second example involves the use of the contour maps of total suspended-solid concentration in combination with a numerical model of West Basin particulate dispersion. Such a model has been developed for Lake Erie (ref. 8). Figure 39 was produced using this model and illustrates the calculated surface currents existing in the West Basin at 9:00 a.m. EDT on March 8. A verification test of the model can be performed using the imagery of a later date to verify the model current prediction. Just as the contour maps extrapolate the data from a number of discrete sampling sites over a larger area, the numerical modeling provides a way of extrapolating measurements at a given time to a later time.

Suspended-solids loading calculations. — An analysis of the West Basin suspended-solids distribution and fate is complex, involving the study of river suspended-solids discharge, dispersion, and settling rates and patterns; resuspension; shore erosion; and sediment transport. An important additional input to the analysis is the total West Basin suspended-solids loading at a given time. Total loads were calculated for a basin area bounded on the east by a line from Little Point to Pelee Island to Sandusky Bay. For this calculation it was assumed that the suspended solids concentration was constant over the vertical water column and equal to the surface value. This is a reasonable assumption since the Basin is quite shallow and well mixed. Table VIII shows the West Basin loading calculated in this way on March 8 and 23, April 12 and 13, and May 12. Included are the monthly totals of suspended solids discharged by the Maumee River and an estimated monthly loading due to shore erosion (ref. 7). The shore erosion estimate is based on the input from U.S. shores only, since

data for the Canadian shore were not available. Also not included is the total suspended-solids discharge from the Detroit River.

The total suspended-solids loads calculated for March 8 and 23 undoubtedly reflect the large Maumee River discharge of February and early March. However, the calculated loads for April 12 and 13 were also quite high even though the April river discharge was very low. These loads are, in fact, an order of magnitude greater than the April river discharge and shore erosion combined. This suggests that a significant portion of the West Basin loading on April 12 and 13 is due to the resuspension of lake bottom sediments. On May 12 the calculated load is again higher than the combined May total Maumee discharge and U.S. shore erosion inputs. It is, however, considerably lower than those calculated for April. Since the winds for those periods were comparable in magnitude and direction, this reduction would indicate that by May there is less bottom sediment left in the West Basin to be resuspended.

The data presented in table VIII support the hypothesis that

(1) The dominant loading mechanism in the very early spring is the Maumee river discharge, a significant portion of which settles within the West Basin.

(2) As the river discharge decreases, wind induced resuspension of lake bottom sediment becomes the dominant loading mechanism. This condition persists for several weeks.

(3) By periodic resuspension, drift, and settling the bottom sediment is redistributed to the deeper mid-basin area and to the Erie Central Basin.

(4) By late spring the bottom sediment deposited by the early spring river discharge has been scoured away, and only background levels of suspended solids are observed in the West basin.

Near-real-time image transmission. — Single-channel imagery available on a near real-time basis can be very useful in planning a ship sampling program by selecting sites that (1) cover the existing range of suspended solids concentrations, (2) are surrounded by larger areas of relatively unchanging concentration, and (3) are not on plume boundaries.

The benefits to a ship-survey team when imagery is available early is illustrated by the survey of March 23. On March 22 at 10 a.m. the Lewis aircraft overflew the entire West Basin (fig. 15). It then proceeded to the Grand River in Michigan, the Menomonee River in Wisconsin, and the Genesee River in New York and returned to the Lewis Research Center at 5 p.m. The data tape was then removed from the aircraft, and an image of the West Basin suitable for transmission by telephone-facsimile was produced. At 11 p.m. that image was

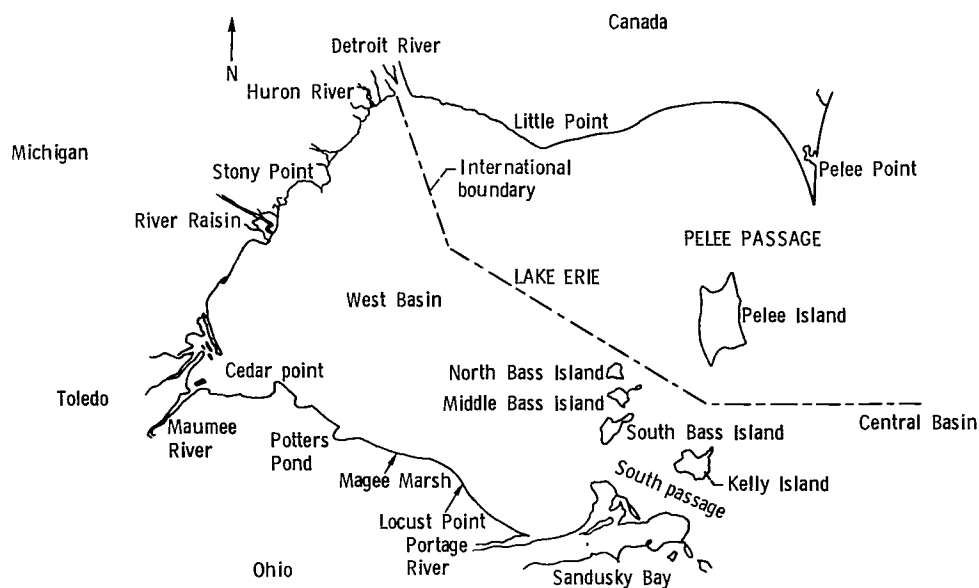


Figure 5. - Maumee River study area.

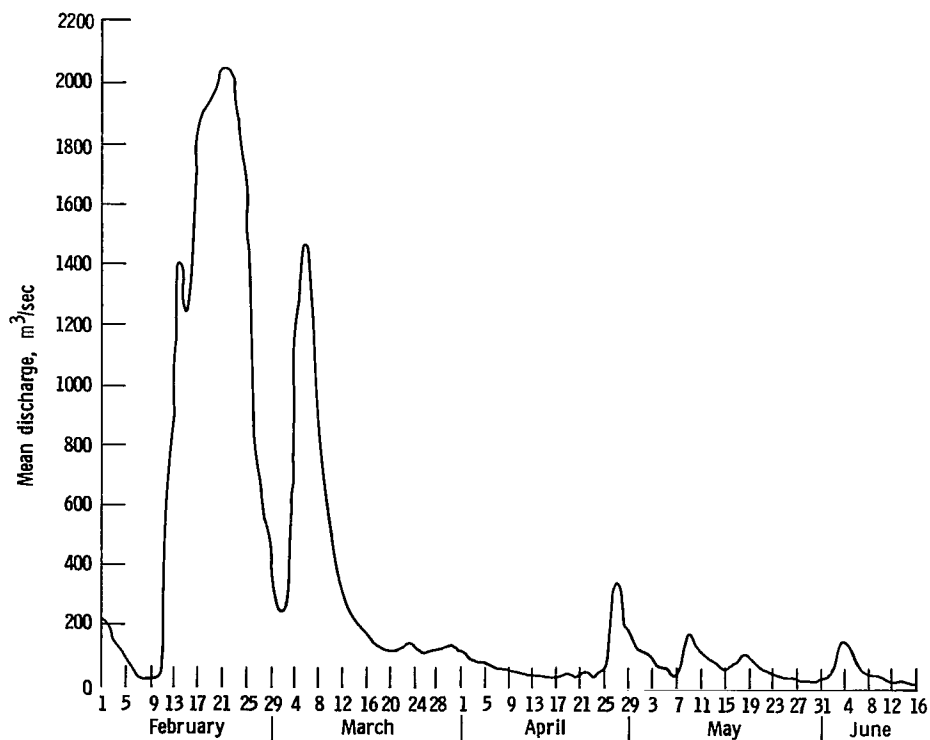


Figure 6. - Maumee River flow at Waterville, Ohio.

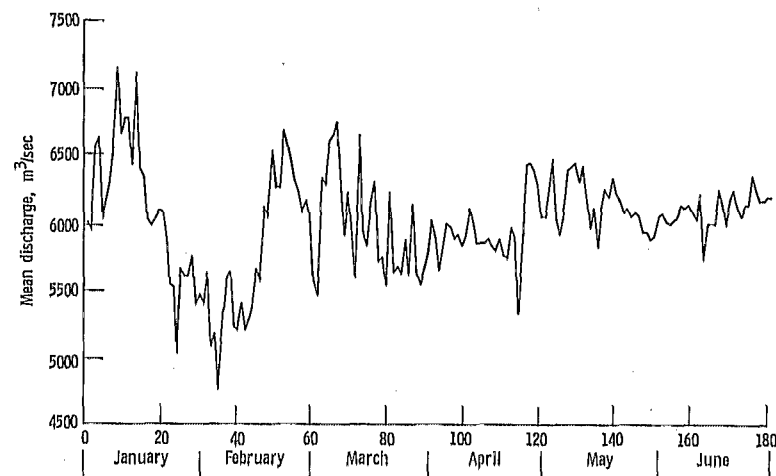


Figure 7. - Detroit River flow.

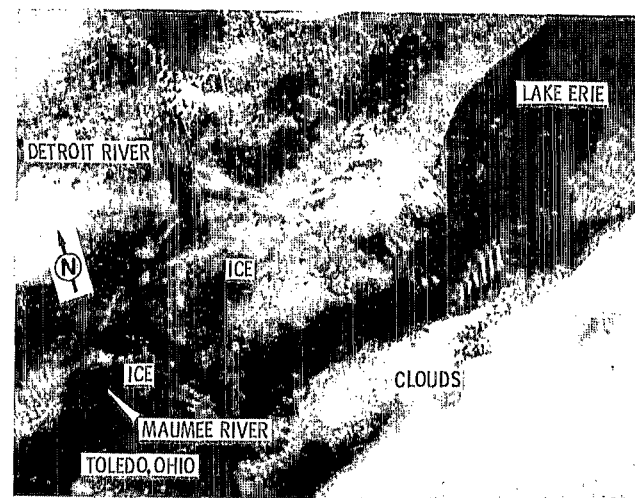


Figure 8. - Landsat image (band 5) of Lake Erie West Basin, February 13, 1976.

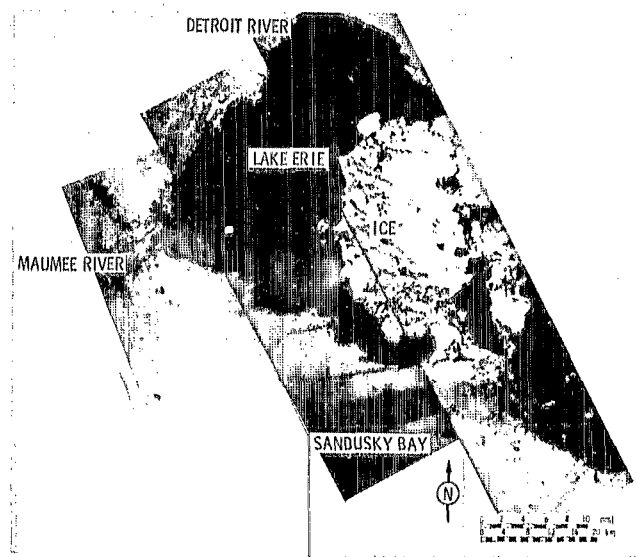


Figure 9. - Image of Lake Erie West Basin, February 23, 1976, OCS scanner channel 8.

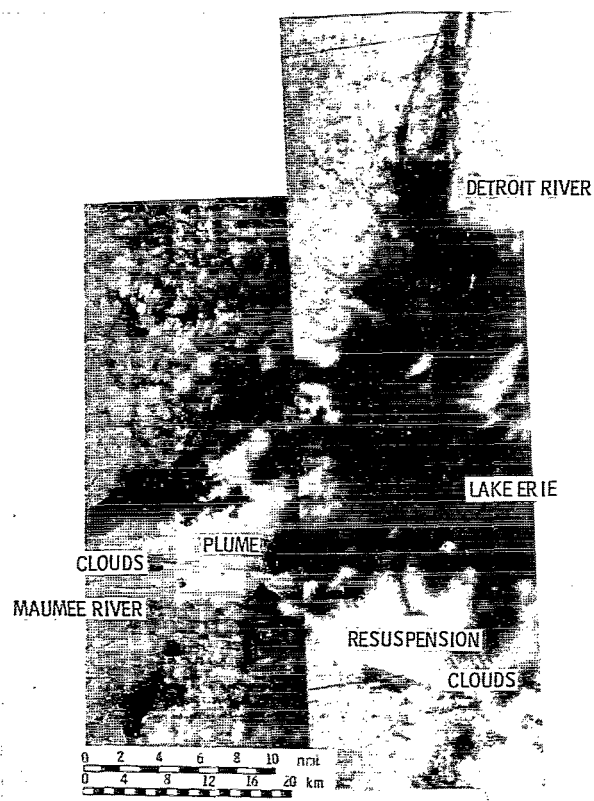


Figure 10. - Image of Lake Erie West Basin, February 25, 1976. OCS scanner channel 8.

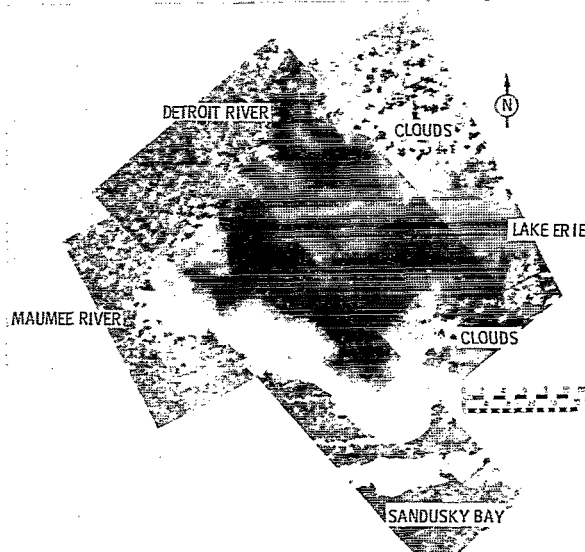


Figure 11. - Image of Lake Erie West Basin, March 8, 1976. OCS scanner channel 8.

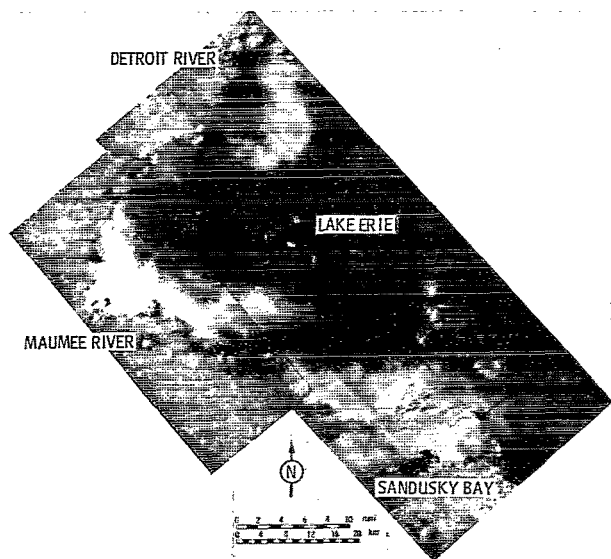


Figure 12. - Image of Lake Erie West Basin, March 11, 1976. OCS scanner channel 8.

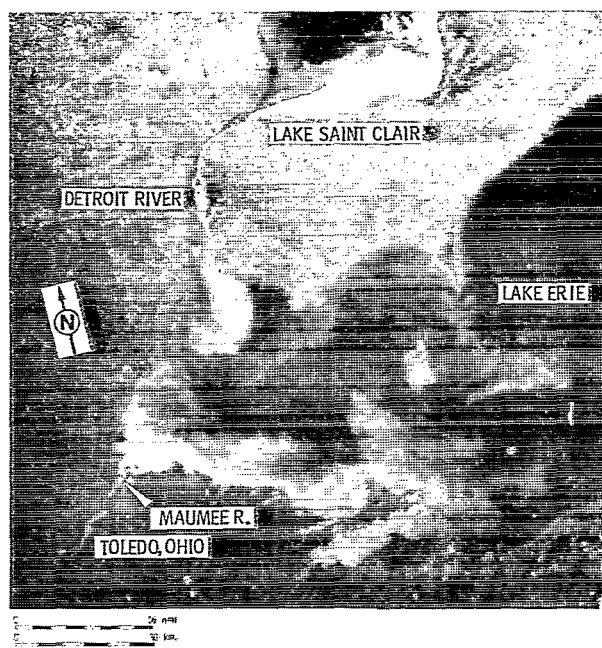


Figure 13. - Landsat image (band 5) of Lake Erie West Basin, March 11, 1976.

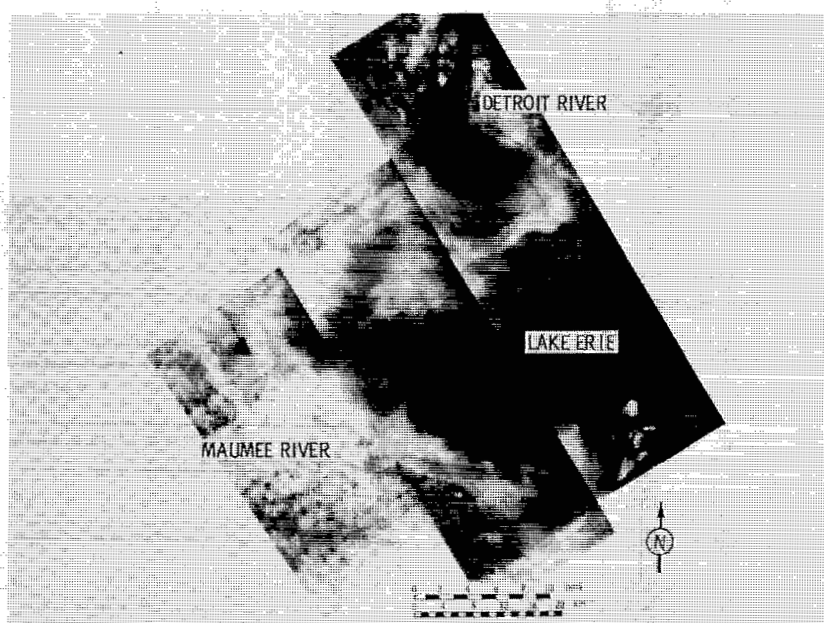


Figure 14. - Image of Lake Erie West Basin, March 15, 1976.
OCS scanner channel 8.

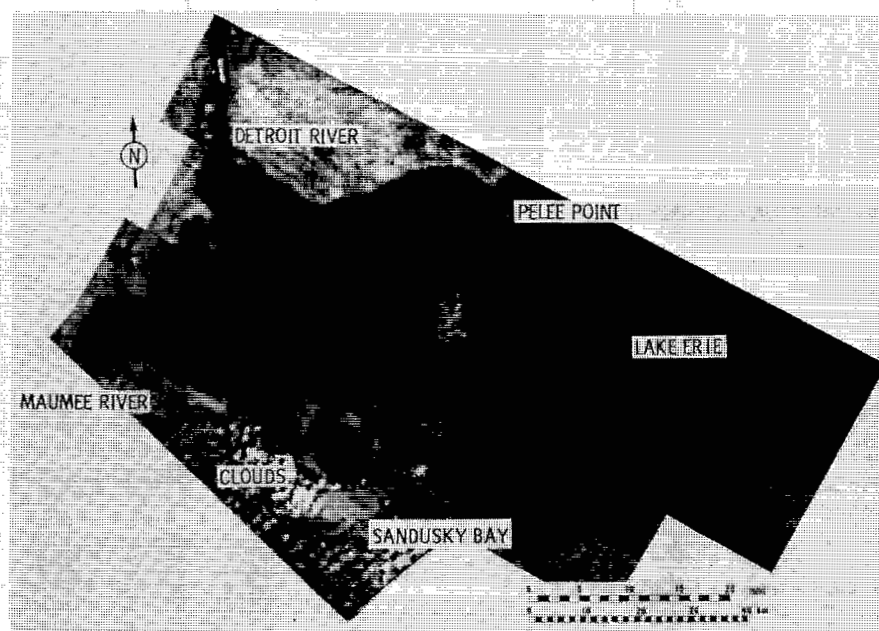


Figure 15. - Image of Lake Erie West Basin, March 22, 1976. OCS scanner channel 8.

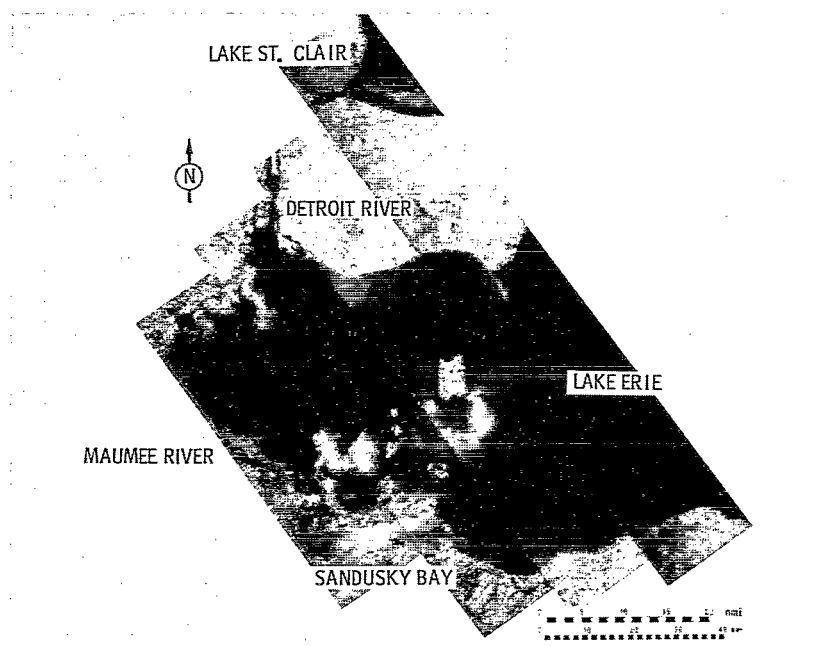


Figure 16. - Image of Lake Erie West Basin, March 23, 1976.
OCS scanner channel 8.

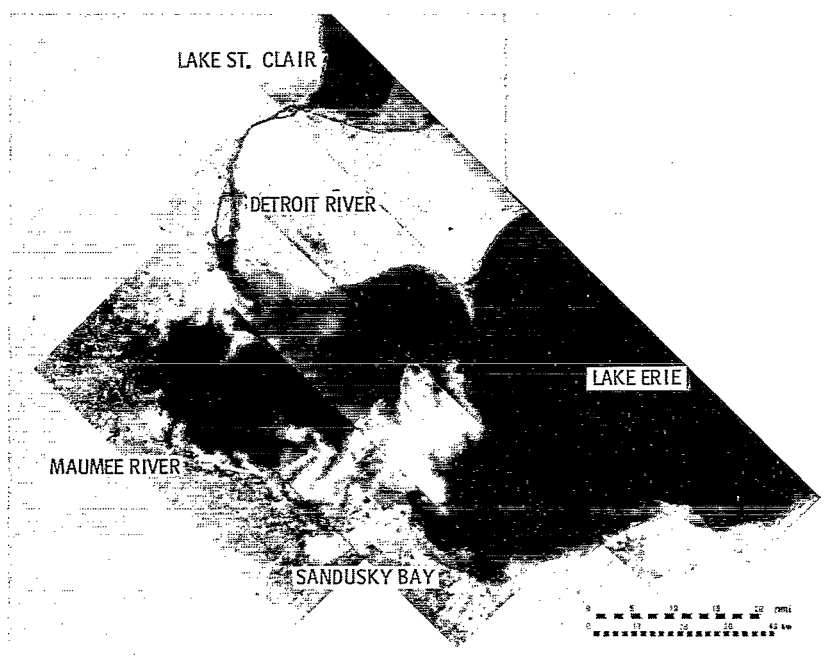


Figure 17. - Image of Lake Erie West Basin, March 25, 1976. OCS scanner channel 8.

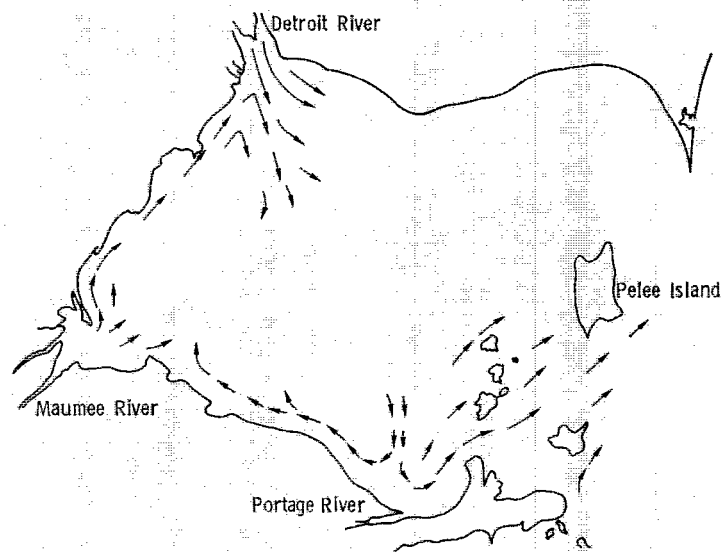


Figure 18. - West Basin transport inferred from overflights on March 22, 23, and 25.

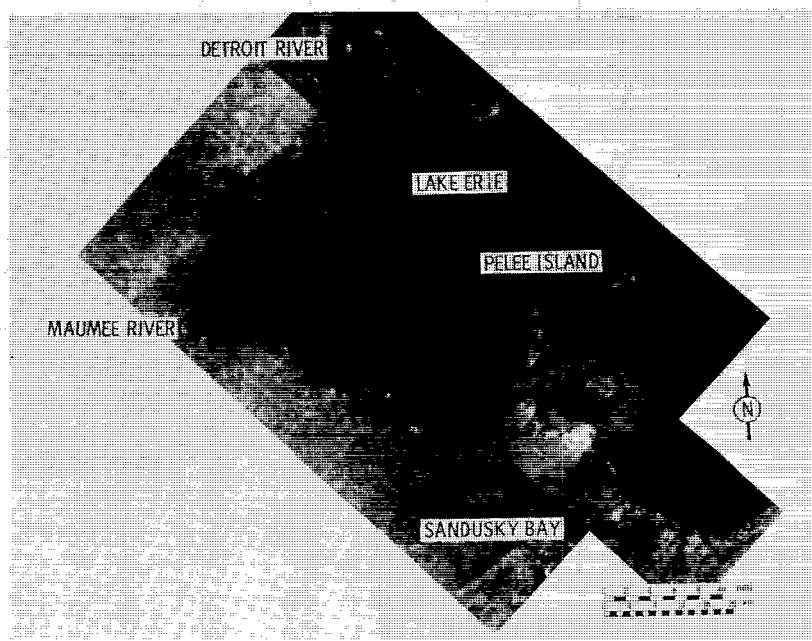


Figure 19. - Image of Lake Erie West Basin, April 3, 1976. OCS scanner channel 8.

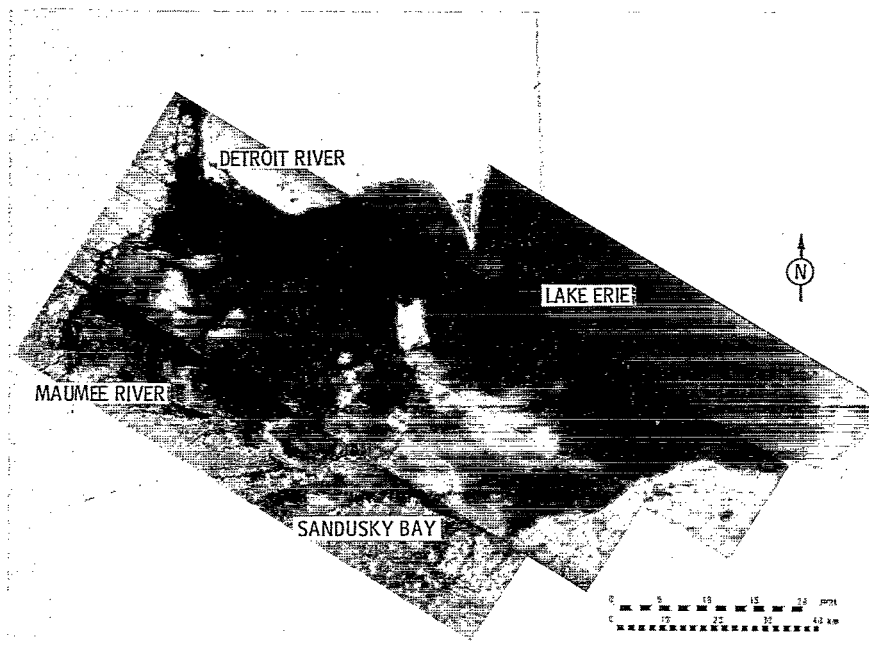


Figure 20. - Image of Lake Erie West Basin, April 5, 1976. OCS scanner channel 8.

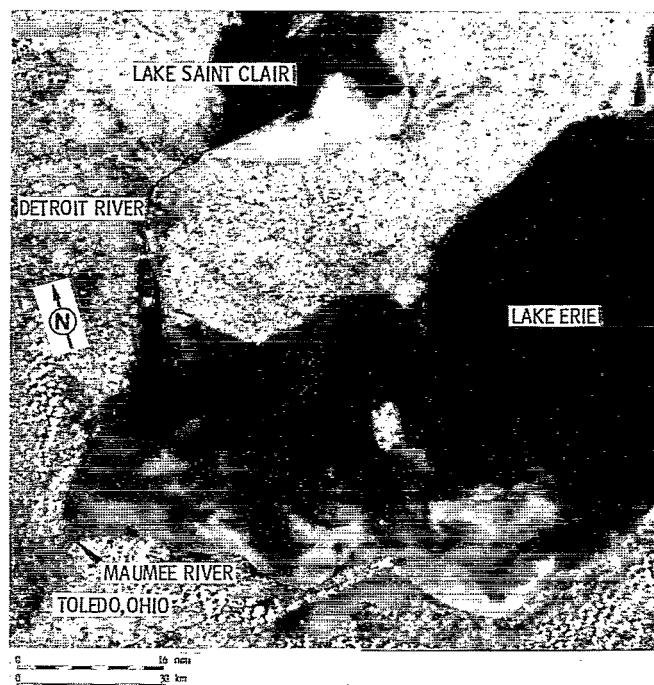


Figure 21. - Landsat image (band 5) of Lake Erie West Basin, April 7, 1976.

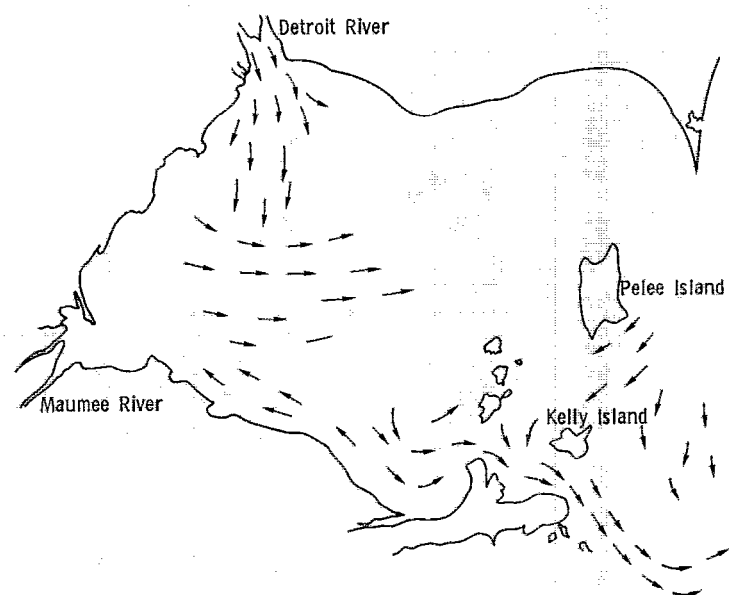


Figure 22. - West Basin transport inferred from overflights on April 3, 5, and 7.

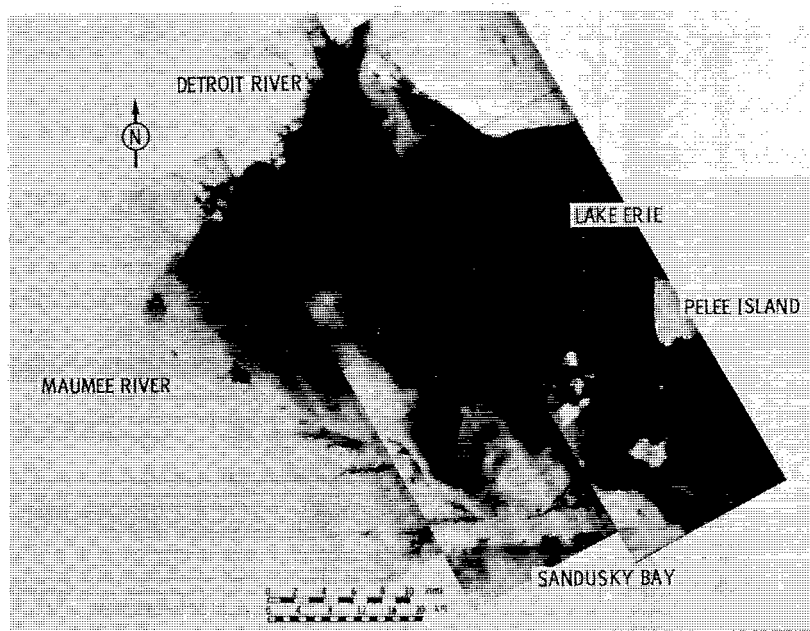


Figure 23. - Image of Lake Erie West Basin, April 12, 1976. OCS scanner channel 8.

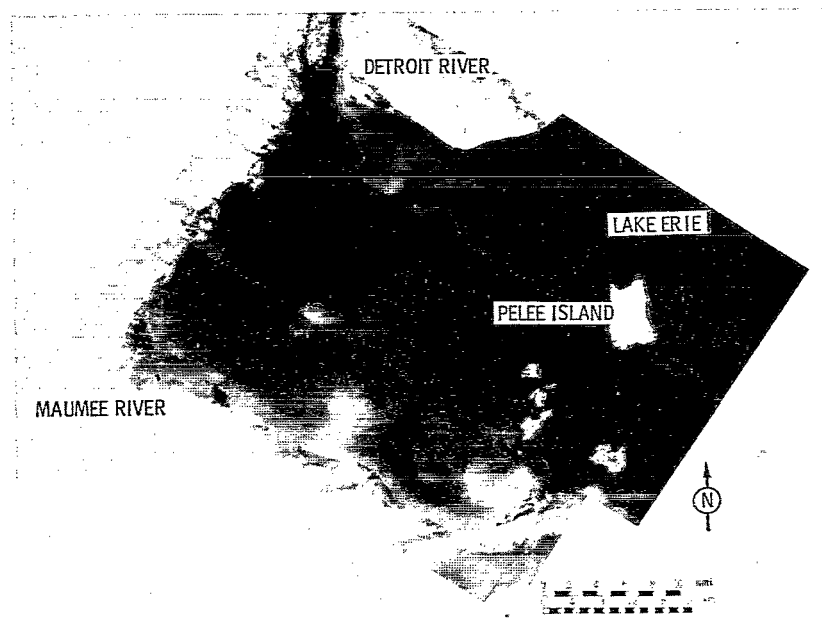


Figure 24. - Image of Lake Erie West Basin, April 13, 1976. OCS scanner channel 8.

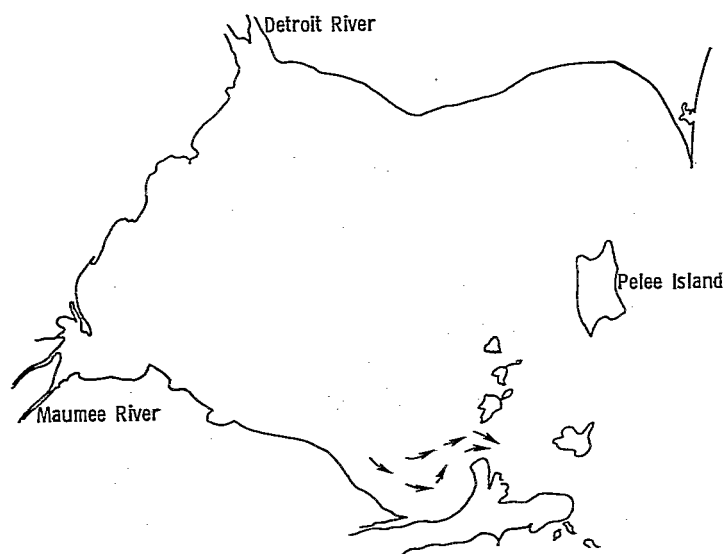


Figure 25. - West Basin transport inferred from overflights on April 12 and 13.

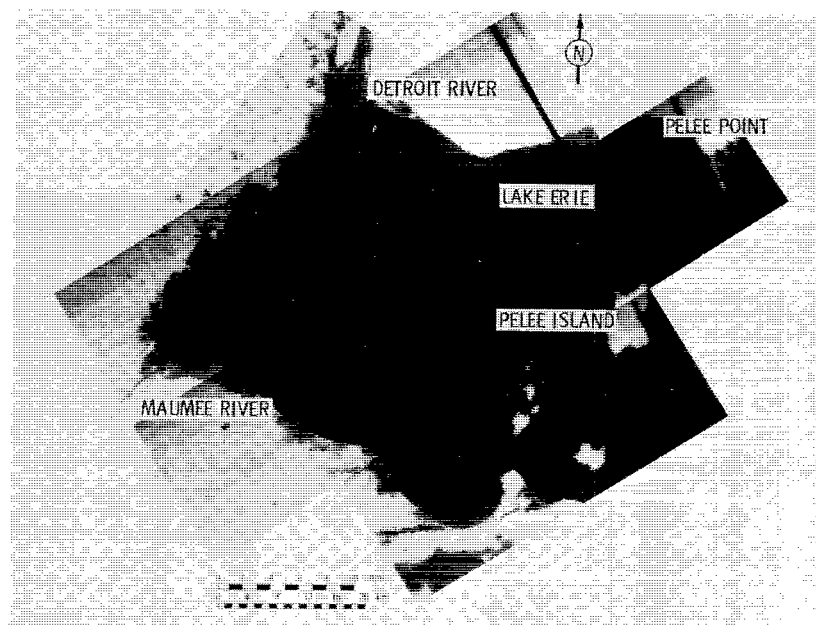


Figure 26. - Image of Lake Erie West Basin, May 12, 1976. OCS scanner channel 8.

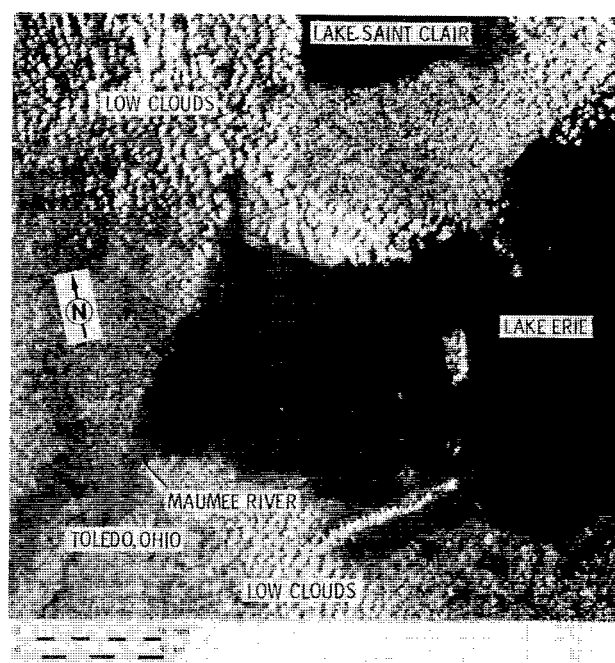


Figure 27. - Landsat image (band 5) of Lake Erie West Basin, May 22, 1976.

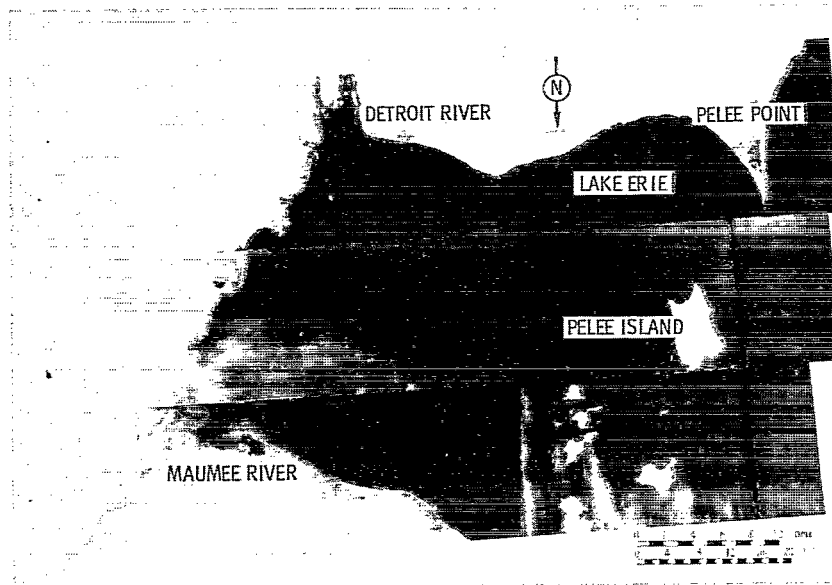


Figure 28. - Image of Lake Erie West Basin, June 5, 1976. OCS scanner channel 8.

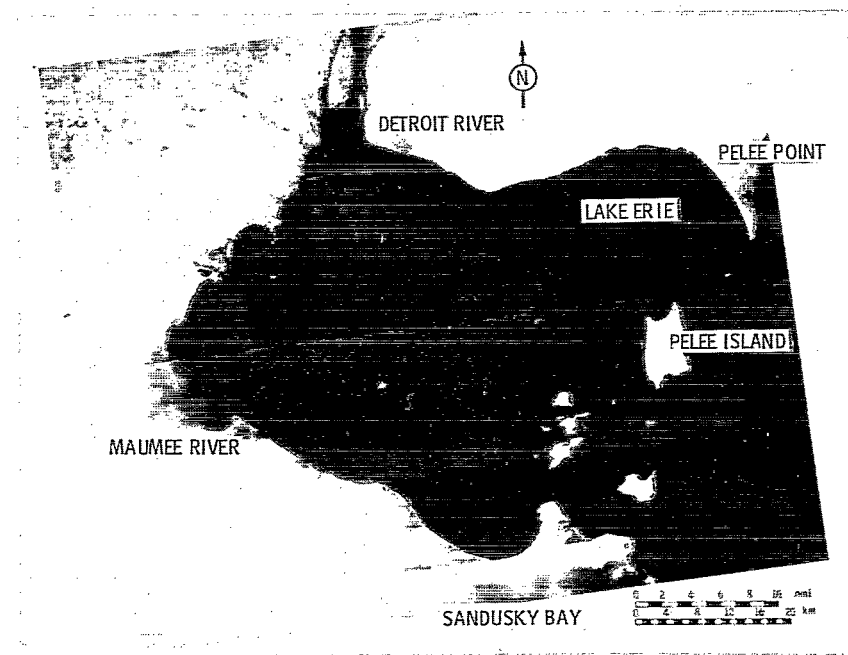


Figure 29. - Image of Lake Erie West Basin, June 7, 1976. OCS scanner channel 8.



Figure 30. - Landsat image (band 5) of Lake Erie West Basin, July 6, 1976.

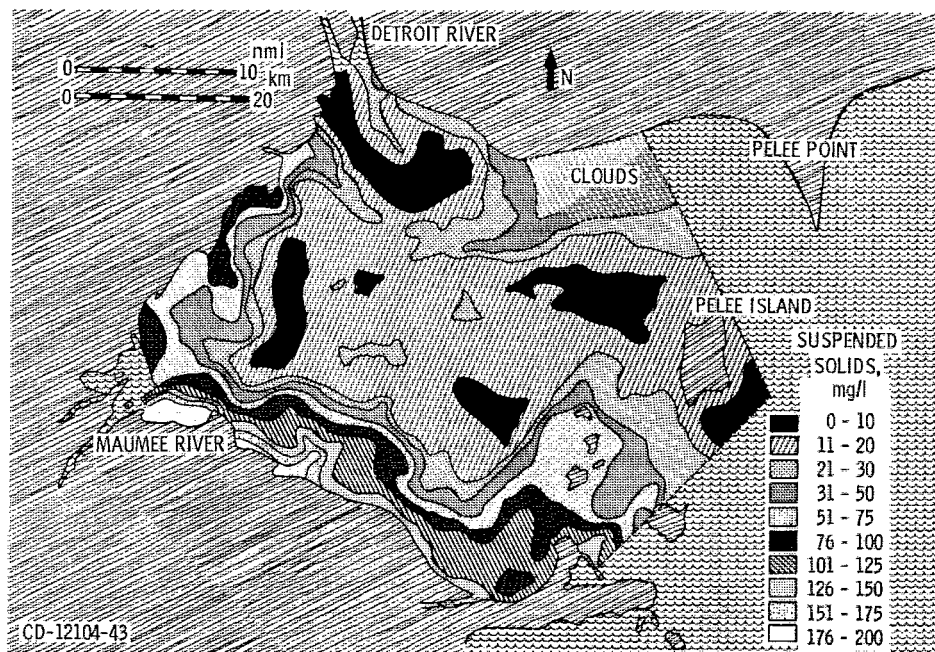


Figure 31. - Map of Lake Erie West Basin total suspended solids concentration, mg/l, for March 8, 1976. OCS scanner channel 8.

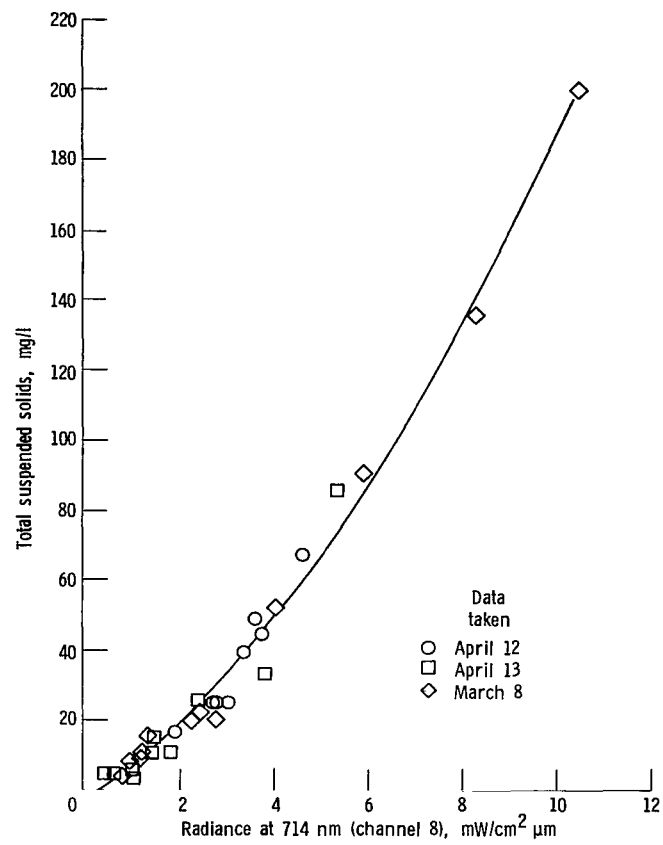


Figure 32. - Generalized correlation applicable to large wavelength data of channel 8 of ocean color scanner for several days of observation.

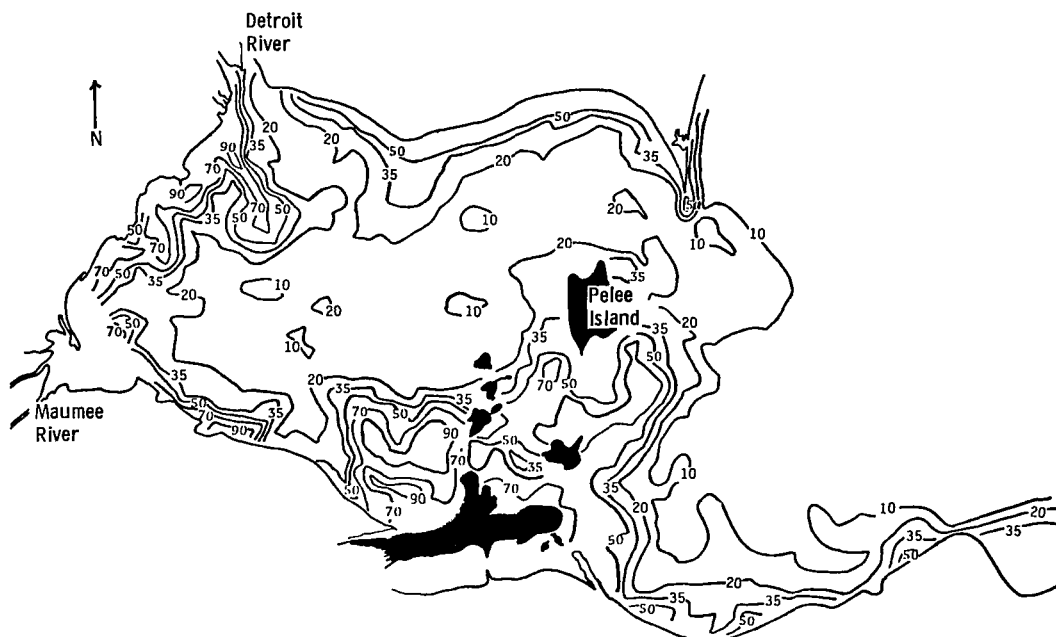


Figure 33. - Contour plot of total suspended solids concentration (in mg/l) for March 23, 1976.

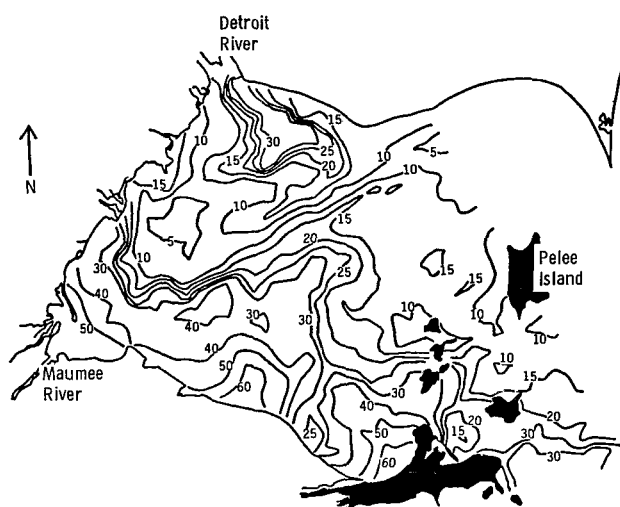


Figure 34. - Contour plot of total suspended solids concentration (in mg/l) for April 12, 1976.

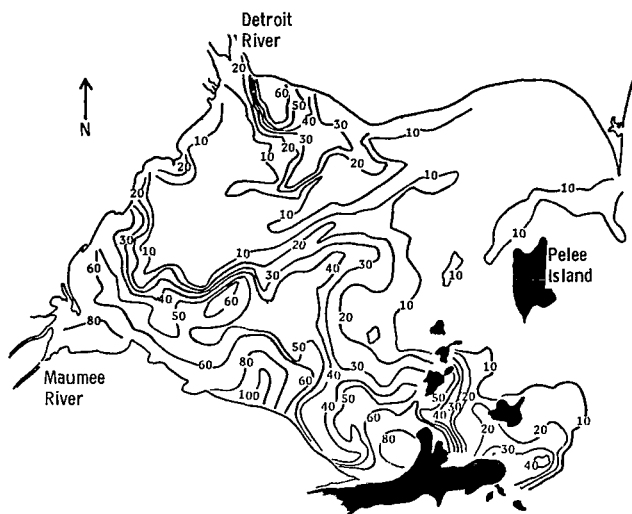


Figure 35. - Contour plot of total suspended solids concentration (in mg/l) for April 13, 1976.

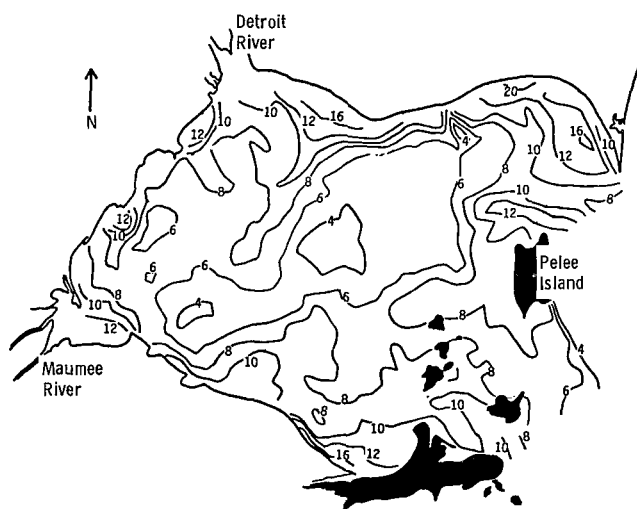


Figure 36. - Contour plot of total suspended solids concentration (in mg/l) for May 12, 1976.

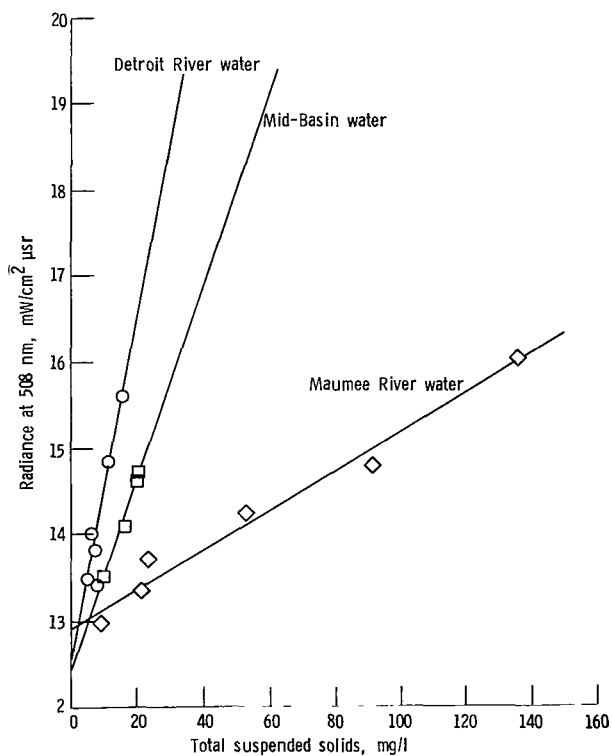


Figure 37. - Separation of three water classes in the West Basin of Lake Erie using 714- and 508-nanometer radiance data.

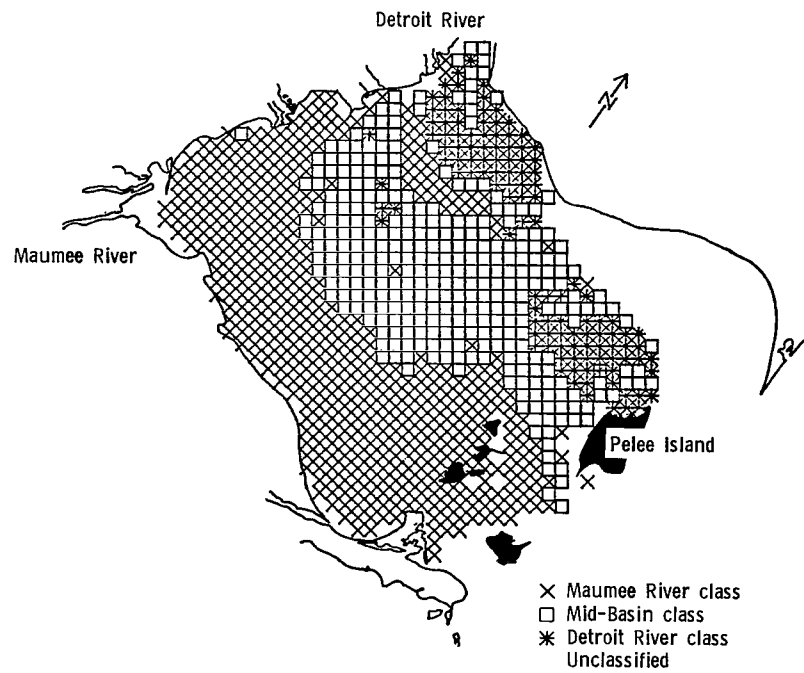


Figure 38. - Classification of three waters.

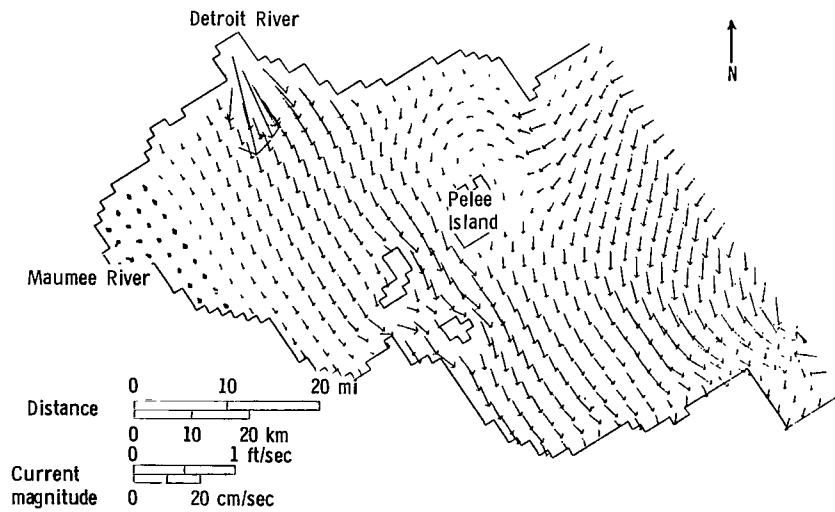


Figure 39. - Calculated West Basin surface currents at 9:00 a.m. on March 8, 1976.

transmitted to the sampling vessels home port. Thus, it was available to the captain of the R.V. Hydra on the morning of March 23 just before that day's cruise. Using that image, the captain added a sampling site to his schedule. That point, located in an area of high sediment concentration about 3 kilometers southeast of Pelee Island (fig. 16) provided the high concentration data point needed to correlate radiance and total suspended solids. It was thus possible to produce a suspended solids map of the entire West Basin (fig. 33). Without that data point no correlation and therefore no map would be available.

Summary of Results

Remote sensing data are reported from 16 overflights of the Lake Erie West Basin between February 23 and June 5, 1976. These data, together with five Landsat images, include coverage of the basin during the period of maximum Maumee River runoff. Same-day water sampling was accomplished during eight of these flights. On five of these days, data were obtained that provided correlations between upwelling radiance and total suspended solids. Other correlations between Secchi depth, turbidity, inorganic solids, total phosphorus, and dissolved oxygen were provided. Contour maps of the surface suspended-solids concentrations over the entire West Basin were generated. Basin loadings and the classification of water loading types were calculated using the remote sensing and these survey data. These quantitative data results along with single-channel imagery of all overflights and the Landsat data permitted a relatively complete assessment of the effects of river plume dispersion, resuspension, shore erosion, and suspended solids transport.

The data indicate that the dominant roles in West Basin dynamics are played by the area's prevailing winds, by the large amount of water discharged by the Detroit River, and by the large amounts of suspended solids discharged by the Maumee River. The prevailing winds, especially in the early spring months are from the west and support a general transport and dispersion of river inputs to the east. (This movement can be inhibited by large area ice cover.) During the spring 1976 study the peak Maumee River inflow occurred in February, and a secondary peak occurred in early March. The first major discharge plume was observed to move east along the south shore. It is hypothesized that considerable settling of that plume load took place. Hence, when the secondary peak discharge plume occurred, its influence on the total basin loading was masked by resuspension events along the south shore and in the islands area. As the river discharge returned to background levels in mid-March, resuspension,

drift and settling followed, which resulted ultimately in the transport of sediment to the deeper mid-basin area and to the Central Basin of Lake Erie. In general, the transport patterns did not reveal any significant movement of suspended solids across international boundaries. By late spring the combined contribution from all three loading mechanisms (river discharge, resuspension, and shore erosion) subsided, and only background levels of suspended-solids concentrations were observed. The part played by shore erosion seemed relatively small throughout the study period.

To the extent that other pollutants correlate with suspended solids, suspended solids may act as a tracer for these materials. Consequently, their movements and distribution patterns are the same. The remote sensing images and suspended solids contour maps thus acquire broader significance, but only in the areas and time periods represented by the ship survey data on which the correlations are based.

In the aircraft-and-ship data correlation analysis, several coordination criteria were noted which affect the correlations and thus potential usefulness in documenting the dynamics of an area. First, it is important that the ship-survey sites be chosen so as to be representative of the overall lake conditions. This means that water samples must be taken in areas ranging from minimum to maximum suspended-solids concentrations. Second, it is important that the sampling sites be within areas of relatively uniform concentration, that is, not on a plume boundary. Finally, the overflight and the ship survey should be as near to being simultaneous as possible. Simultaneity can be approached by minimizing the number of ship sampling sites.

Good coordination requires that the ship survey team be provided with lake imagery on a timely basis. This was demonstrated on March 22 and 23 when the ship survey manager added to his March 23 sampling schedule a site critical to the data analysis. The site location was determined from an image made on March 22, which had been sent to him late on that date by telephone-facsimile transmission. Since there was not much change in the sediment distribution from that day to the next, the near-real-time availability served well. If rapidly changing basin conditions existed, the same accomplishment would require real-time data transmission to the survey ship.

Genesee River Results

The Genesee River discharges into Lake Ontario at Rochester, New York. The river water enters the lake 670 meters offshore through a 150-meter-wide chan-

nel. Discharge rates for the spring of 1976 are shown in figure 40. A dam is located 64 kilometers upstream at Mount Morris and is operated by the Corps of Engineers to control flow rates into the lake. As a result, during periods of high runoff, the shape and location of discharge peaks may be different than they would be if the water flow were unrestricted.

In 1976 the snow melt runoff peaked on March 6. The peak was sharp, but a relatively high runoff period existed from early February until the end of March. Discharge peaks following this time period are associated with rain runoffs.

The Great Lakes Laboratory (GLL) at the State University College at Buffalo conducted ship surveys on 8 days as shown in figure 40. On two of these days, March 31 and April 28, sampling was limited because of inclement weather. On April 1 and August 3 ship sampling covered stations for the International Field Year for the Great Lakes (IFYGL) as part of the river runoff studies. A background study survey in preparation for a wind resuspension event was done on June 22, and the actual wind resuspension-study cruises occurred on August 19 and September 24.

NASA attempted to overfly all runoff and resuspension ship survey sites. Figure 40 shows the flights and ship cruises. In some cases when clouds precluded the collection of remote sensing data on the day of a ship survey, an overflight was made on the next clear day. High altitude flights using the OCS are reported for March 22, April 3, April 29, and June 3. Lower altitude flights with the M²S were made on August 3 and 19, both of which were also days of ship surveys.

History of Events

Images from the six days of aircraft coverage as well as six selected Landsat images are presented chronologically in figures 41 to 56. The images span the period from March 22 to August 19.

From the time of the first overflight to the end of May, resuspension and/or shore erosion, is observed in nearly all of the images. Estimates for shoreline erosion rates in the Great Lakes are given in reference 7, where erosion rates on Lake Ontario are somewhat below the average in the Great Lakes. On a per mile basis, the erosion rates show an overall increase from west to east going from Niagara to Orleans to Monroe (Rochester) to Wayne counties, although Orleans County actually has the lowest rate. It is not clear what fraction of the suspended material observed should be attributed to resuspension and what fraction to shoreline erosion, so that in all further discussions, resuspension may be assumed to include possible shoreline erosion.

The OCS flights of March 22 and April 3 (figs. 41 and 42) show plumes emerging from the Genesee River and heading east. Resuspension is also evident to the east of the Genesee on March 22. These two images correspond to the end of the snow melt runoff period. Plumes observed after this are due to rain runoff events.

The plume seen in the image of April 29 (fig. 45) presents an interesting phenomena. Even though there was a heavy runoff during the previous couple of days, the plume did not extend very far into the lake. At the same time there is also evidence of a significant amount of resuspension or shoreline erosion occurring. Wind speeds at Rochester were 7.2, 7.6, and 4.8 m/sec, and wind directions were north-west, west-northwest, and west-northwest for April 27, 28, and 29, respectively. Evidently the wind was strong enough to drive the plume parallel to shore before it made any headway into the lake. The strong winds were consistent with the Great Lakes Laboratory experience on April 28, which was a sampling survey day, but the mission had to be terminated after sampling three stations because of high wind and waves. The Landsat image of April 30 (fig. 46) further illustrates the effects of persistent northwest winds during a time of high river discharge.

Included among the Landsat images are two from April 13 and May 10 (figs. 44 and 47), which show the eastern tip of Lake Erie in addition to the major portion of the south shore of Lake Ontario. On April 13 a large ice pack existed at the east end of Lake Erie, which had resulted from the ice boom at Buffalo. Suspended particulate entered Lake Ontario from the Niagara River as well as from the Welland Canal. On May 10 after the ice had disappeared, the plume from the Niagara was large, and the runoff from the Welland Canal increased. The source of the particulate entering Lake Ontario at the Niagara River appears to be resuspension and shore erosion in Lake Erie, which can be seen along the Canadian shore in Eastern Lake Erie. A small additional contribution may come from the Niagara River. However, flow rates obtained by the U.S. Geological Survey at Niagara Falls show fairly constant flow rates throughout the year. There are no major contributing streams between Niagara Falls and Lake Ontario and consequently the Niagara River makes a fairly constant loading throughout the year. The large plume from the Niagara River spreads to the east and merges into a region of near-shore resuspension, which exists along the entire shoreline. A small plume exists at the Genesee, but is barely visible when compared with the background resuspension. While the Genesee River makes a noticeable contribution to particulate loading into Lake Ontario, loadings from Lake Erie via the Niagara River are more significant,

at least on this date. In addition, resuspension due to winds and possibly shore erosion are also significant sources of suspended particulate.

The final six images are M²S (figs. 51 to 56) scanner images from the C-47 overflights for the rain runoff plume on August 3 and the resuspension study on August 19. On both dates concurrent in-the-water data were collected. Enlargements of the area around the mouth of the Genesee (figs. 53 and 56) indicate the sampling stations on these dates.

The rain runoff event on August 3 produced a large plume that moved westward. Images in two channels, channel 3 (515 nm) and channel 5 (600 nm) (figs. 51 and 52), are presented for comparison in order to outline the total area affected by the runoff. As the wave length increases, absorption of light by water increases rapidly above about 500 nanometers. Therefore, with increasing wavelength, less particulate in the deeper water is seen and only the areas with particulate nearer the surface stand out. Thus the apparent size of the plume is a little smaller in the channel 5 image than in the channel 3 image. It should be noted that the channel that produces the larger plume is not necessarily the best for correlating scanner and ship data. In fact, the best correlations of radiance with suspended-solid loadings have been produced from the longer wavelength data.

An enlargement of the area near the river mouth (fig. 53), shows the 12 IFYGL stations sampled. Data were taken at three additional stations that were within the sampling grid shown, but were too close together to be individually identifiable on the scale of the figure. These were stations determined by GLL at the time of sampling and were within the plume, on the edge of the plume, and outside of the plume.

Figures 54 and 55 show the Genesee River outflow under conditions of very low flow (45 m³/sec) on August 19. A resuspension event had been anticipated on August 19 because of high winds on the preceeding days. However, resuspension was minimal, and little suspended particulate leaving the Genesee was apparent. The winds did cause considerable wave action, but were mostly westerly, which probably was the reason for the lack of resuspension activity. Surface sampled stations are shown in figure 56.

Data Analysis and Discussion

The two days on which concurrent aircraft scanner data and water samples were acquired were August 3 and August 19. Data from both days were analyzed and correlations were attempted.

The rain runoff on August 3 provided a good opportunity to evaluate the effect of a rain event on Lake Ontario. The Genesee River discharge during

this time was at the highest level of the summer. Since no significant amount of resuspension is apparent, the particulate loadings in the plume represent river runoff contributions only. On this date the Great Lakes Laboratory sampled from late morning to early evening. The NASA C-47 overflight occurred from 3 to 4 p.m., which was in the middle of the sampling period.

The correlation analysis for the August 3 data illustrated some of the problems of the lack of aircraft-ship coordination discussed earlier in this report. The preassigned ship sampling sites were located over a sampling grid area which was small compared with the size of the plume (figs. 52 and 53). The sites that were sampled over a 5- to 6-hour period were located in the most dynamic region of the plume. Also, several sites were located in regions of large gradients in particulate concentration. This may be why some of the duplicate water samples showed wide variations, even though quality checks for individual samples were good. Because of these problems, a large scatter in the data was found when a correlation of aircraft with ship data was tested. Since some of the ship data were collected at times that were significantly different from the overflight time, these data and the inconsistent duplicate values were eliminated, and the correlation analysis repeated. The use of the reduced data set resulted in a correlation of M²S channel 5 and suspended solids. The analysis indicated that channels 4 to 7 correlated nearly as well but that the channel 5 correlation provided the lowest standard error. This correlation was linear over a range of 0 to 38 mg/l, consistent with the results from the other rivers. The suspended-solids contour map shown in figure 57 was produced from this correlation.

Figure 57 also indicates the corresponding contour values for chlorophyll *a* concentration. Chlorophyll is the only other parameter for which an indirect correlation was obtained. Correlations were attempted for particulate phosphorus, total solids, silica, and turbidity, but none were obtained. Correlations for chemical parameters were not attempted since these parameters were not available at the time of the analysis.

For the data of August 19, surface samples were obtained at a grid of stations that were selected for studying resuspension effects. Reported suspended solids concentrations were about 11 mg/l at all sites, which was the lower detectable limit. However, the scanner data (fig. 56) shows evidence that suspended-solids concentrations at the near-shore stations were higher than for the offshore stations at that time. Therefore, the low concentrations sampled did not provide a sufficient range to permit a suspended solids correlation with scanner data. The lack of a

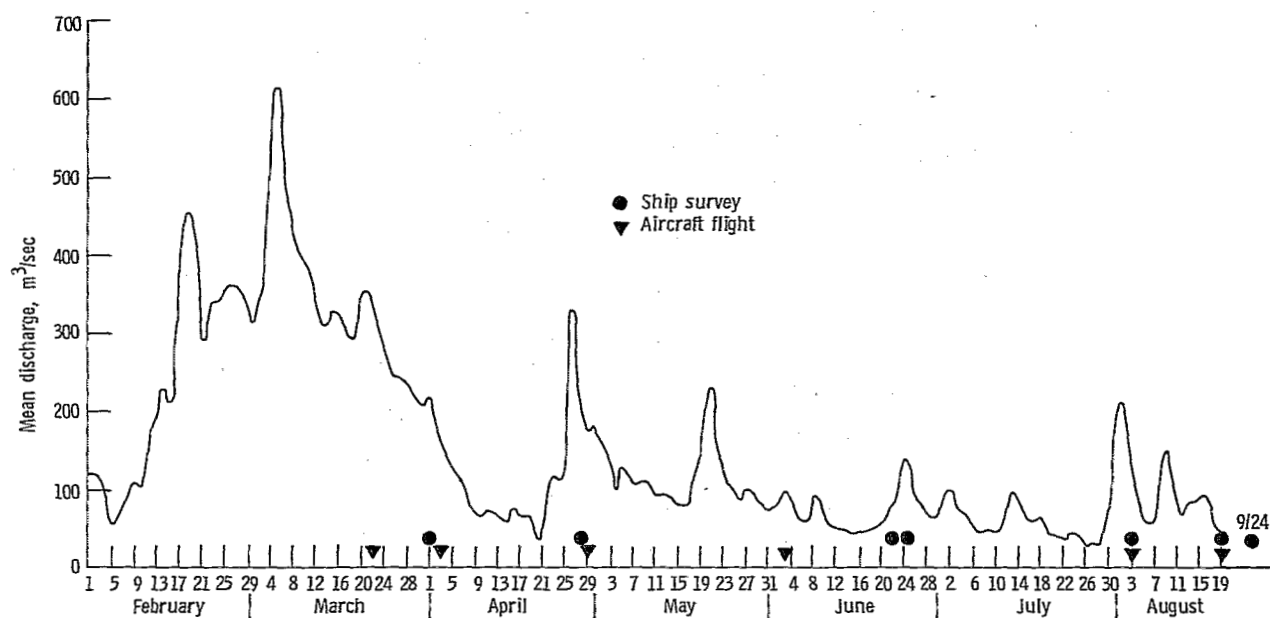


Figure 40. - Mean discharge of Genesee River and summary of remote-sensing and ship surveys.

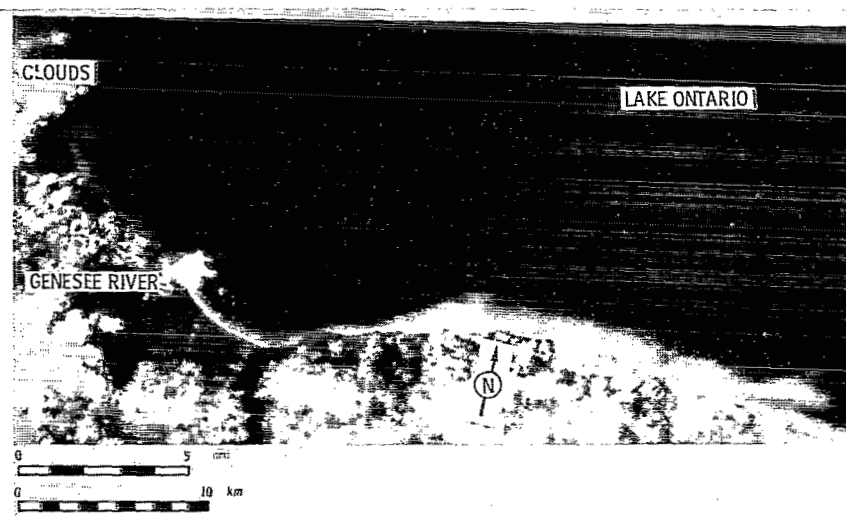


Figure 41. - Image of Genesee River-Lake Ontario, March 22, 1976. OCS scanner channel 6.

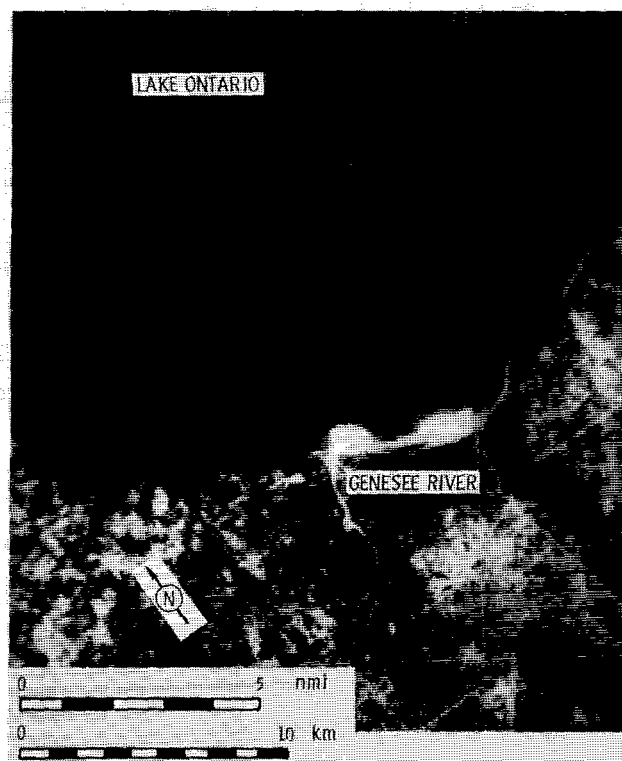


Figure 42. - Image of Genesee River-Lake Ontario, April 3, 1976.
OCS scanner channel 6.



Figure 43. - Landsat image (band 5) of Genesee River-Lake Ontario, April 12, 1976.

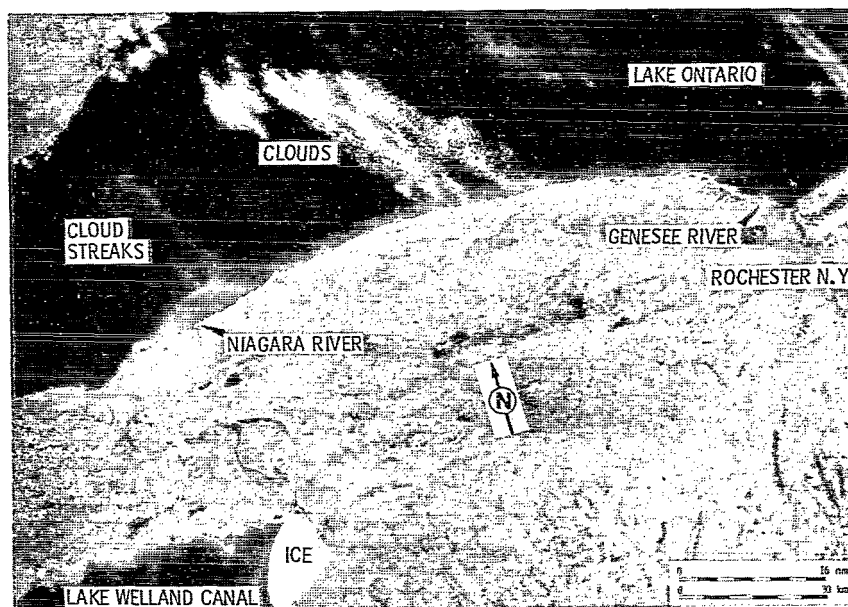


Figure 44. - Landsat image (band 5) of Genesee River-Lake Ontario, April 13, 1976.

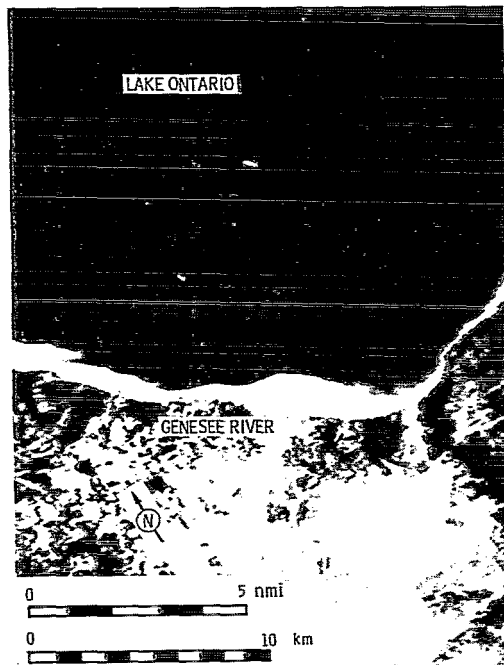


Figure 45. - Image of Genesee River-Lake Ontario, April 29, 1976. OCS scanner channel 6.

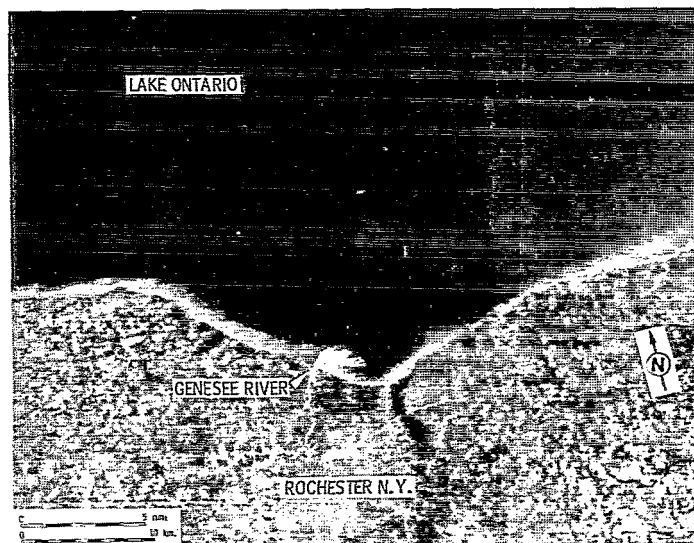


Figure 46. - Landsat image (band 5) of Genesee River-Lake Ontario, April 30, 1976.

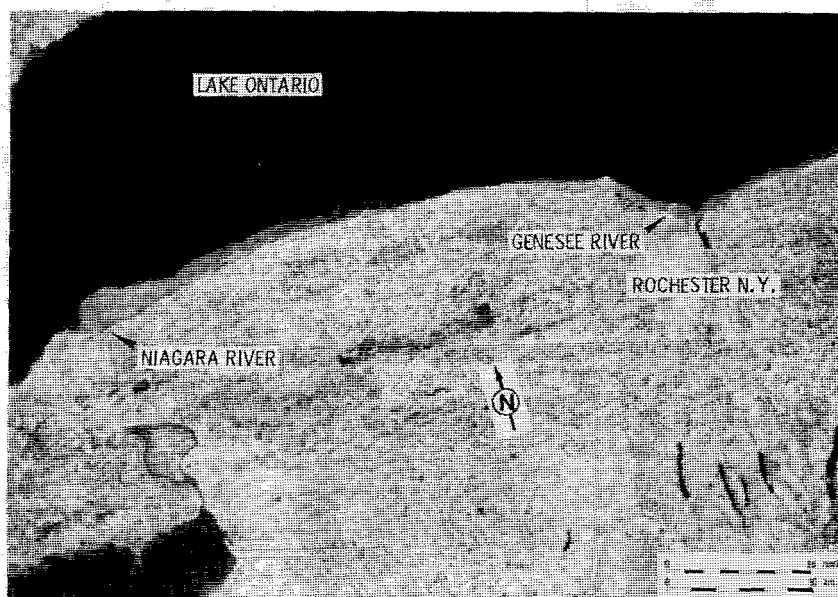


Figure 47. - Landsat image (band 5) of Genesee River-Lake Ontario, May 10, 1976.

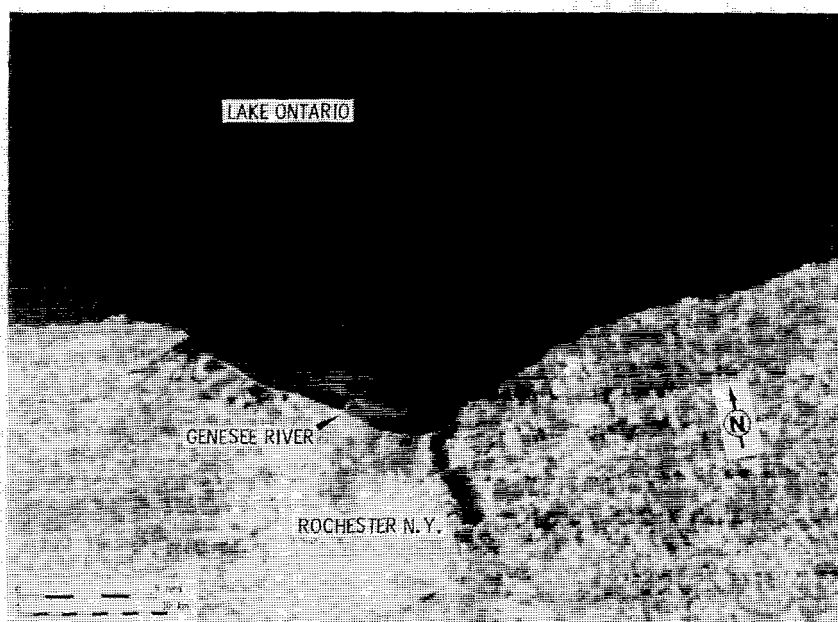


Figure 48. - Landsat image (band 5) of Genesee River-Lake Ontario, May 27, 1976.

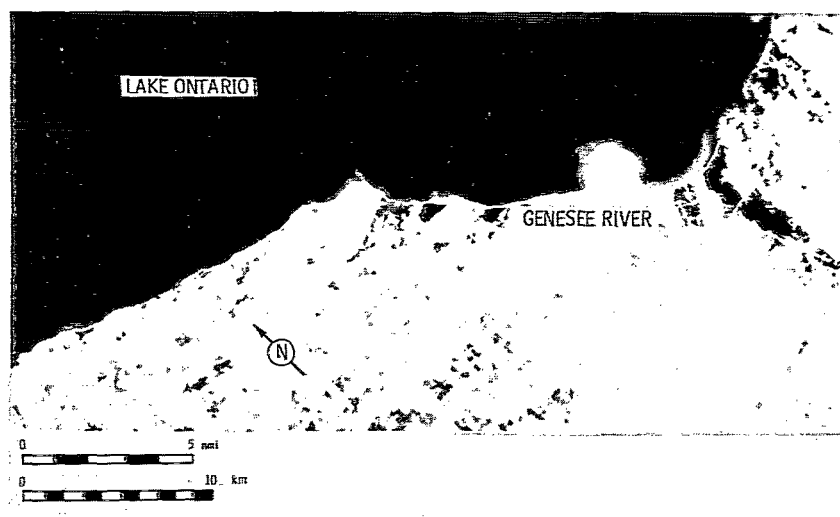


Figure 49. - Image of Genesee River-Lake Ontario, June 3, 1976. OCS scanner channel 6.

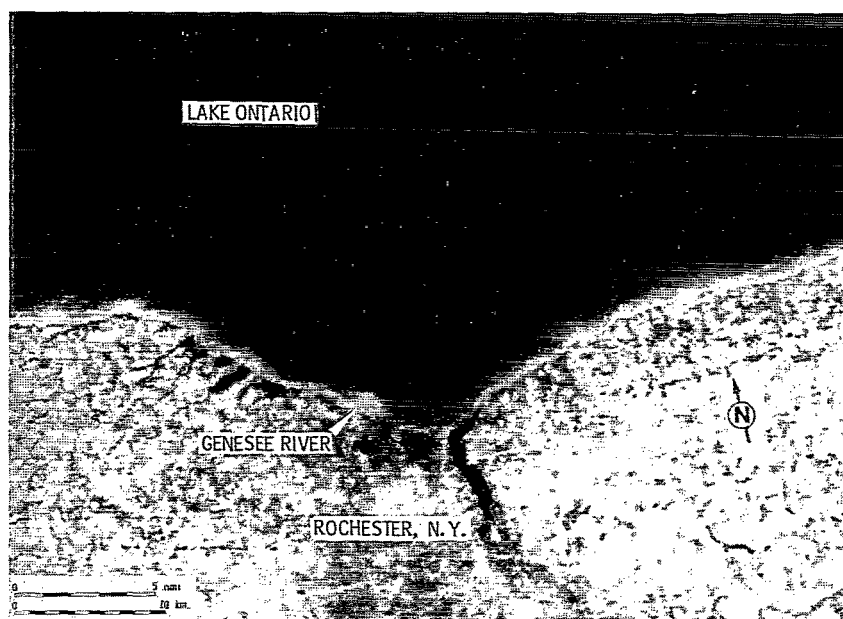


Figure 50. - Landsat image (band 5) of Genesee River-Lake Ontario, June 5, 1976.

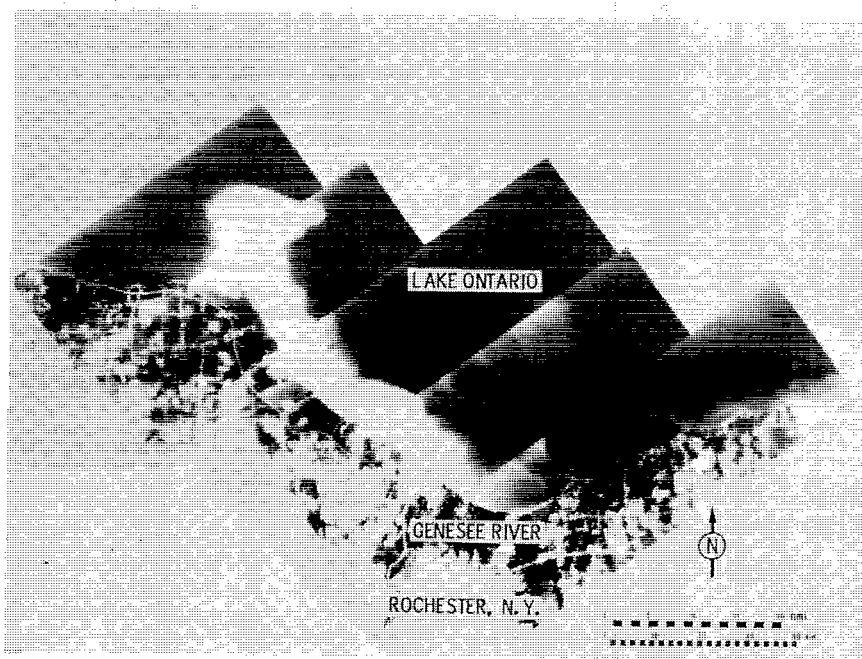


Figure 51. - Image of Genesee River-Lake Ontario, August 3, 1976. M²S scanner channel 3.

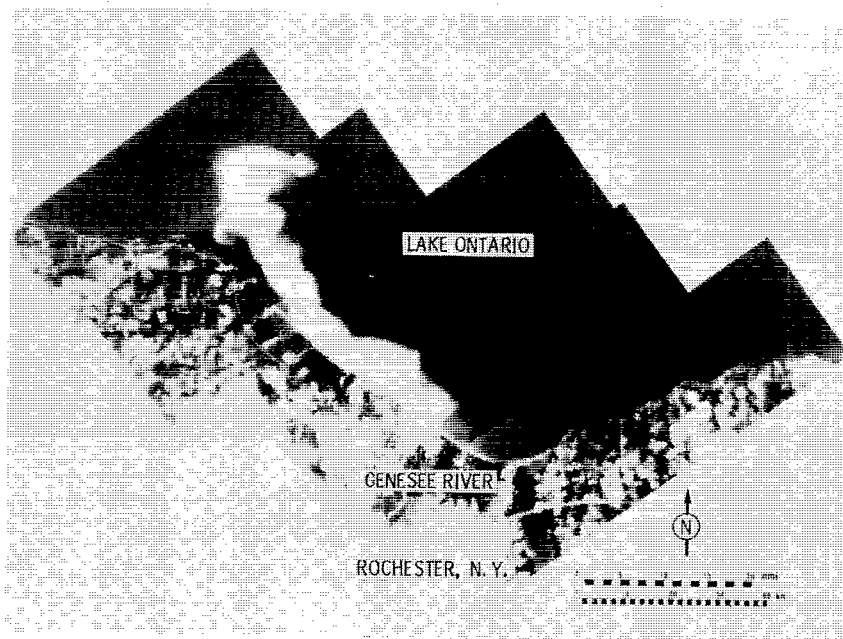


Figure 52. - Image of Genesee River-Lake Ontario, August 3, 1976. M²S scanner channel 5.



Figure 53. - Image of Genesee River-Lake Ontario, August 3, 1976. M²S scanner channel 5.

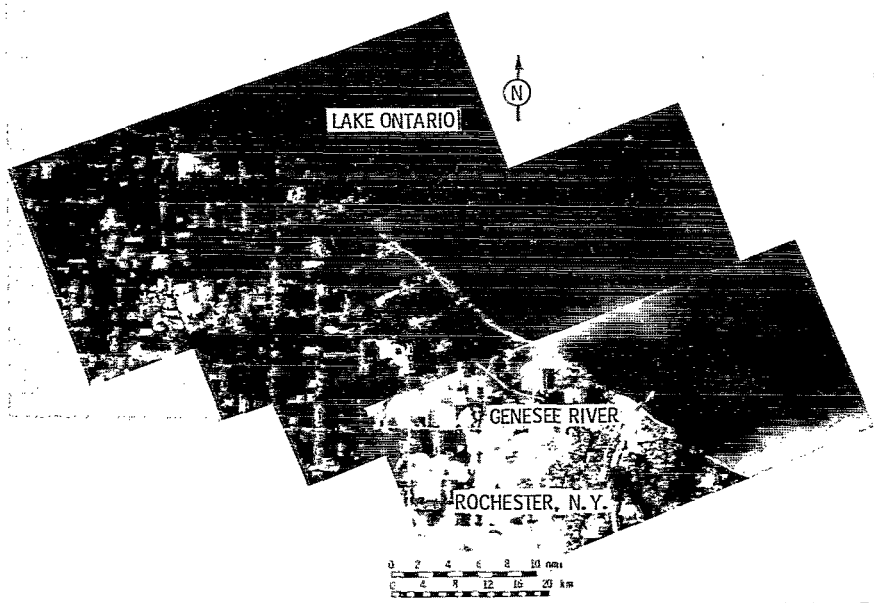


Figure 54. - Image of Genesee River-Lake Ontario, August 19, 1976. M²S scanner channel 3.

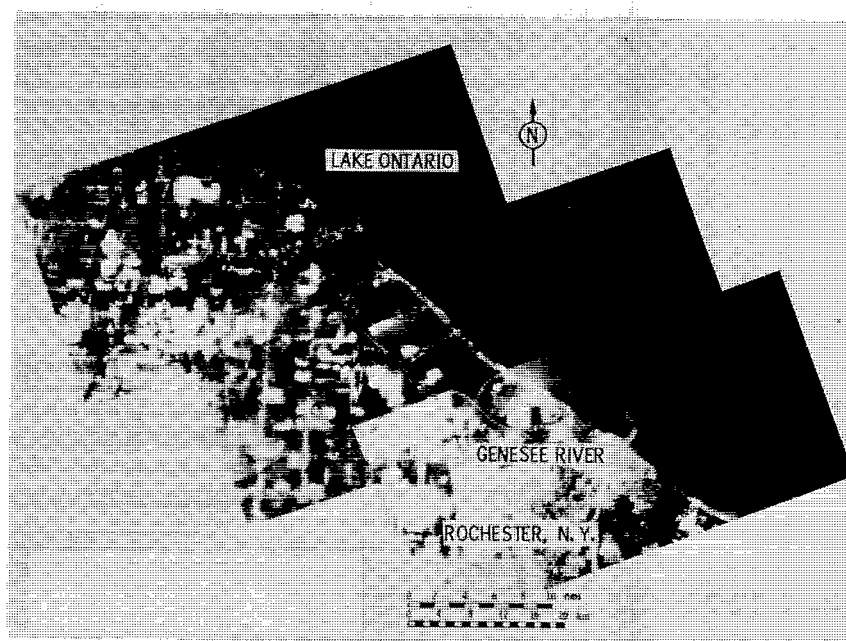


Figure 55. - Image of Genesee River-Lake Ontario, August 19, 1976. M^2S scanner channel 5.



Figure 56. - Image of Genesee River-Lake Ontario, August 19, 1976. M^2S scanner channel 5.

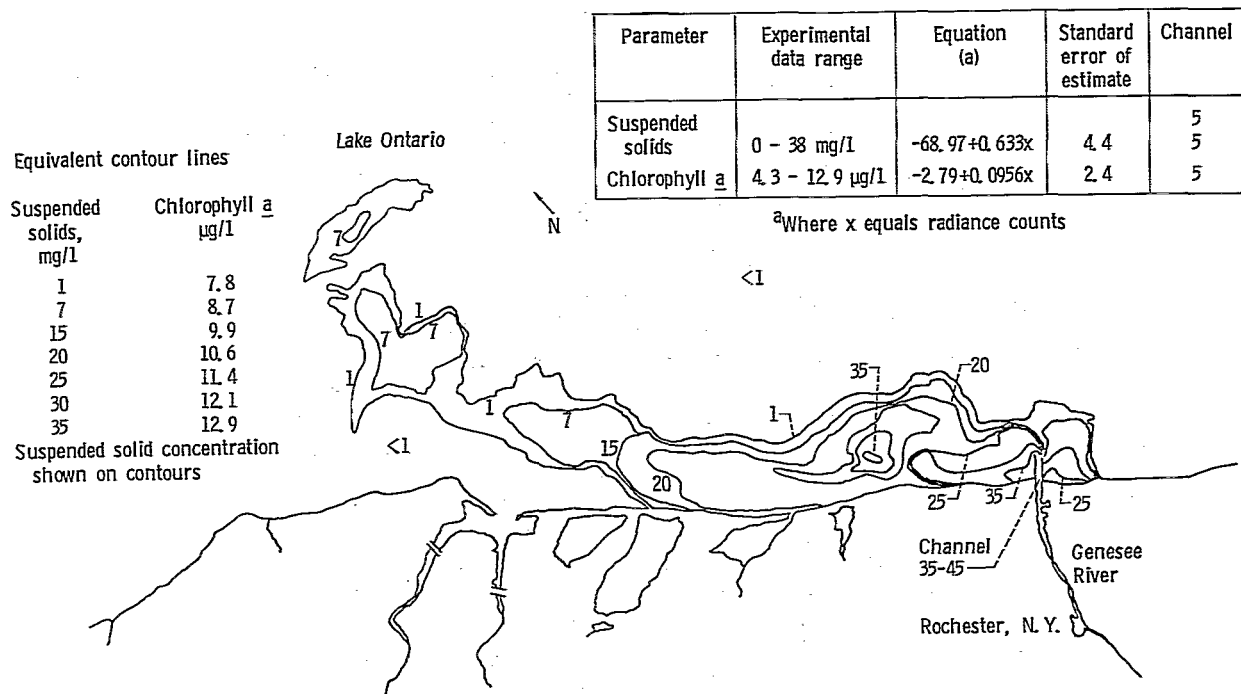


Figure 57. - Contour plot of suspended solids and chlorophyll a.

suspended-solids correlations precludes any indirect correlations for chemical parameters for which suspended solids might be a tracer.

Summary of Results

Remote sensing data are reported from six aircraft overflights over Lake Ontario near the Genesee River. Four of the flights were made during the spring period from March 22 to June 3, and two were made in August. Six Landsat images of the area during this period are also presented. The flights on August 3 and 19 coincided with ship surveys.

Based on a study of all of the imagery, wind induced resuspension and possibly shore erosion are seen to occur frequently and to produce a significant impact along the south shore of Lake Ontario. Runoff material from the Genesee River also produced a measurable suspended-solids input into Lake Ontario but did not appear to be as important as resuspension and shore erosion effects. Landsat imagery revealed that a significant particulate loading of the south shore area of Lake Ontario results from the outflow of the Niagara River and the Welland Canal. The eastern end of Lake Erie is the apparent source of this material.

Correlation analyses were performed on the data of August 3 and 19. A correlation of surface suspended-solids data with multispectral scanner data was obtained for the August 3 rain runoff event, and a suspended solids contour map based on this correlation was prepared. An indirect correlation of chlorophyll *a* distribution with the scanner data was also made. All reported suspended solids measurements on August 19 were uniformly low and precluded a correlation in the scanner data.

Menomonee River Results

The Menomonee River flows into Lake Michigan at Milwaukee, Wisconsin. There are two features of the Menomonee that are unique among the five rivers studied. Three rivers, the Menomonee, Milwaukee, and Kinnikinnic Rivers, merge at Milwaukee, and the effluent into Lake Michigan is the sum of these three. In the case of the other rivers in the study, a single dominant river exists. The volume flow of the Menomonee is the lowest of the five rivers studied. Also, a breakwall with three entrances is located 1.3 kilometers offshore and encloses the Milwaukee lakefront. This breakwall acts as a barrier, limiting plume dispersion. (The breakwall is shown in fig. 73.)

The ship surveys for runoff events began on February 13 and 25 for the snow melt and continued

on July 28, August 28, and September 9 for rain runoffs. No large snow melt runoff occurred. The snow and ice that did accumulate ran off in several low volume peaks (fig. 58). Rain runoffs in March were more significant. A background study, which included the effects of resuspension, was made on April 8. All ship survey work was conducted by the Wisconsin Department of Natural Resources (DNR).

High-altitude aircraft overflight data were obtained with the Lear Jet on February 23 and 25, March 19 and 22, and June 2 and 7. A lower altitude C-47 overflight was made on April 8. The two days on which coincident overflights and boat surveys were conducted were February 25 and April 8. The weather was clear on both days, and the scanner data from both days were analyzed in some detail.

History of Events

With the relatively low river outflow, compared with the other rivers, and the breakwall restricting plume expansion, aircraft coverage of runoff events could have been better achieved using the low-altitude C-47 aircraft. However, because of the logistics and flight time required to send the C-47 to Milwaukee from Cleveland it was decided to use the faster, high-altitude aircraft whenever possible. Furthermore, the Menomonee typically has a discharge peak of very short duration, lasting only a few hours. Thus even though the aircraft were on standby throughout the spring study period, advance notice was not sufficient to enable coverage of a peak discharge. This problem did not occur at the other river sites where at least 24 hours advance notice of a discharge peak was possible.

Actual aircraft coverage began in February and ended in June. Single-channel images for six high-altitude OCS overflights, one low-altitude C-47 overflight, and six selected Landsat overpasses are shown in figures 59 to 72. The images cover the period from February 23 until June 7. Two images for channel 4 (560 nm) of the M²S are shown for the C-47 overflight of April 8. Figure 69 is an enlarged view of figure 66 showing the harbor area and sampling site locations.

In all of the images there is evidence of suspended particulate near shore. The larger scale Landsat images show several instances where significant near-shore suspended particulate extended over a large portion of the west shore of Lake Michigan, both north and south of Milwaukee. It is not clear to what extent this should be ascribed to wind induced resuspension and to what extent shore erosion. (Hereinafter where reference is made to resuspension, it can be assumed to include possible shoreline erosion.) Estimates were made by counting of the

yearly contribution of shoreline erosion to sediment loadings into the Great Lakes (ref. 7). One of the major contributors in the Great Lakes was Ozaukee County which is just north of Milwaukee. Milwaukee and Racine Counties were estimated to contribute about half as much as Ozaukee County on a per mile of shoreline basis. However, Wind Point, which is just south of Milwaukee in Racine County, seems especially active, which may indicate that at Wind Point resuspension rather than shoreline erosion is dominant.

A study of table IX of the recorded wind data for each day indicates that the transport pattern of the suspended particulate is consistent with the wind direction, especially when the wind has been blowing in the same direction for the preceding few days. If the wind direction has been variable for the previous few days, such as occurred before the February 23 overflight, the suspended particulate exhibits no particular directional features. A consistently high wind speed seems to cause more activity offshore, but not necessarily near shore.

On some days resuspension is observed inside the breakwall. For example, it can be seen within the breakwall in the vicinity of the north entrance on March 22 (fig. 64) and near the south entrance on April 29 (fig. 69). It may also have been present on other days but the small size of the harbor area in the large-scale Landsat images sometimes makes it difficult to visually differentiate river runoff and resuspension in the harbor.

A number of rain runoff events occurred after the snow melt in February. The one that probably best illustrates the effect of the breakwall as a boundary for plume dispersion can be seen in the Landsat image of March 15 (fig. 62). This image was made two days after a relatively high rain runoff. No identifiable plume dispersion is noted beyond the breakwall. Four days later, on March 19, an OCS image still shows what appears to be residual suspended particulate within the breakwall and no observable dispersion beyond the wall (fig. 63).

In the Landsat image of April 2 (fig. 65), which followed another high rain runoff on March 27, the harbor again shows the effect of particulate loading. However, for the suspended particulate seen outside of the south end of the harbor, it is not possible to distinguish particulate due to runoff from that originating from near-shore resuspension. In general, when there is a high degree of resuspension in the vicinity of Milwaukee, it is difficult to identify the extent of plume dispersion beyond the breakwall solely from a visual interpretation of the OCS or Landsat images.

On days of low river discharge, a small plume that appears dark against the harbor water can frequently

be seen inside the breakwall on the OCS and Landsat images. Perhaps the best example is seen in the image of March 22 (fig. 64), in which the oval-shaped plume extends from the river mouth almost to the breakwall. The low radiance of the plume implies that either the water within the plume boundary is relatively low in particulates or there is a suspended or dissolved material in the plume which absorbs highly at the OCS channel 6 wavelength (632 nm).

In order to resolve this question, an analysis of coincident overflight and boat survey data was needed. There were two days on which a coincident overflight and boat survey were made. The first was on February 25, two days before a minor runoff peak. (The February snow melt resulted in a series of relatively small runoffs rather than one large one.) Measured suspended particulate concentrations on February 25 ranged from a high in the harbor area of 18 mg/l, to 6 mg/l measured in the lake 4.0 kilometers east of the harbor entrance. The suspended particulate consisted primarily of nonvolatile components. A high percentage of nonvolatiles indicates that the suspended particulate was mostly inorganic material. Since runoff from the land in the early spring is predominately composed of inorganic silt and clay minerals, this high nonvolatile percentage was expected.

The second coincident aircraft and ship survey was made on April 8. The purpose of these surveys was to obtain a set of data representing background conditions, that is, low river discharge conditions. This was achieved. At the same time, a condition of high resuspension was observed along the shore north of the breakwall.

Several water classes were observed on this day. A small river plume emerged out of the river mouth and formed a semicircular pattern extending about two-thirds of the way to the breakwall. While resuspension occurred along the near north shore, offshore the water was clean. This situation provided three classes of water for analysis at one time, plus possible variations inside the breakwall. The Wisconsin DNR sample analysis results show that the river plume is predominately organic and that the resuspended material is predominately inorganic. The low flow rate ($2.5 \text{ m}^2/\text{sec}$) resulted in a well defined plume that settled within the breakwall area. This may be contrasted to February 25 when the higher flow rate ($9 \text{ m}^3/\text{sec}$) resulted in a plume which filled the entire breakwall area.

Data Analysis and Discussion

On both days of coincident aircraft and ship surveys (February 25 and April 8) correlations were attempted between scanner data and ship survey

data. Sampling sites for both days were concentrated around Milwaukee within the breakwall area and included a station out in the lake along the transect going east through the center breakwall entrance. The correlation analyses were attempted for suspended solids and all other available chemical parameters. Chlorophyll levels were below detectable limits and thus no correlations involving chlorophyll were attempted.

For February 25 successful correlations of scanner data with suspended solids, total chlorides, total phosphorus, particulate phosphorous, $\text{NO}_2 + \text{NO}_3$ nitrogen, NH_3 nitrogen, total solids, and dissolved oxygen are reported. The analyses indicated that the relationships were linear over the range of the experimental data. Channel 8 (714 nm) correlated best with suspended solids, although channels 6 (632 nm) and 7 (674 nm) were also good.

Results for the other parameters indicated that both channels 7 and 8 correlated well with the ship data, with channel 7 being slightly better. The correlations with the chemical parameters are regarded as indirect correlations in the sense defined earlier in the report; that is, the correlations are possible because the suspended solids act as a tracer for the chemical parameters and correlate directly with them.

All correlation results are summarized in table X. Figure 73 is a suspended-solids contour map derived from the correlation of channel 8 with suspended solids. Table XI shows the equivalent contour line values for the other parameters. Since no samples were taken in the area of resuspension, the contours for the chemical parameters may not apply in the near-shore resuspension areas. However, they should apply in the offshore, open-lake water.

In analyzing the data of April 8 it became apparent that several different water classes existed in the study area. The water in the river and in the plume was predominantly organic and the other water in the harbor area was generally inorganic. The other water included areas of resuspension, nonplume water inside the breakwall (which may have included residual suspended particulate from the rain runoff on March 29), and background water in the lake.

The existence of the various water classes may have been the reason that the correlation analyses for the April 8 data were less successful than those for the February 25 data. The channel 7 data correlated well with all suspended-solids data except at one station at the river mouth, where the measured concentration appeared to be high. However, no correlations were found for any of the other measured parameters. The analyses indicated that the data corresponding to the three stations in the river and to the station directly out of the river mouth in the plume showed a dif-

ferent spectral character. Consequently, the correlation analyses were repeated, omitting the data from these four stations. This yielded correlations for suspended solids (channel 5 gave the best correlation) and for particulate phosphorus. These are reported in table X. The resulting suspended-solids contour map is presented in figure 74 with equivalent contour values for particulate phosphorous given in table XI. Since the plume data were omitted from the correlation, no suspended solids values could be calculated within the plume. The values of 5 to 8 mg/l in the plume appearing on figure 74 were based on the ship measurements.

The limited success in correlating the data of April 8 may have been due to the complication introduced by the presence of several water classes in the sampling grid. Whereas on February 25 the sampling grid was contained entirely within areas of snow melt runoff, the sampling stations of April 8 were in areas composed of at least three different classes of water. In addition, some points were sampled at locations of rapidly changing water conditions whereby small uncertainties in the boat locations could cause large errors in registering the corresponding scanner data. The lack of success in correlating properties other than suspended solids and particulate phosphorus does not necessarily imply that correlations do not exist.

Summary of Results

Remote sensing data are reported from seven aircraft overflights over Lake Michigan near the Milwaukee Harbor between February 23 and June 7, 1976. Six Landsat images of the area during the study period are also presented. Ship surveys conducted by the Wisconsin Department of Natural Resources included same-day water sampling during two of the overflights (February 25 and April 8).

Based on a study of all of the data, the combination of the Menomonee, Milwaukee, and Kinnikinnic Rivers does not appear to be a major source for loading of suspended material into Lake Michigan. Plumes from the common outlet of these rivers were observed within Milwaukee Harbor. However, the Milwaukee Harbor breakwall acts as an effective barrier, retaining much of the particulate discharged by the rivers. It is possible that during other years a much larger snow melt or rain runoff could generate sufficient flow for the river plume particulate to leave the breakwall area. Under these circumstances particulate along with dissolved pollutants could enter Lake Michigan.

The imagery revealed that wind induced resuspension and possible shore erosion have a major effect along the western shore of Lake Michigan in the

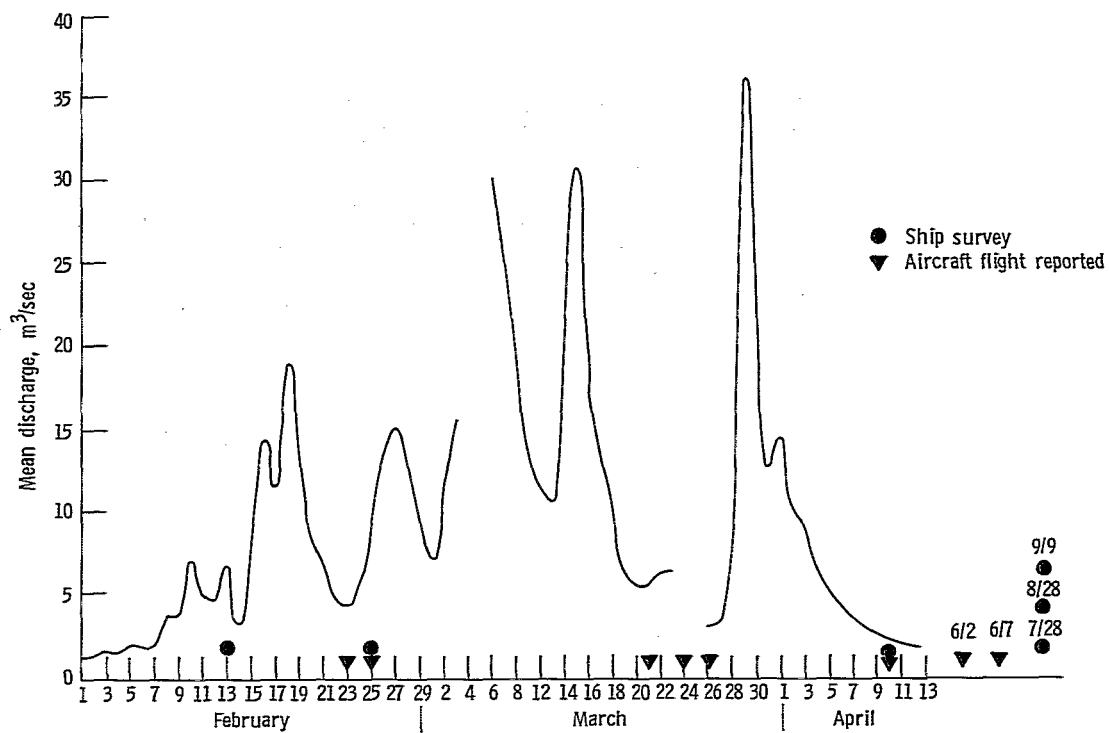


Figure 58. - Mean discharge of Menomonee River and summary of remote sensing and ship surveys.

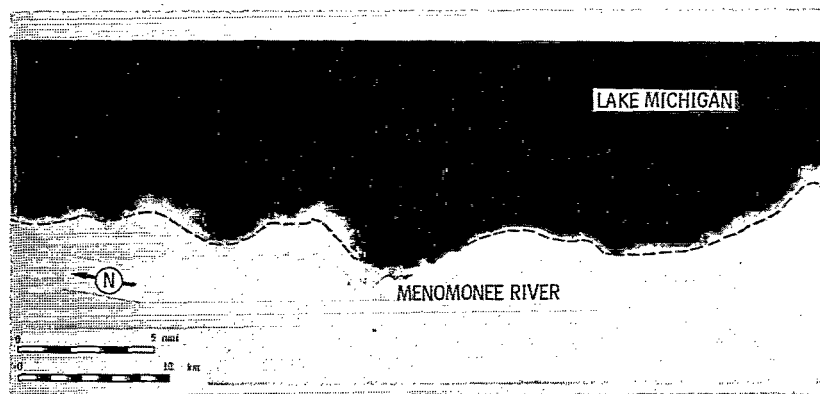


Figure 59. - Image of Menomonee River-Lake Michigan, February 23, 1976. OCS scanner channel 6.

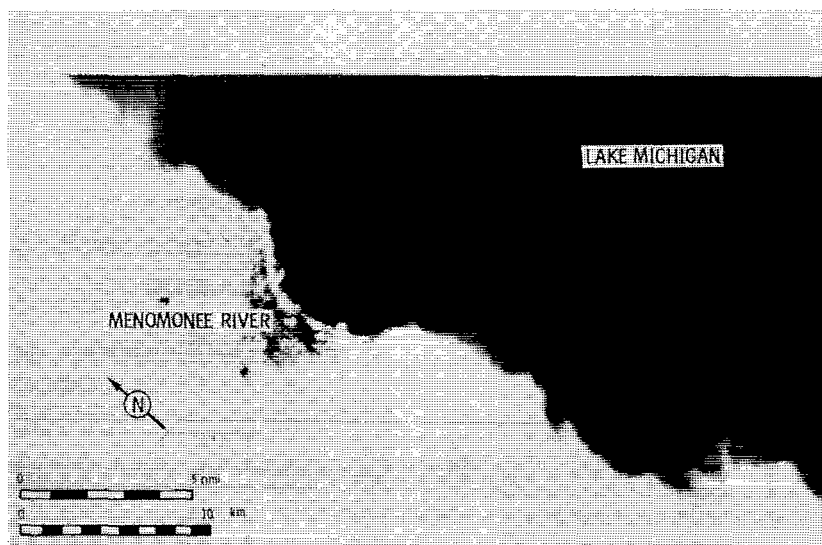


Figure 60. - Image of Menomonee River-Lake Michigan, February 25, 1976. OCS scanner channel 6.

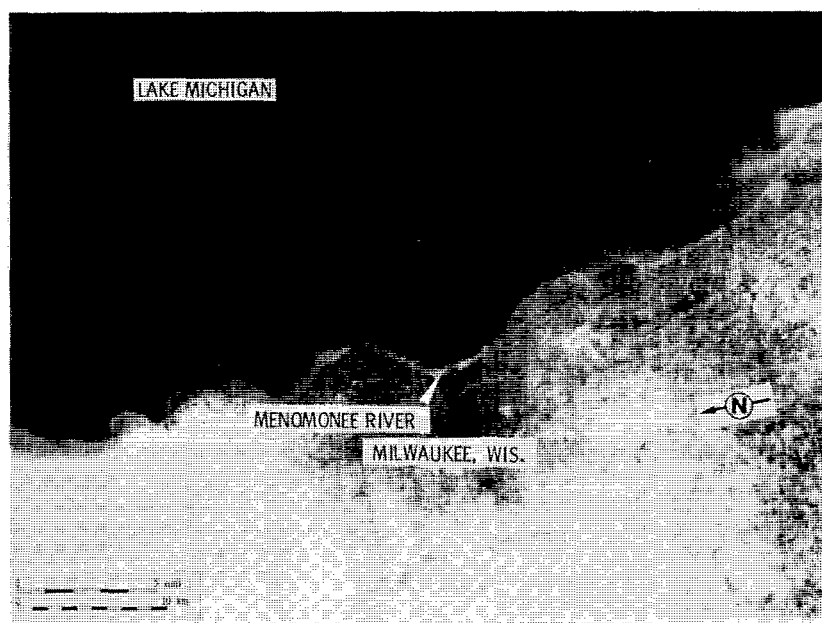


Figure 61. - Landsat image (band 5) of Menomonee River-Lake Michigan, February 26, 1976.

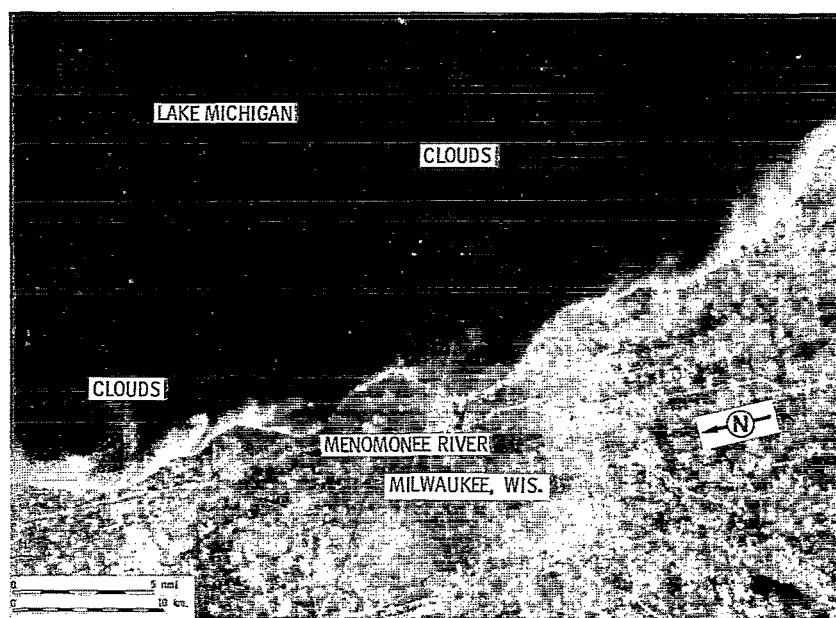


Figure 62 - Landsat image (band 5) of Menomonee River-Lake Michigan, March 15, 1976.

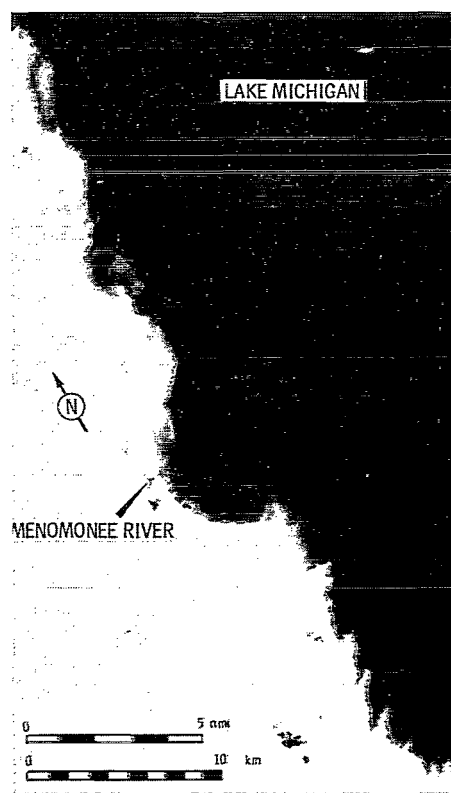


Figure 63. - Image of Menomonee River-Lake Michigan, March 19, 1976. OCS scanner channel 6.

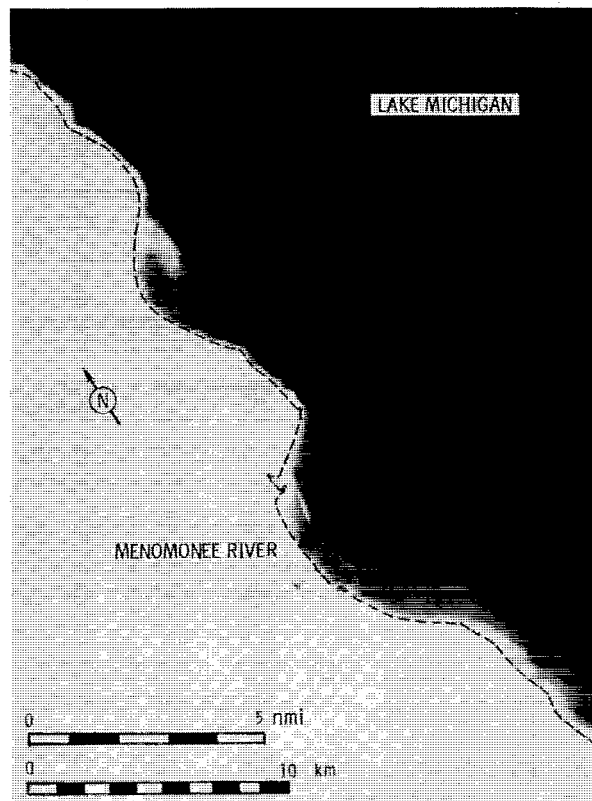


Figure 64. - Image of Menomonee River-Lake Michigan, March 22, 1976. OCS scanner channel 6.

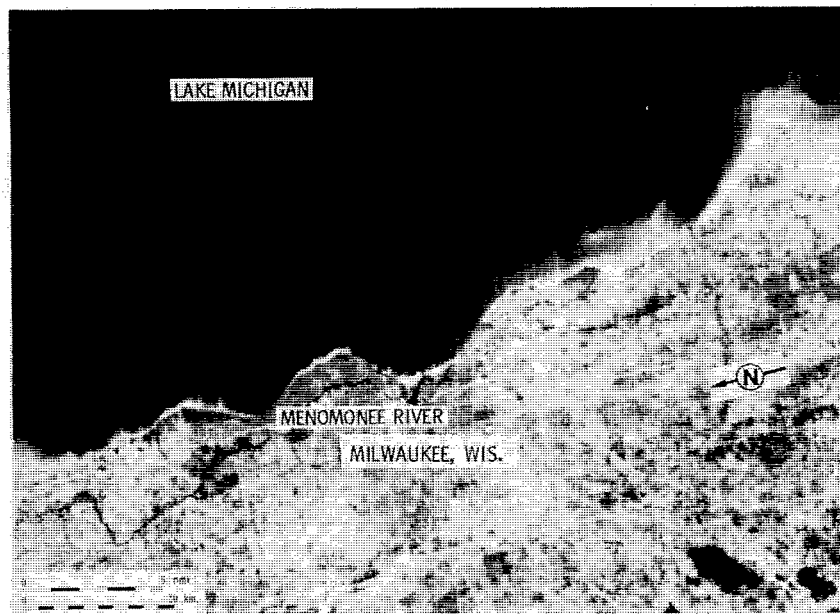


Figure 65. - Landsat image (band 5) of Menomonee River-Lake Michigan, April 2, 1976.

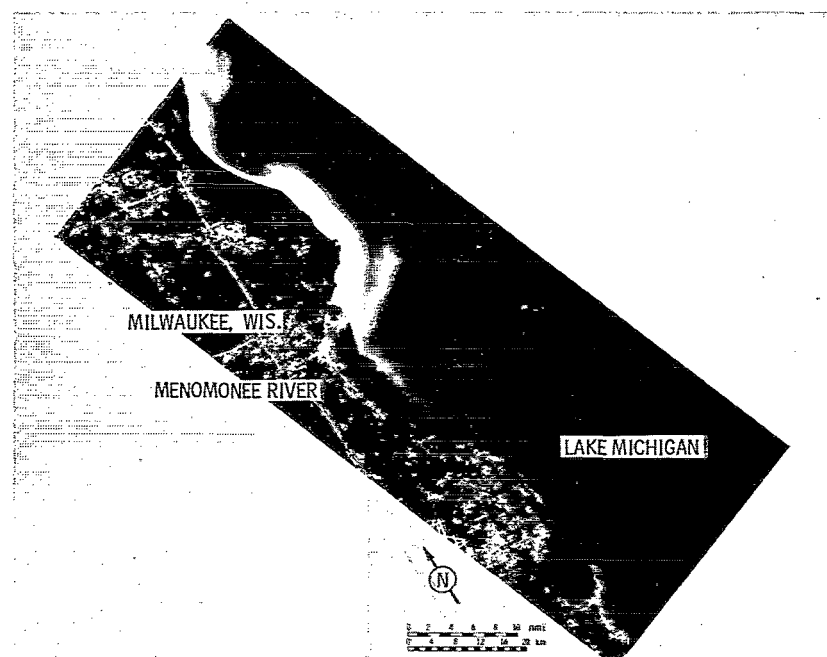


Figure 66. - Image of Menomonee River-Lake Michigan, April 8, 1976. M²S scanner channel 4.

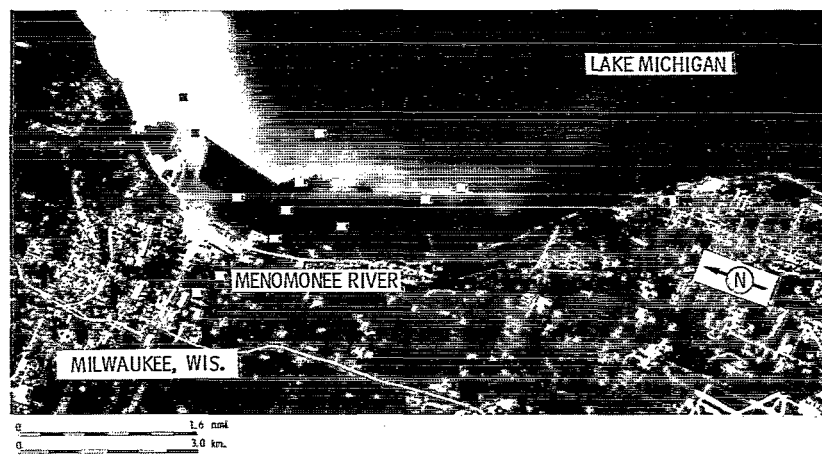


Figure 67. - Image of Menomonee River-Lake Michigan, April 8, 1976. M²S scanner channel 4.

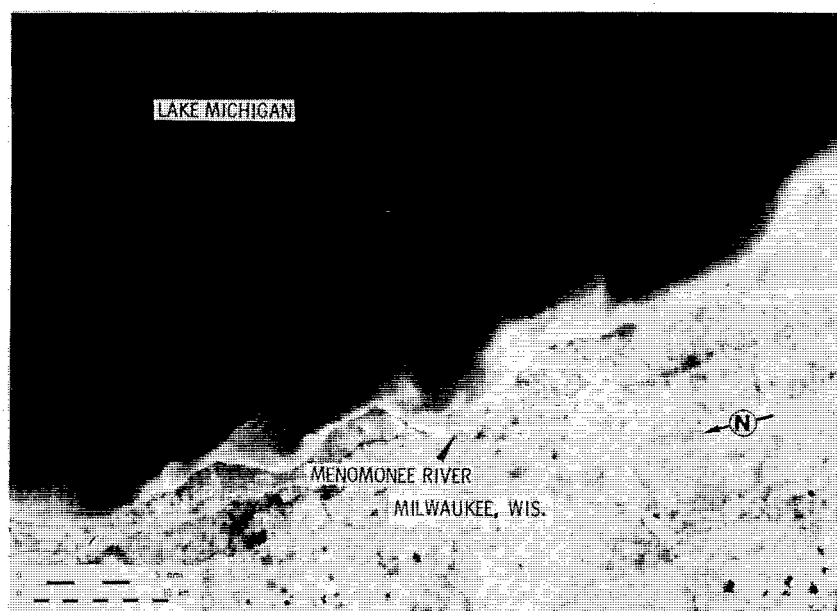


Figure 68. - Landsat image (band 5) of Menomonee River-Lake Michigan, April 28, 1976.

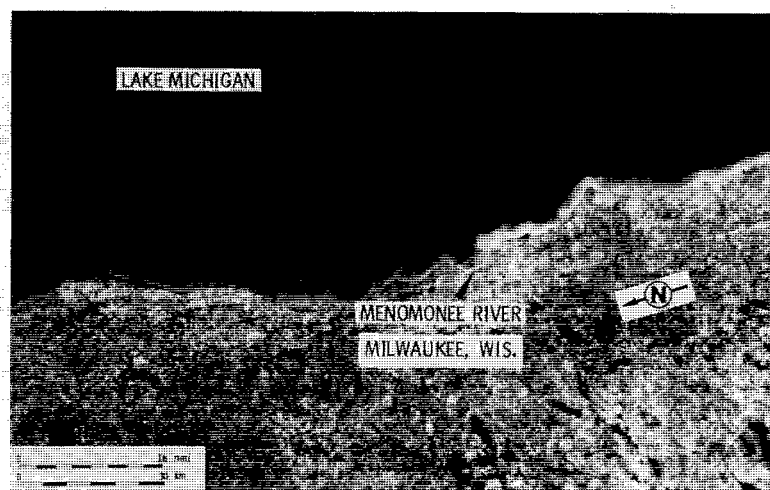


Figure 69. - Landsat image (band 5) of Menomonee River-Lake Michigan, April 29, 1976.



Figure 70. - Landsat image (band 5) of Menomonee River-Lake Michigan, May 8, 1976.

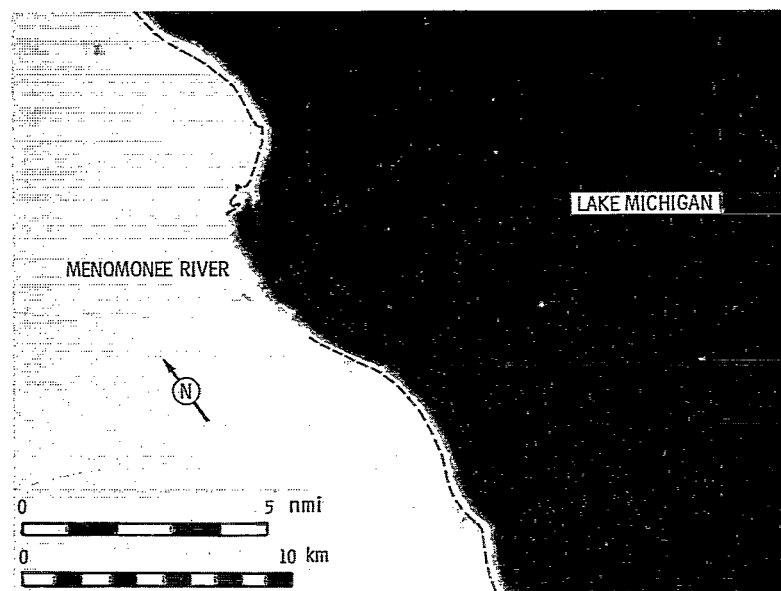


Figure 71. - Image of Menomonee River-Lake Michigan, June 2, 1976. OCS scanner channel 6.

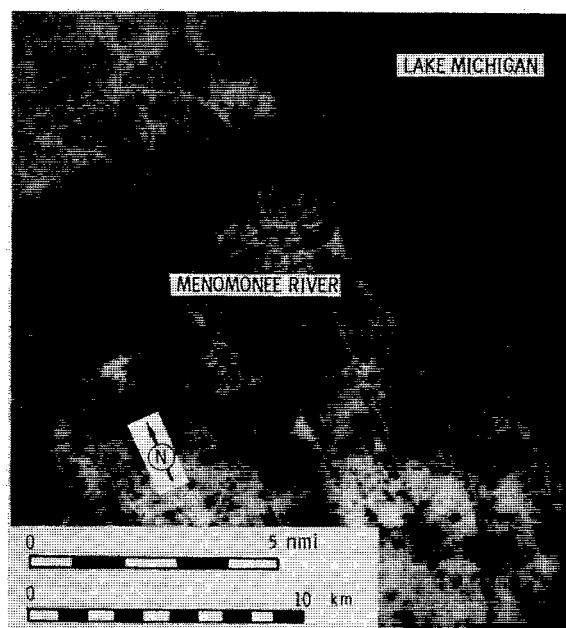


Figure 72. - Image of Menomonee River-Lake Michigan, June 7, 1976. OCS scanner channel 6.

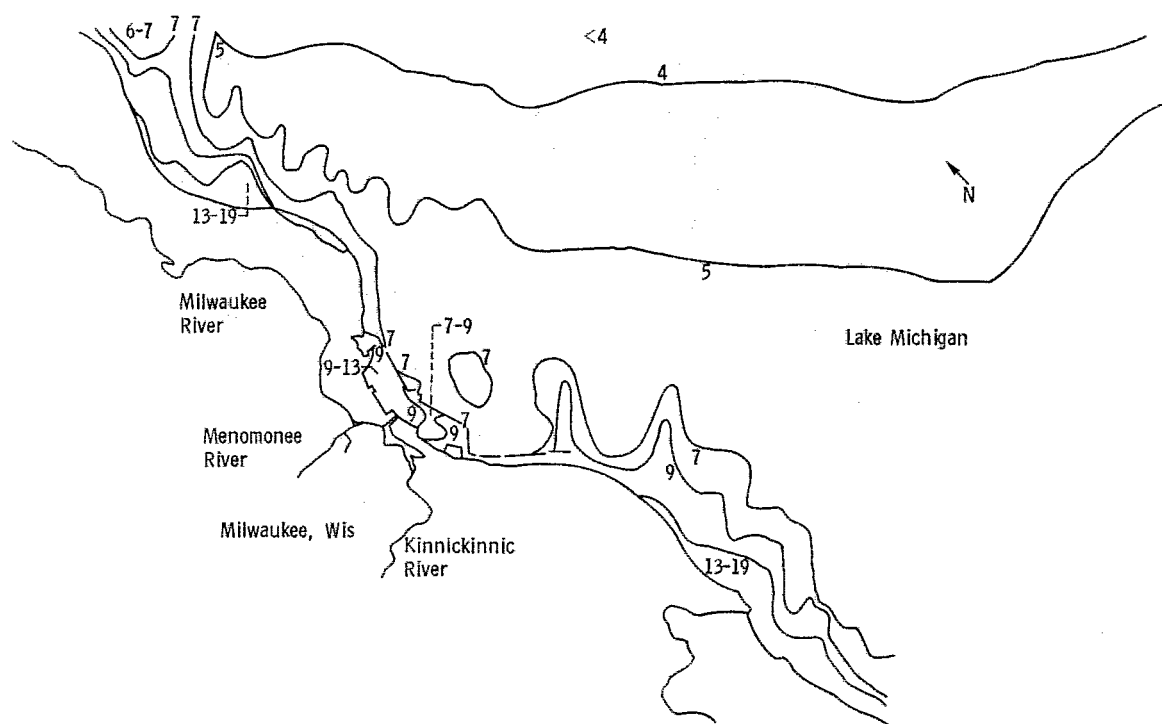


Figure 73. - Contour plot of suspended solids (mg/l). See tables X and XI for chemical parameters.

vicinity of Milwaukee. In all images until June suspended particulate was observed both north and south of Milwaukee and was especially heavy at certain locations such as Wind Point. The large-scale satellite images, in particular, reveal instances of widespread near-shore suspended material along the west shore. In general, it does not appear possible to make a distinction between resuspension and shore erosion from imagery alone.

Correlations between remote-sensing data and measured suspended-solids and particulate-phosphorous values were obtained for the two days of simultaneous aircraft overflight and ship survey (February 25 and April 8). Based on these correlations, suspended solids contour maps were generated for the two days. On April 8 the correlation applied only to the region outside of the harbor plume. Correlations for total chloride, total phosphorus, $\text{NO}_2 + \text{NO}_3$ nitrogen, NH_3 nitrogen, total solids, and dissolved oxygen were obtained for the February 25 data but not for the data of April 8. The chemical parameter correlations are indirect correlations; that is, the correlations are possible because the suspended solids act as a tracer for the chemical parameters and correlate directly with them. The lack of additional correlations on April 8 probably was due to the existence of several different water classes in the harbor area that were not identified.

Grand River Results

This section describes the results of the remote-sensing flights over Lake Michigan in the vicinity of the Grand River. All flights were made at 12.5 kilometers (41 000 ft) using the ocean color scanner (OCS), which has a field of view of 24.5 kilometers at this altitude. Although the Grand River sediment plume generally covered an area of less than 10 square kilometers, the scanner data revealed that the region of possible river impact extends as far as 50 kilometers from the river mouth.

Nine overflights of the Grand River area were made. The first flight was made on February 23, with ice still present along the eastern shore of the lake, and the last flight occurred on April 2. Multichannel OCS imagery made from data taken on these flights will be presented. Computer-drawn contour plots of suspended sediment in the surface water are presented; the plots are based on correlations of the scanner data with in-the-water data recorded by the Great Lakes Environmental Research Laboratory (GLERL) ship survey team. Radiance spectral curves are included to aid in determining the origin of the high radiance areas observed in the imagery.

Four cloud-free Landsat images are included for formulating sediment distribution patterns in the

vicinity of the Grand River and to determine the origin of the extensive areas of turbid water observed.

Another objective of the remote sensing flights was to aid the ship survey team in choosing sampling stations. A general observation was that the plume direction changed so rapidly that near real-time imagery must be received by the boat rather than 12-to 24-hour old imagery provided.

Of importance in discussing the remote-sensing data are the Grand River flow data and the wind data. (These are shown in fig. 75 and table XII; fig. 75 also shows the dates on which the aircraft and ship surveys were made.) The wind speeds and directions shown in table XII were measured at Muskegon, Michigan, about 15 miles north of the river. The wind data indicated persistent onshore winds during the study arising equally from the northwest and the southwest.

History of Events

A Landsat image for February 7 (fig. 76) shows shore ice extending 5 to 8 kilometers offshore near the Grand River. There is no indication of sediment in the water beyond the ice. The river discharge was the lowest occurring at any time during the study ($110 \text{ m}^3/\text{sec}$).

The first aircraft overflight of the area for which cloud-free multispectral scanner data were obtained occurred on February 23. At this time the river discharge, had reached the first peak flow of $540 \text{ m}^3/\text{sec}$. In the scanner image of the area (fig. 77) the plume from the Grand River covers an area of about 10 square kilometer and is turned to shore by the southwest winds. The northern part of the plume spreads out and turn towards the south, possibly due to the littoral current which runs from north to south in this part of Lake Michigan (ref. 7). Detailed spectral analysis of the data is precluded by the presence of the floating ice. The area of extremely high radiance at the river mouth, for instance, could be caused, in part, by floating ice.

Two days later on February 25 the area was again overflown. Figure 78 shows that the shore ice persists and no sediment plume appears. The predominately onshore winds during this period have moved the ice into a band along the shore extending approximately 1.5 kilometers into the lake so that the river sediment discharge occurs under the ice. The surface water sampling results for this date indicated that the river was discharging suspended solids at concentrations of 27 to 30 mg/l. (But mean discharge of river doubled by March 10.)

Scanner data for the overflight on March 11 is shown in figure 79. A large sediment plume is observed south of the river with no indication of turbid

water north of the river. A smaller plume approximately 10 miles south of the Grand River emanates from Pigeon Creek. As indicated in figure 75, the Grand River discharge rate was still very high at 620 m³/sec, with the spring maximum runoff level occurring three days earlier. The plume in figure 79 is the largest observed during the study. The plume direction relative to the wind is unusual in that the plume extends to the south while the wind is out of the southeast. Wind velocities were low, however, and the littoral current is in the direction of the plume. The northwest wind on the preceding day would also have imparted a southerly momentum to the plume.

On March 15 an overflight of the area was made, and the resulting imagery is shown in figure 80. Although there is some cloud interference, the sediment plume appears similar to the March 11 plume, but smaller. The river flow is less on this date and the wind is from the northwest at 3.4 m/sec.

Data for the March 19 flight are shown in figure 81. The winds were from the southwest at 8.5 m/sec, and significant suspended sediment is present south of the river plume. The question of whether this sediment comes from shore erosion or is resuspended material from earlier river discharges will be discussed later. Extensive surface sampling was performed on this date and these data were compared with the radiance data. The suspended solids concentration in the river was 12 mg/l compared with 27 mg/l measured on the previous dates.

Three consecutive overflights were made on March 22, 23, and 24. Landsat images are also presented for March 22 and 23. The images are shown in figures 82 to 86. During this three-day period the river discharge was essentially constant at 280 m³/sec. The winds were variable in magnitude but generally out of the southwest. There was extensive ship sampling on March 23. The suspended solids concentration in the river was 18 to 20 mg/l. The imagery for March 22 and 23 again shows significant suspended particulate south of the Grand River. The plume contrast is not as good in the Landsat images, primarily because Landsat gains and offsets are optimized for land rather than water data. The digital scanner data from the March 23 overflight will be analyzed in greater detail to show the sediment distributions quantitatively.

It is interesting to note the shift in plume direction indicated by the imagery of March 22 and 23. The variable water currents during the shifting of the plume must be taken into account when collecting and analyzing ship data. Information from the March 22 flight showing the southern direction of the plume was transmitted to GLERL early on the 23rd. However, this information was already outdated, since a wind change had shifted the plume to the

north. This points out the need to provide remote sensing data to survey ships in near real time.

Figure 87 is an image made from data obtained on April 2 on the last overflight of the study period. Suspended sediment is again evident south of the river. In addition, surface sampling on this date revealed chlorophyll concentrations as high as 30 mg/m³, representative of bloom conditions. The sediment concentration on April 2 was 27 mg/l, which is the same level as measured during peak flow conditions, although the river flow remained essentially constant from March 19 when the sediment concentration was 12 mg/l.

Figure 88 presents a Landsat image for April 28. The image clearly shows the Grand River plume south of the river and an indication of slightly turbid water along the entire shoreline and out into the lake about 12 kilometers. A significant area of shore erosion at the outlet of Muskegon Lake is also apparent.

Data Analysis and Discussion

Much of the imagery of the Grand River area of Lake Michigan indicates the existence of extensive areas of suspended sediment. On certain days such as March 11 (fig. 79) on which wind conditions were calm, it appears that the suspended particulate is due primarily to the Grand River inflow. However, on windy days such as March 19 (fig. 81), it appears that resuspension of bottom material or shore erosion may be contributing to the suspended particulate.

In order to determine if there is a difference in the sediments in the plume and in the large areas off shore, the radiance spectra shown in figure 89 for scanner data recorded on March 19 were examined. If the particulate types differ, the shapes of the spectra should also differ. (Here shape refers to spectral variations and not the expected intensity shifts due to concentration differences.) The similarity between the spectra for the resuspension area south of the river and the river plume indicates that the material in the water could be the same.

Spectra are also presented for the other two days on which concurrent aircraft and ship data were collected. In figure 90 spectra are shown for areas inside the March 23 plume boundaries. Included in figure 90 is a spectra for the apparently cleaner water 15 miles offshore from Muskegon for which no ship data are available. Again, no significant differences in shape are noted. The spectra for four areas in the Grand River plume of April 2 are plotted in figure 91. These spectra are markedly different in shape from those presented in the previous two figures. It is believed that the differences are due to the high photoplankton concentrations present on April 2, which were not present on March 19 or 23.

Suspended sediment is again evident south of the river. In addition, surface sampling on this date revealed chlorophyll concentrations as high as 30 mg/m³, representative of bloom conditions. The sediment concentration on April 2 was 27 mg/l, which is the same level as measured during peak flow conditions, although the river flow remained essentially constant from March 19 when the sediment concentration was 12 mg/l.

Figure 88 presents a Landsat image for April 28. The image clearly shows the Grand River plume south of the river and an indication of slightly turbid water along the entire shoreline and out into the lake about 12 kilometers. A significant area of shore erosion at the outlet of Muskegon Lake is also apparent.

Data Analysis and Discussion

Much of the imagery of the Grand River area of Lake Michigan indicates the existence of extensive areas of suspended sediment. On certain days such as March 11 (fig. 79) on which wind conditions were calm, it appears that the suspended particulate is due primarily to the Grand River inflow. However, on windy days such as March 19 (fig. 81), it appears that resuspension of bottom material or shore erosion may be contributing to the suspended particulate.

In order to determine if there is a difference in the sediments in the plume and in the large areas off shore, the radiance spectra shown in figure 89 for scanner data recorded on March 19 were examined. If the particulate types differ, the shapes of the spectra should also differ. (Here shape refers to spectral variations and not the expected intensity shifts due to concentration differences.) The similarity between the spectra for the resuspension area south of the river and the river plume indicates that the material in the water could be the same.

Spectra are also presented for the other two days on which concurrent aircraft and ship data were collected. In figure 90 spectra are shown for areas inside the March 23 plume boundaries. Included in figure 90 is a spectra for the apparently cleaner water 15 miles offshore from Muskegon for which no ship data are available. Again, no significant differences in shape are noted. The spectra for four areas in the Grand River plume of April 2 are plotted in figure 91. These spectra are markedly different in shape from those presented in the previous two figures. It is believed that the differences are due to the high photoplankton concentrations present on April 2, which were not present on March 19 or 23.

The origin of much of the suspended material seen in the imagery of the lake water off Muskegon and Ottawa Counties is not certain. Large quantities of material are eroded into the lake along these shores;

however, the shore is mostly sand (ref. 7). Since most sand has a large grain size, it does not remain suspended in lake waters for very long (ref. 9). Therefore, shore erosion is probably not a major source of the observed suspended material. Large quantities of suspended sediment are transported into the lake by the Grand River. The prevailing littoral current would deposit more of this river sediment south of the river. This is consistent with the observed resuspension being predominantly south of the river. A fraction of the shore material is undoubtedly silts and clay contributed by shore erosion, but the Grand River contributes most of the material, which accumulates and ultimately contributes to the observed resuspension.

Figure 92 shows the assigned linear correlations between the radiance of OCS channel 8 (714 nm) and suspended sediment concentration for March 19 and 23 and April 2. The data from March 23 and April 2 fall on the same line, whereas the data of March 19 exhibit a different linear relationship most likely due to observed atmospheric haze effects. The correlations were constrained to be linear because the small number of data points did not justify the use of the nonlinear relationship expected on the basis of modeling studies of the scattering of light by particulate distributions (ref. 10). The small number of points is not due to any lack of sampling but rather to the large number of sampling sites located on or near the plume boundary. Some ship data were not included in the correlation analyses because of uncertainties in determining the boat's location relative to the plume boundary.

The correlations of figure 92 were used to produce the suspended solids contour maps for March 19 and 23 and April 2 shown in figures 93 to 95. The contour lines are generally parallel to the shoreline except for the effects of the Grand River and Pigeon Creek that influence the contours to a distance of about 5 kilometers offshore. Beyond 13 kilometers offshore the water appears uniform, and the suspended solids concentrations drop below 1 mg/l.

Figures 96 and 97 present plots of eight water quality parameters as functions of suspended solids concentrations. These data were measured by GLERL on the three dates for which both remote sensing and ship data were recorded. To the extent that a correlation exists between suspended solids and any of the parameters on a given date, the suspended solids contour plots for that date also serves as a contour plot of the parameter. For some parameters, a single correlation appears to serve for each of the three days (e.g., Ca and Mg in figs. 96(a) and (b)), whereas for other parameters different correlations are required for different days (e.g., chlorophyll in fig. 96(d)).

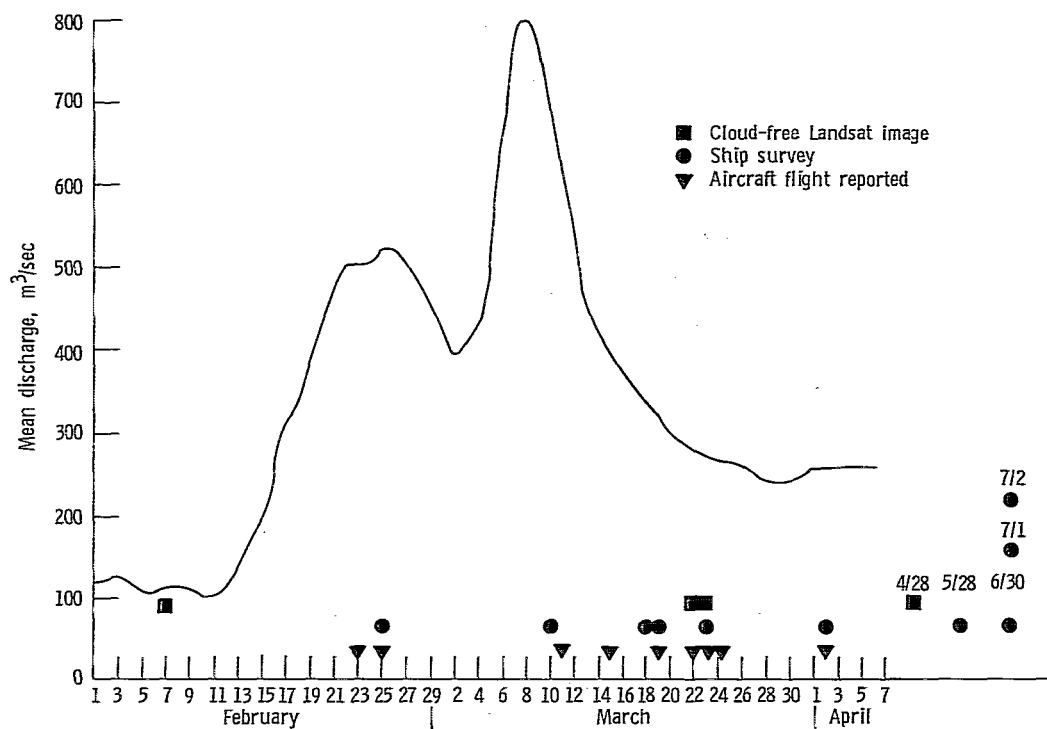


Figure 75. - Mean discharge of Grand River and summary of remote-sensing and ship surveys.

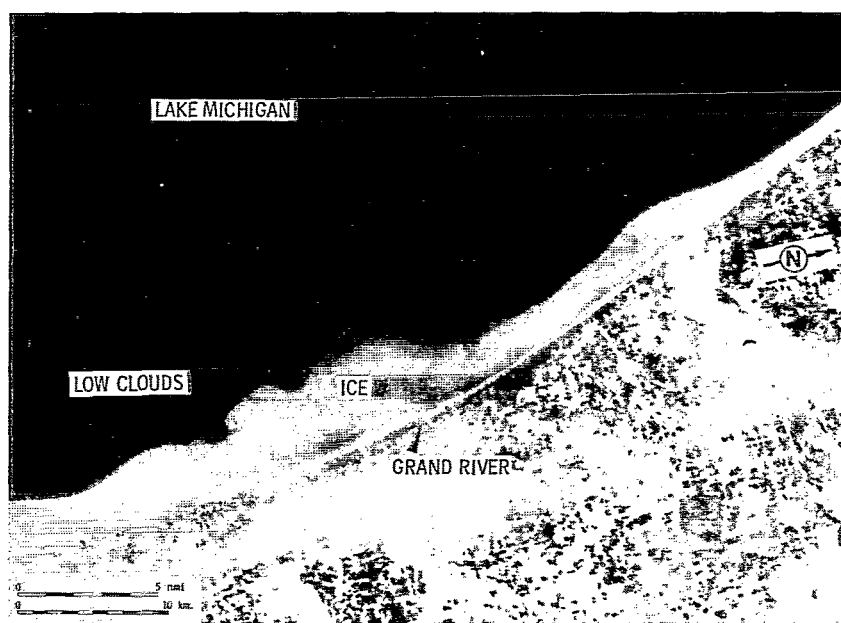


Figure 76. - Landsat image (band 5) of Grand River-Lake Michigan, February 7, 1976.

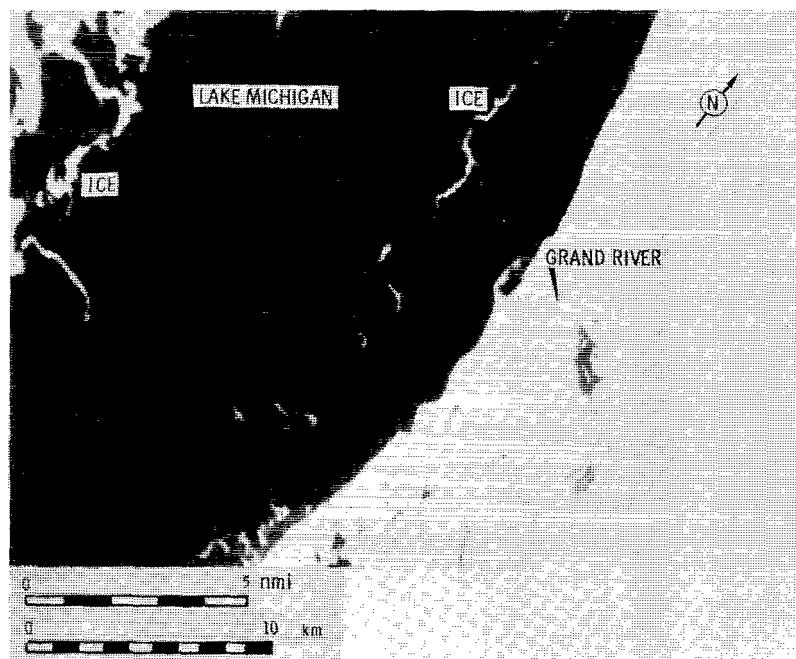


Figure 77. - Image of Grand River-Lake Michigan, February 23, 1976. OCS scanner channel 6.

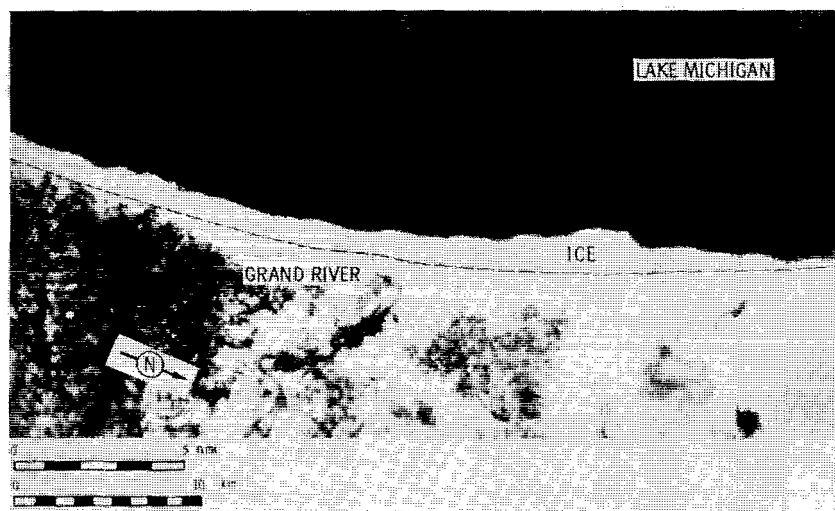


Figure 78. - Image of Grand River-Lake Michigan, February 25, 1976. OCS scanner channel 6.

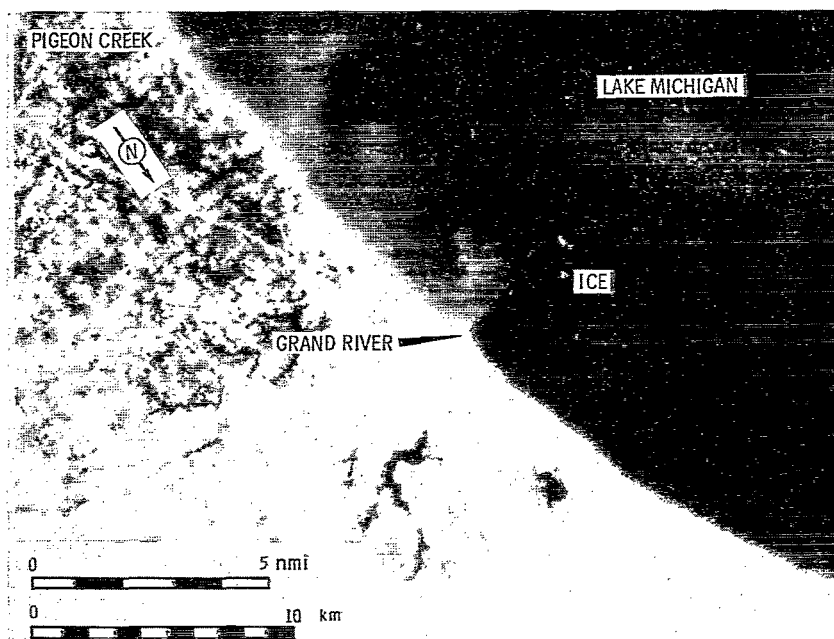


Figure 79. - Image of Grand River-Lake Michigan, March 11, 1976. OCS scanner channel 6.

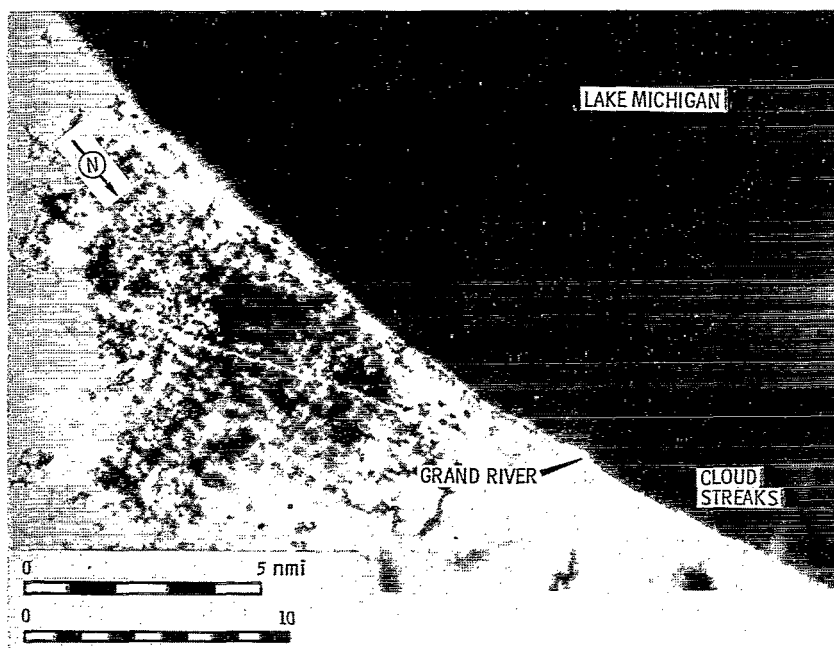


Figure 80. - Image of Grand River-Lake Michigan, March 15, 1976. OCS scanner channel 6.

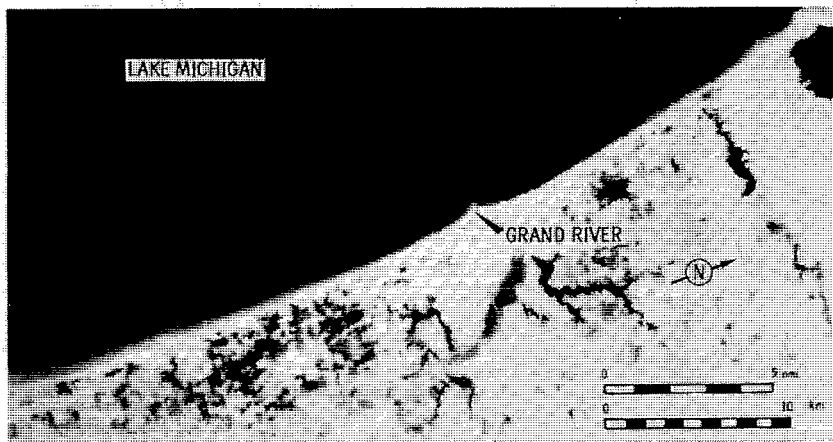


Figure 81. - Image of Grand River-Lake Michigan, March 19, 1976. OCS scanner channel 6.

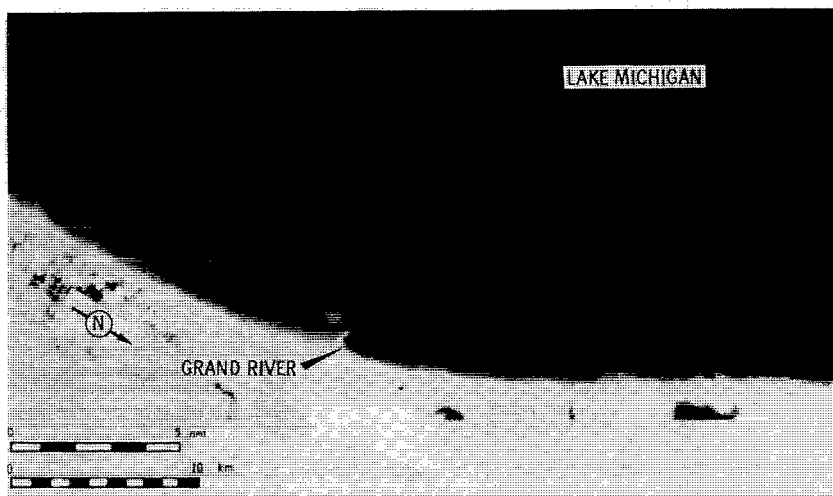


Figure 82. - Image of Grand River-Lake Michigan, March 22, 1976. OCS scanner channel 6.

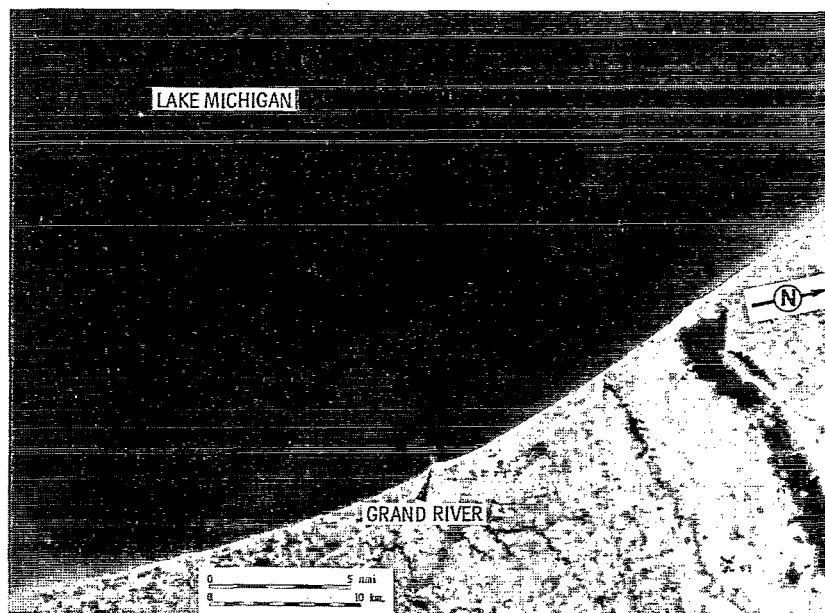


Figure 83. - Landsat image (band 5) of Grand River-Lake Michigan, March 22, 1976.

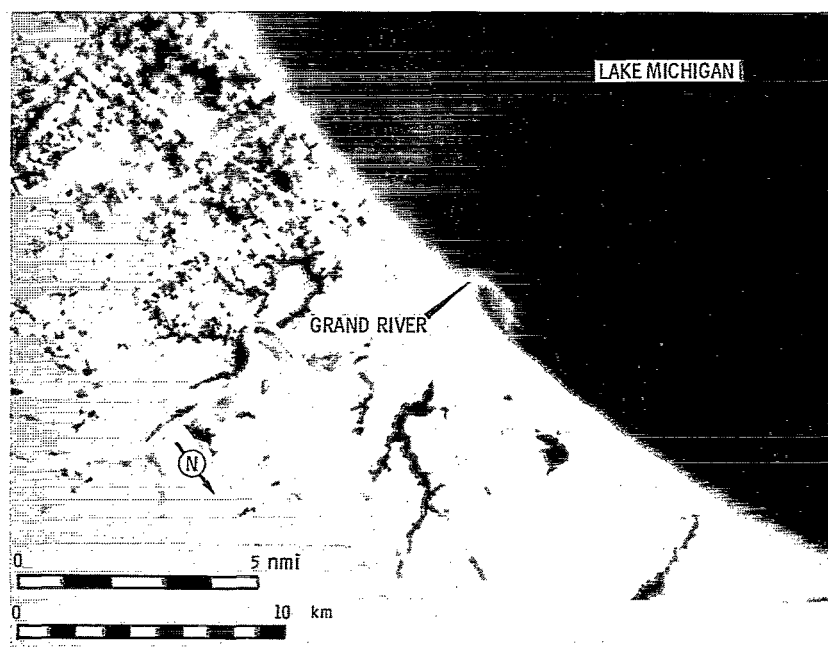


Figure 84. - Image of Grand River-Lake Michigan, March 23, 1976. OCS scanner channel 6.



Figure 85. - Landsat image (band 5) of Grand River-Lake Michigan, March 23, 1976.

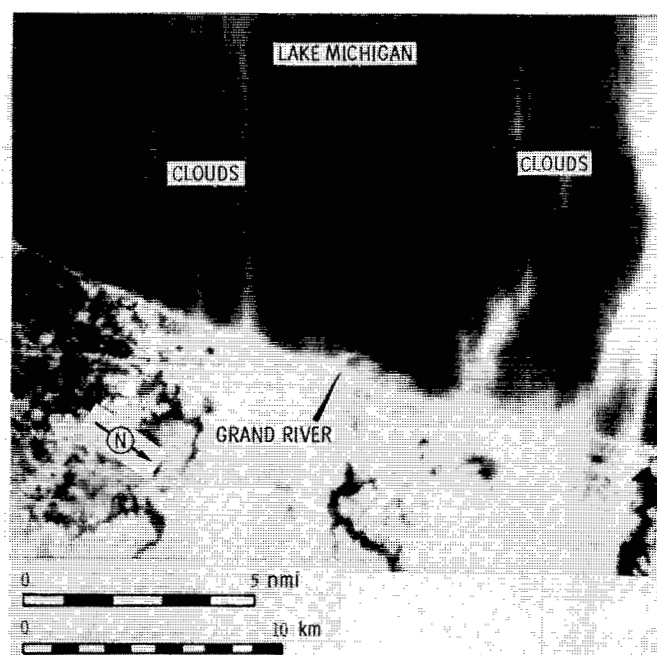


Figure 86. - Image of Grand River-Lake Michigan, March 24, 1976. OCS scanner channel 6.

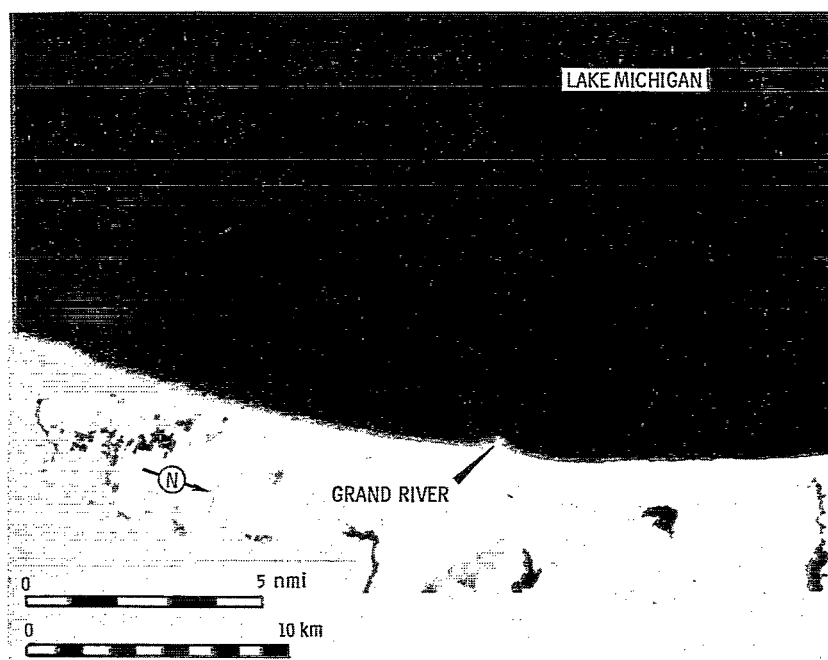


Figure 87. - Image of Grand River-Lake Michigan, April 2, 1976. OCS scanner channel 6.

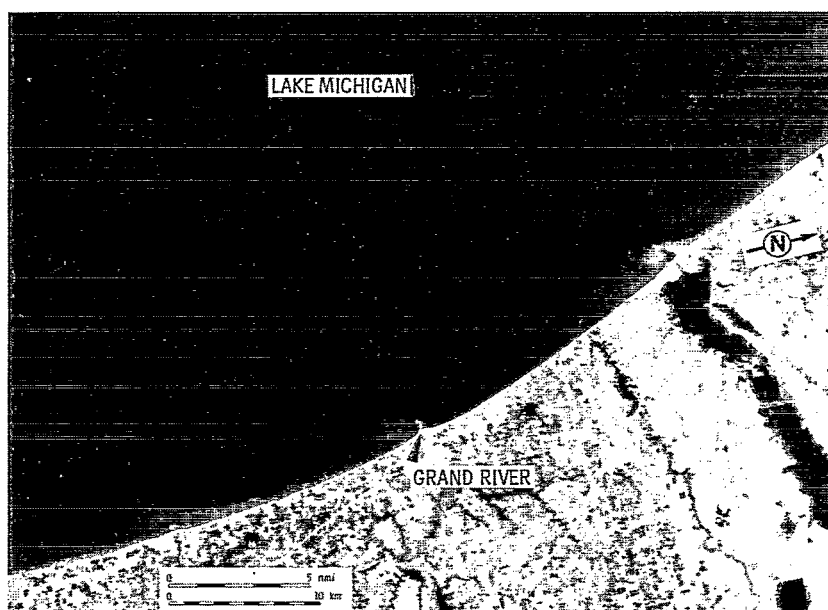


Figure 88. - Landsat image (band 5) of Grand River-Lake Michigan, April 28, 1976.

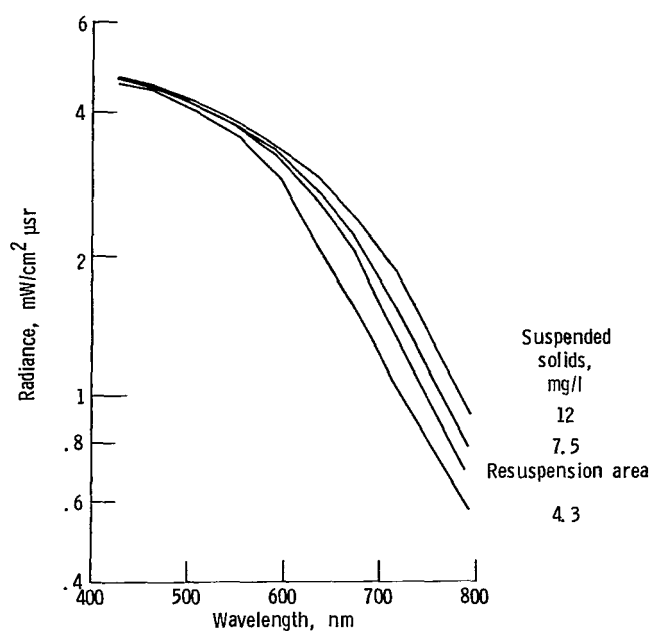


Figure 89. - Spectra from March 19 Grand River plume having low phytoplankton concentration.

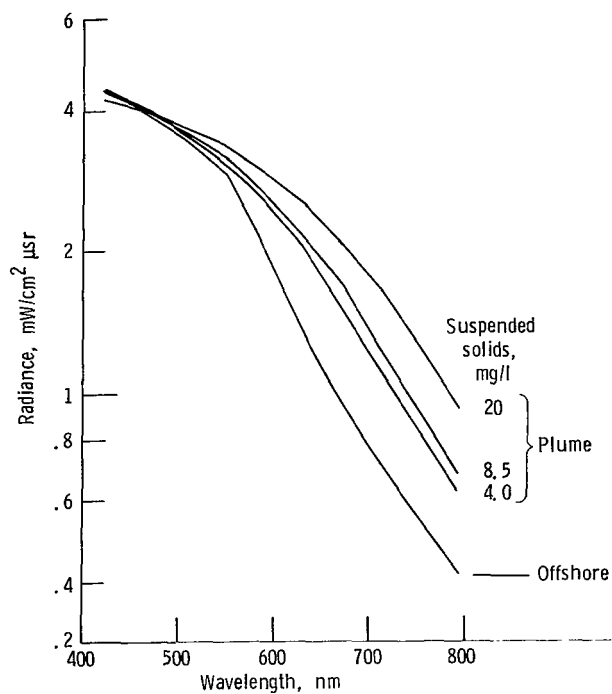


Figure 90. - Spectra from March 23 Grand River plume having low phytoplankton concentration.

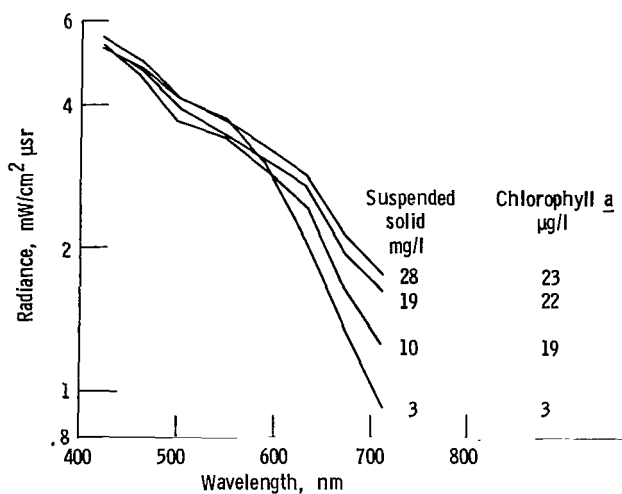


Figure 91 - Spectra from April 2 Grand River plume showing effects of high phytoplankton concentration.

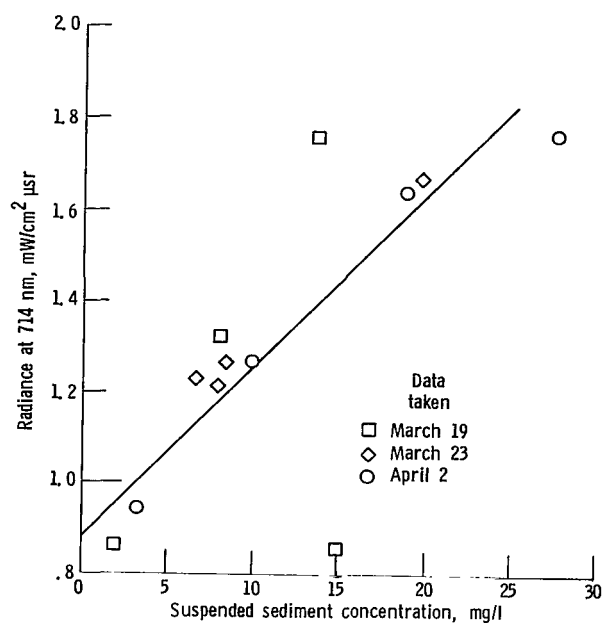


Figure 92. - Correlation of measured radiance at 714 nm with total suspended solids.

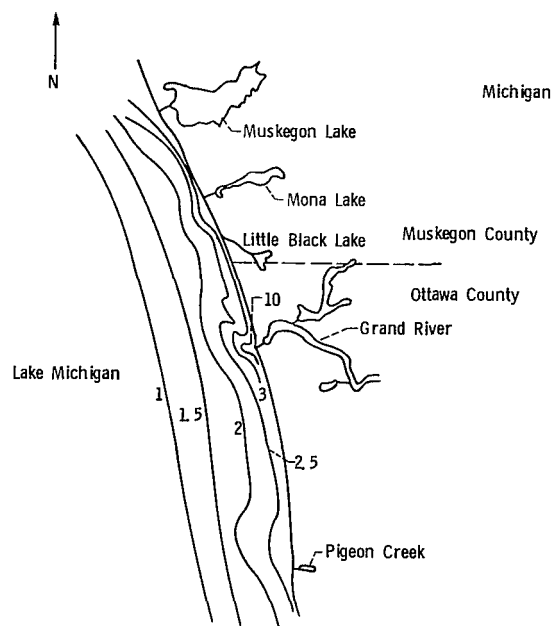


Figure 93. - Contour plot of total suspended-solids concentration (in mg/l) for March 19, 1976.

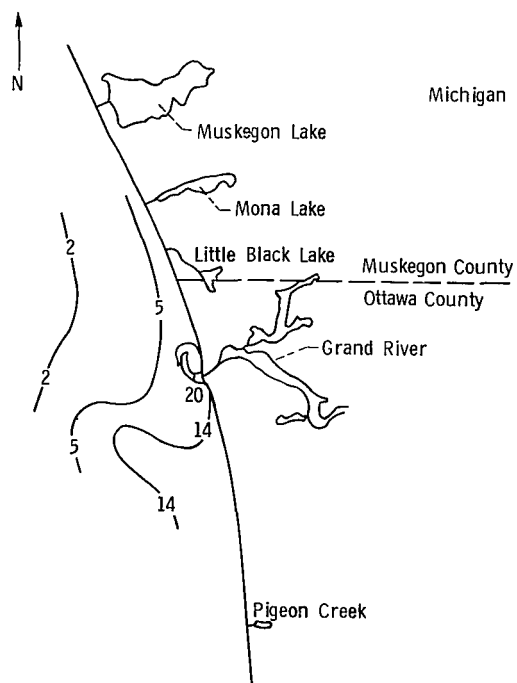


Figure 94. - Contour plot of total suspended-solids concentration (in mg/l) for March 23.

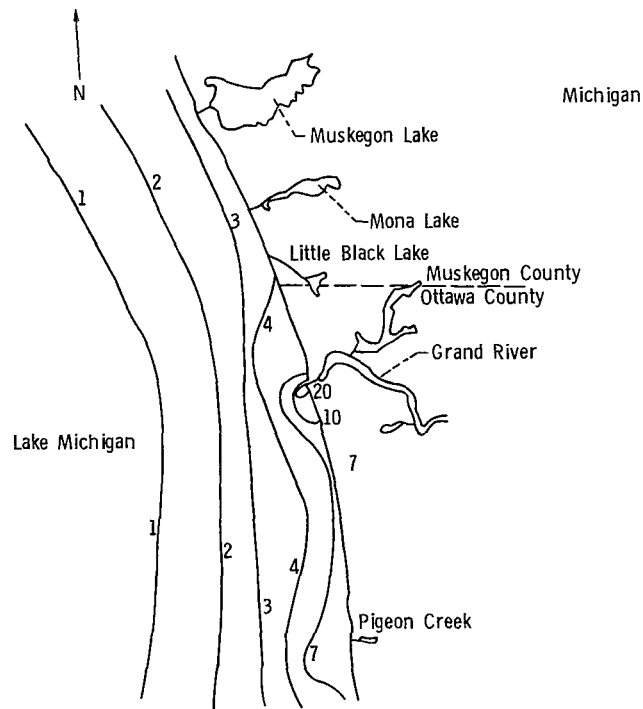


Figure 95. - Contour plot of total suspended-solids concentration (in mg/l) for April 2.

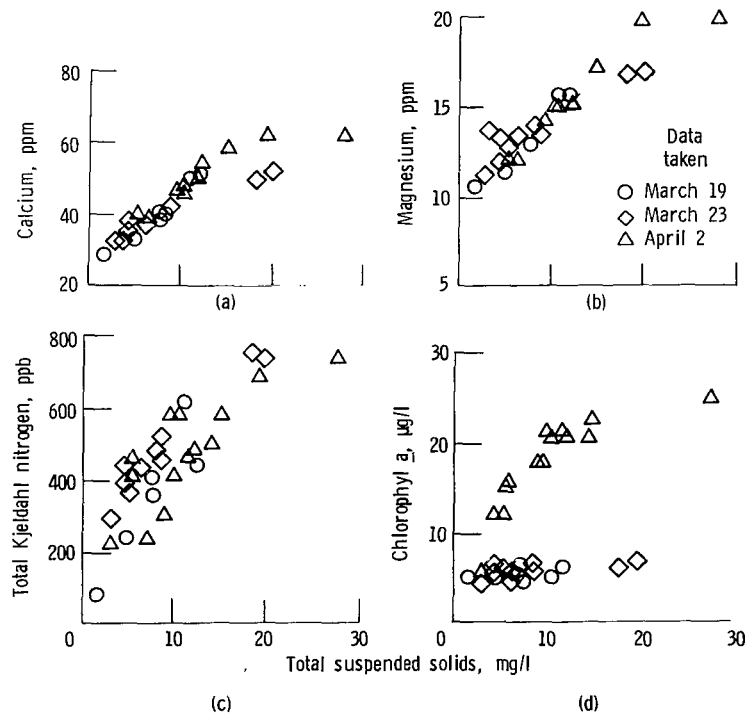


Figure 96. - Water-quality parameters versus total suspended solids.

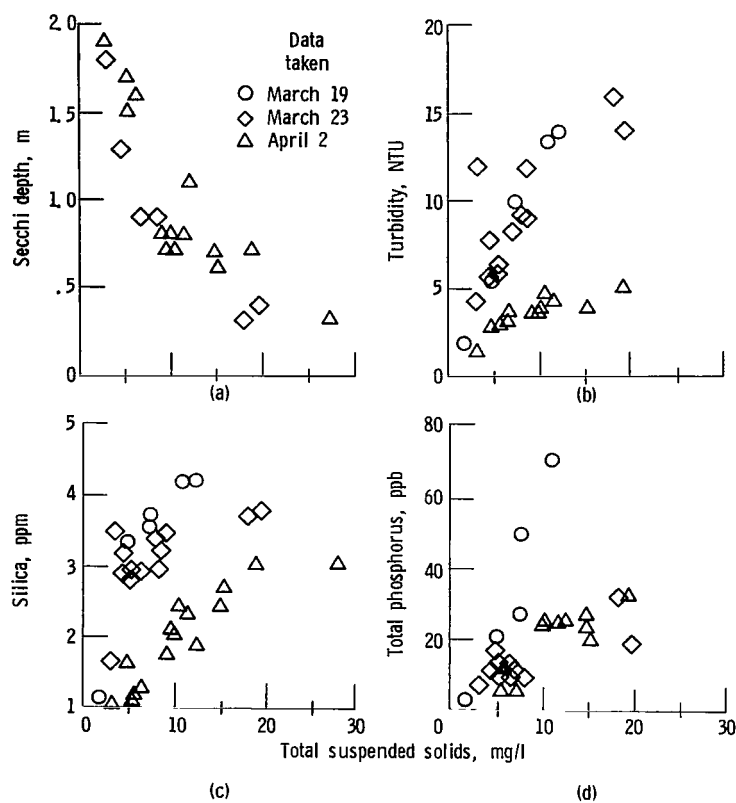


Figure 97. - Water-quality parameters versus total suspended solids. (NTU denotes Nephelometer turbidity unit.)

Summary of Results

A total of nine remote sensing aircraft flights were made over Lake Michigan near the Grand River during a six-week period from February 23 to April 2. Multispectral scanner data from these flights showed the extent of the Grand River sediment plume during the spring, including the maximum runoff period. Of greatest importance, the data showed large areas extending south of the river and beyond the main river plume having significant suspended sediment. This material is apparently carried south by the prevailing littoral current from the mouth of the Grand River along the lake shore and then resuspended by wind and wave action. Shore erosion is not believed to be a major input to the suspended material in these off-shore areas.

Contour plots derived from correlations of the in-the-water measurements of suspended-solids concentrations and the OCS scanner channel 8 (714 nm) radiance data are presented for the March 19 and 23 and April 2 overflights. These contours reveal the effects of the Grand River outflow on the near-shore distribution patterns of suspended solids in the waters off of Muskegon and Ottawa Counties. To the extent that the other measured water parameters correlate with suspended solids, the contours also reveal the distribution of these parameters.

The remote-sensing data are capable of revealing the location and distribution of suspended solids in sufficient detail to assist survey ships in selecting sampling sites. However, in view of the rapid response of the sediments to changing winds the information must reach the ship in near-real time to be of value.

Nemadji River Results

The Nemadji River entering the western arm of Lake Superior at the Duluth-Superior Harbor (fig. 98) is the chief runoff source of red clay sediment in the lake. This fine red-clay particulate is the most severe naturally occurring suspended-solids contaminant in the lake and has been considered a natural tracer for the dispersion of point-source pollutants entering the otherwise clean, open lake waters. Past studies have shown that the Nemadji River contributes over 70 percent of the stream-eroded red clay input into the lake, and the spring runoff period, in turn, typically accounts for about 30 percent of the river's yearly sediment output (106 000 metric tons in 1975 runoff period). Landsat satellite investigations conducted in the study area (refs. 5, 11, 12) have shown that remote sensing can monitor suspended red clay accumulation and dispersion. The Nemadji red-clay particulate is readily traced by remote sens-

ing, but a number of other contributing pollutant sources tend to obscure simple visual interpretation of the data. Actually, the dominant source of red-clay turbidity does not result from tributary runoff but from lake shore erosion. Erosion of the red clay banks along the Wisconsin shore contributes over 70 percent of the yearly lake turbidity (average yearly rate of 2.3×10^6 metric tons). In addition to this, another distinct water type dominates the runoff from some of the other major tributaries in the area. Dark "tannin" water, high in organic and dissolved solids, is typically found in the St. Louis River. A study of the Nemadji River source dispersion requires isolation of the river's loading from the other contaminant sources.

A summary of the Nemadji River survey activities and how they were related to the river runoff is shown in figure 99. All of the ship-survey measurements were made by research personnel from the University of Minnesota at Duluth. Coordinated ship and aircraft operations conducted over a nine-day period from March 31 to April 8 resulted in successful coverage of a majority of the river runoff and dispersion phenomena characteristic of the study area. During this period there were five boat sampling cruises and six aircraft-scanner overflights, which resulted in concurrent coverage on April 1, 4, 5, and 6. Detailed chemical analyses (as defined in table II) were performed on the water samples acquired on April 1 and 4. Supporting Landsat satellite data were also acquired on April 5 and 6. A concurrent ship-and-aircraft operation was also conducted on April 9 with the low-altitude aircraft; but only isolated site data were taken for detailed study, and no large area coverage was attempted. Additional ship sampling data were taken at regular intervals through May 21 with detailed chemical analysis performed on the data of May 11. Additional aircraft overflights were conducted on June 7 and July 8. The data taken after April 8 will not be discussed in detail because they were acquired well past the peak river runoff period.

The ship sampling stations were concentrated in an area southeast of the Superior harbor entry and extended on one day as far east as the Amnicon River. One additional station was located outside the Duluth harbor entry and one or more stations were located in an area of clean lake water. Between 8 and 12 stations were sampled during each cruise. The aircraft data normally covered an area the entire width of the Western Arm of Lake Superior, southwest from a line running between Two Harbors and the Iron River. On some occasions the coverage was extended to the northeast as far as Silver Bay and Bark Point. All the scanner data were acquired between 10 a.m. and 2 p.m. CST. Whenever possible, uncorrected black and white imagery from one channel of

the scanner data was transmitted by telecopier to the University of Minnesota as an aid for selecting future ship sampling sites. Imagery from April 1 and 2 was transmitted at 8:30 p.m. EST on April 2. Imagery from April 4 and 5 was sent on the same day it was acquired at 8:15 p.m. and 10 p.m. EST, respectively.

History of Events

Although the analog preprocessed imagery from one channel of the scanner is only qualitative, it can provide a useful description of the overall plume dispersion and flow patterns. Before a discussion of the quantitative processed data analysis, this imagery along with pertinent Landsat imagery will be used to provide a narrative history of the study period activities. During the narrative, frequent reference will be made to the numerical current and transport modeling results described by Sydor, et al. (ref. 13). These results have been consulted extensively to assure an accurate interpretation of the dispersion conditions.

The Landsat imagery in figure 100 is illustrative of the extremely low suspended sediment background conditions that exist in the lake's western arm in the absence of river sediment outflow and shore erosion. During this period in late winter (February 21) the tributaries were still clogged with ice, and the red clay banks of the shores were frozen or snow covered. By the end of March the Nemadji's stage had increased through snow melt and/or rains and ice jams, which lasted until March 31. Because of impending heavy flow conditions, the ship team began sampling on March 31 and then repeated the sampling the next day when simultaneous remote-sensing data were acquired. The aircraft imagery from April 1 (fig. 101) shows that, although the ice in the river had broken up, the amount of sedimented river water flowing from the Superior entry into the lake was still low because of ice in the harbor and entry. The bright area due southeast of the entry contains a large amount of broken ice. The red clay plume was also swept due southeast along the Wisconsin shore. This transport condition is consistent with that predicted by the Sydor current model for the prevalent northwest winds of the previous days. Because of the ice packs in the harbor, little mixing of the red clay occurs, and no sedimented water is seen at the Duluth entry or along the exterior harbor wall.

The dominant feature in the imagery is the large extent of heavy sediment along the Wisconsin shore. Because the imagery was enhanced to reveal small sediment concentrations, the shore boundary is obscured by the heavy near-shore red clay concentrations. Large red clay concentrations extend up to 8 kilometers offshore near the Amnicon and Poplar

River mouths. Spatial resolution of the scanner does not permit isolation of the smaller river mouths along the shore but a visible observation from the aircraft noted only minor sediment contributions from these rivers. Based on the results of preceding years, Sydor estimates that the combined Amnicon, Poplar, and Middle River outputs to be only 10 percent of the Nemadji River output. This information, coupled with the diffuse nature of the sediment laden areas and a knowledge of the previous day's 5- to 10-m/sec northwest winds, indicates that these large red-clay concentrations are the result of shore erosion (along with some possible resuspension) rather than tributary runoff. The eroded sediment flow is shown to be easterly along the Wisconsin shore. This behavior is again consistent with Sydor's transport model predictions.

By April 2 the Nemadji River was free flowing, and ice was rapidly breaking out of the Superior entry. By the time the imagery in figure 102 was acquired, the entry was nearly clear of ice. A plume consisting of a mixture of red-clay sediment and brash ice can be seen extending over 3 kilometers out into the lake. The plume pattern indicates an eddy type of circular current near the entry with a general transport toward the northeast along the axis of the Western Arm. Because of the light and variable winds (average 2 m/sec) on April 1 and 2, the plume transport near the entry was probably dominated by the high inertial flow from the harbor. Heavy red-clay concentrations can be seen again along the Wisconsin shore. The material in the near-shore area appears to be still moving to the northeast, while that in the open lake appears to be flowing slightly to the west. The lighter areas near the northern shore are caused by high thin clouds and should not be confused with sediment.

The peak Nemadji suspended loading came on April 3 and was accompanied by a change to rather strong (10 to 12 m/sec) northeasterly winds which persisted until April 4. This resulted in the first significant transport of Nemadji runoff material to the open lake, as can be seen in the imagery from April 4 (fig. 103). The Nemadji plume was generally isolated from the shoreline turbidity and snaked its way out 16 kilometers from the entry, up the axis of the Western Arm. A small stringer of ice still existed straight out the harbor entry. But both the entry and harbor were free of ice jams, and a small amount of sediment can be seen emanating from the Duluth entry.

Different flow patterns can also be seen in the eroded and resuspended red clay along the southern shore. The distinct hook patterns of this material are the result of the sediment immediately adjacent to the shore moving southwest while that 4 to 6 kilometers

offshore was moving northeast. All of these changes in the plume transport and shoreline current were accurately predicted by Sydor's model. It also appears that the near-shore red-clay concentrations east of Brule Point have diminished significantly.

During the day on April 4 the winds diminished and became light (average <3 m/sec) and variable. This condition existed through April 6 and resulted in the general transport patterns shown in figures 104 to 106. Although portions of the aircraft imagery for April 5 (fig. 104) are obscured by clouds, the main areas of turbidity are clear and are identical to those shown in the Landsat imagery (fig. 105). The aircraft data were acquired between noon and 1 p.m. CST, and the satellite data were acquired at 10 a.m. CST. The circulating eddy-current patterns cause hooking of the sediment plume and result in isolated patches of high red-clay concentrations. These patches are also observed in the imagery of subsequent days and prove useful in tracing the transport patterns. This aspect of the study will be discussed later.

On April 5 (figs. 104 and 105) the Superior entry outflow returned to its previous flow direction and is seen moving due southeast, while the sediment along the Wisconsin shore is being swept to the west along the shore and to the north out into the lake. The farthest extent of Nemadji River sediment transport appears to be a patch about 18 kilometers from the Superior entry and 10 kilometers offshore. The sediment output from the Duluth entry has increased and can be seen to be coming straight out the entry and then diffusing radially. There is a band of turbidity along the harbor wall, although it appears to be dispersing into a larger area of minor turbidity extending out into the lake. These features are easier to see in the aircraft imagery (fig. 104) because this imagery was enhanced during processing. An area of low turbidity also exists along the northern shore out into the lake. The general circulation-relaxation current pattern inferred by the imagery is predicted quite well by Sydor's transport model.

The imagery for April 6 (fig. 106) looks very similar to that of the previous day, and the patches of heavy turbidity are still evident. In fact, they appear to be becoming even more isolated, while moving and diffusing only slightly. The Nemadji input continues due southeast, while the Wisconsin shoreline sediment continues to flow west and north. The shoreline pattern is particularly clear just west of Brule Point. A pocket of heavy sediment remains in the southwest corner of the Arm. Turbidity emanating from the Duluth entry is now isolated in the northwest corner of the Arm while the area along the harbor wall and north shore are quite clear. There is one small area of sediment near the mouth and northeast of the Lester River on the Minnesota shore.

A diagnostic distribution pattern based on low-altitude imagery acquired on April 8 (fig. 107) again shows what can be assumed to be the same turbidity patches although they have diffused considerably. A new patch has also formed just northwest of the Superior entry. Although the Nemadji plume is again heading northeast, sometime before to the imagery acquisition, a counterclockwise rotational flow pattern resulted in the formation of the new area of turbidity. A pocket of heavy red-clay concentration still remains in the Arm's southwest corner where most of the Nemadji River sediment input appears to be trapped. The shoreline sediment along the Wisconsin shore has diminished significantly, particularly east of the Poplar River. Because of the better resolution of the low-altitude imagery, the outflow of the Amnicon, Middle, and Poplar Rivers can be seen distinctly. Plumes from the Amnicon and Middle Rivers extend due northwest into the lake and diffuse radially. The plume from the Poplar River hooks back westerly toward the shore. In each case these river plumes appear to have less sediment than the surrounding lake waters, indicating again that the large areas of turbidity along the Wisconsin shore are the result of either shore erosion or resuspension and not tributary loading.

The period of high river loadings (~ 2000 metric tons/day) lasted only 10 days, and, since the summer was dry, the Nemadji output after late April was negligible. This is supported by the imagery shown in figures 108 to 111. Imagery for May 11 (fig. 108) shows the entire Western Arm to be relatively free of turbidity with only minor shore erosion along the Wisconsin shoreline. The only significant river activity appears in the July 8 imagery (fig. 111) with areas of high red-clay concentrations at the mouths of the Nemadji, Amnicon, and Poplar Rivers.

Data Analysis and Discussion

As previously stated, concurrent ship sampling and aircraft overflights occurred on four days. These data provided measurement pairs for the quantitative correlation of upwelling radiance measured by the scanner and in the water measurements as described earlier. On two of the days, the ship data were subjected to chemical analysis, and correlations were attempted with all the measured parameters. Results of all the significant correlations are summarized in table XIII and graphically illustrated in the subsequent contour plots. In all cases the values represent surface or near surface measurements. The vertical variation of the listed parameters with depth was negligible over the correlated channel's optical depth of penetration.

The most straightforward correlations were obtained for total suspended solids and Secchi depths because they involve the use of data from only one channel of the scanner. Furthermore, in the case of suspended solids, a linear first-order equation was sufficient to provide a satisfactory correlation over the range of 0 to 20 mg/l. This range was representative of the measured lake plume suspended solid values. Although on some days there were isolated values greater than 20 mg/l, these represented samples taken either directly in or at the mouth of the Superior entry. Because of the dynamic mixing in these small regions, any correlation of those data would probably be fortuitous and possibly misleading. It was also found that, for suspended solids concentrations above 20 mg/l, the correlations required were of second or higher order.

On three of the days, data from channel 8 was correlated for suspended solids because it provided the smallest standard error of estimate. On April 5, OCS channel 8 was not operational, and data from OCS channel 10 were used with little loss in accuracy. Because the regression coefficients calculated for the data from April 1 and April 4 were quite similar, these data were combined, and a general relationship was obtained to represent both days with the correlation parameters listed in table XIII. This enabled confident extrapolation of the April 1 data up to concentrations of 20 mg/l.

Exact correlations could not be established for April 2 because no ship data were acquired on that day. A relationship was established, however, to predict suspended solids for that day, based on the in situ measurements and the combined correlations for April 1 and 4. The resultant calculated suspended solids for April 2 were considered representative of the values present that day, and a contour plot has been included for completeness of coverage.

The suspended solids contour plots presented in figures 112 to 116 contain essentially the same information shown in the imagery except that it is now quantitative and provides more detail on the red clay concentrations, particularly in the very turbid areas. The contours were generated from calculated suspended solids values at discrete locations spaced at 1-kilometer intervals. The shoreline shown was also generated from the same 1- by 1-kilometer grid array. The intersecting lines representing the major rivers were added manually later. Even with the degraded spatial resolution due to the contour's grid array, the sources of the sediment and subsequent transport patterns are in many cases easier to visualize from these plots. For example, in figure 112 the concentrated source between the Amnicon and Poplar River is much easier to discern. In the same plot the sediment from the smaller river mouths can

also easily be seen. The band of turbidity along the harbor wall on April 4 (fig. 114) is very evident, as is the turbidity southwest of the Lester River. Subsequent clearing of turbidity along the harbor wall on April 5 and 6 can be followed in figures 115 and 116. Through all of these suspended solids plots, the buildup and retention of a heavy red-clay concentration can be observed along the southwest shoreline.

Data used to generate the suspended-solids contours can also be used to produce crude sediment loading estimates by multiplying the surface-solids values and the lake depth at each grid point by an area of 1 square kilometer. Such calculations were made and summed for a total area covering the southern half of the Western Arm from the Duluth-Superior harbor to Brule Point. For April 1, 4, and 6 the calculated loadings are 1.33×10^4 , 1.88×10^4 , and 1.75×10^4 metric tons, respectively. On April 1 the input from the Nemadji was negligible; hence, it is easy to establish that the bulk of the loading was contributed by shore erosion and resuspension. Any estimates of the relative contributions of the various inputs to the April 4 and 6 loadings are obviously much more complicated and would require a knowledge of settling rates, particle sizes, vertical current profiles, etc. Such an analysis is not attempted here but the total suspended loadings calculated by Sydor in his model computations do compare favorably and do contain estimates of the contributing sources. Sydor's values are 1.18×10^4 metric tons on April 1, 2.70×10^4 metric tons on April 4, and 2.66×10^4 metric tons on April 6.

The Secchi depth correlations and plots (figs. 117 and 118) proved to be of little value and were not used in the transport interpretations. Of much greater value were the chemical parameter correlations for the April 1 and 4 data. Based on the work of Sydor, et al., it was quickly determined that significant correlations could not be determined simply between the chemical parameters and suspended solids, hence the red-clay turbidity could not be used directly as a tracer for these pollutants. Areas of turbidity affected by the Duluth entry were consistently higher in nutrients and dissolved salts than similar areas in the southern half of the Arm. This fact is consistent with published data concerning the tannin water coming from the St. Louis River and other rivers along the Minnesota shore. Because this tannin water is known to have distinctive optical properties, including high absorptivity in the lower visible wavelength spectrum (ref. 11), correlations were attempted using multiple OCS channels. Significant correlations were found (see table XIII) for total phosphorus, total organic nitrogen, silica, and sulfates when using a combination of OCS channels 4 and 8. No other significant correlations were obtained.

The radiance-suspended solid correlations for channel 8 were unaffected by the tannin water because of a naturally low depth of penetration in this wavelength region (714 nm) even at very low turbidity levels. Optical measurements on water samples obtained during this study revealed that, even for nearly clean lake water (i.e., 1 mg/l or less of suspended red clay particulate), the depth of penetration was less than a meter at a wavelength of 700 nm. In contrast, the radiance measured in OCS channel 4 (549 nm) was affected by the absorption by the tannin water, and the channel 4 data were proportionately lower for similar values of sediment when measured in the tannin-water region. Previous Landsat remote sensing studies by Sydor have used these distinct optical properties to discriminate water types.

Examination of the contour plots for the chemical parameters (figs. 119 to 126) reveal information that was not available in the suspended solids contours. Areas along the northern shore and near the Duluth entry are seen to have high values of nutrients and salts even though the turbidity is low. On the other hand, the chemical values along the southern shore are sometimes low even in areas of relatively high sediment. The restricted pocket of effluents in the southwest corner of the Arm is also seen more clearly in the chemical plots.

Through the use of the imagery discussed in the previous section and the contour plots in this section the movement of several distinct patches of the Nemadji River plume can be traced on April 4, 5, 6, and 8. The transport of three isolated patches is shown in figure 127 with the direction of travel indicated by the arrows beginning with the position on April 4 and ending with the position on April 8. These are the same areas tracked by the University of Minnesota using April 4 and 5 Landsat data (ref. 13). The area labels are identical to those used by the University of Minnesota. The largest transports occurred between April 4 and 5 as a result of the current reversal previously discussed. The most significant movement between April 6 and 8 was 3 kilometers for patch 1 as it moved southward toward the shore. Perhaps the most striking movement or nonmovement is that of patch 2. Although it did diffuse between April 5 and April 8, its change in position is negligible for this time period and it appears trapped by eddy currents. These eddy circulations have been predicted by the University of Minnesota numerical current-model calculations and are thought to be able to entrap pollutants in the Western Arm for long periods.

Although the results of these analyses for sediment and chemical parameters have yielded significant information on the transport and fate of pollutants in the Western Arm, one question remains unresolved

and cannot be adequately answered in this study. It has not been clearly shown that the Nemadji River input can be isolated if it becomes mixed with the surrounding sediment concentrations caused by shore erosion and resuspension. Although the eventual fate of the Nemadji runoff can be assumed to be the same as the encompassing red-clay particulate, the extent of its dispersion cannot be accurately determined. Unfortunately, any further analysis of the river runoff transport after mixing is beyond the scope of the data acquired in this study.

Summary of Results

Through the coordinated efforts of ship sampling and aircraft remote sensing overflights, the quality of water offshore of the Nemadji River mouth was successfully monitored during the 1976 spring runoff period. The spring runoff characteristics were considered typical for the river, and data were obtained before, during, and well after the days of peak flow and peak suspended loading. All of these events took place in the nine days from March 31 through April 8, and the emphasis of the data analysis was directed to those days, although measurements were made far beyond that time. The initial transport direction of the river outflow was always easily determined and in some cases the short-term fate of the river effluents could be established. By combining the results of University of Minnesota current-model calculations with remote sensing imagery and quantitative contour plots, the dispersion of sediment could be traced over a large segment of the Western Arm. The model proved to be a good predictor of the transport conditions, and the remote sensing data allowed extrapolation of the ship measurements over a much larger area.

By far the largest loading of suspended red-clay sediment in the lake resulted from shore erosion or resuspension along the southern shore. No determination could be made as to the relative contribution, if any, of the resuspended sediments to the total suspended loading. Under all but strong non-prevalent wind conditions, the Nemadji River runoff mixed with the surrounding suspended material, and a pocket of sediment was formed in the southwestern area of the arm. The transport of this material out of the Western Arm into the main body of Lake Superior was not observed during the study period. Once the river plume mixed with the eroded or resuspended sediment, its identity was lost. Thus the overall dispersion of the plume could not be exactly determined. It is reasonable to assume, however, that the dispersion followed the general transport of the entire body of material.

The Nemadji River did contribute significant amounts of nutrients and salts to the lake. The

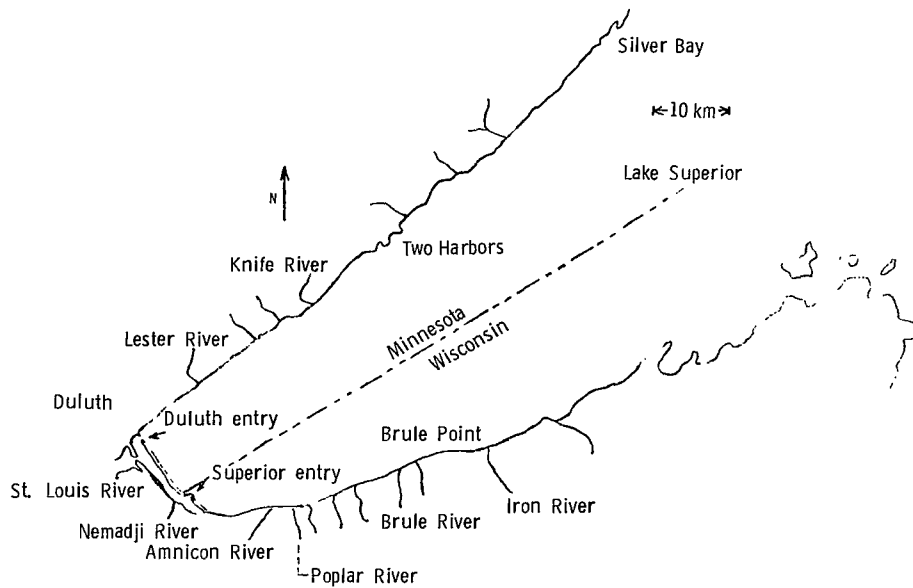


Figure 98. - Nemadji River area in the western arm of Lake Superior.

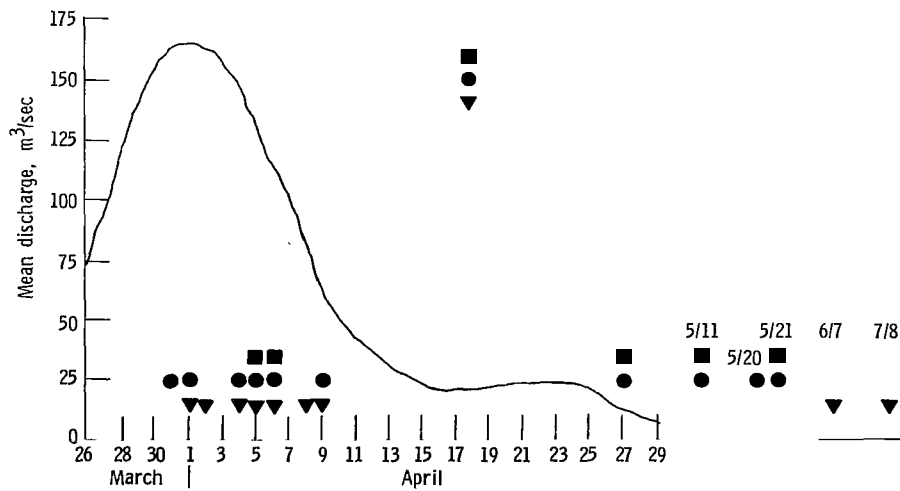


Figure 99. - Mean discharge of Nemadji River and summary of remote sensing and ship surveys.

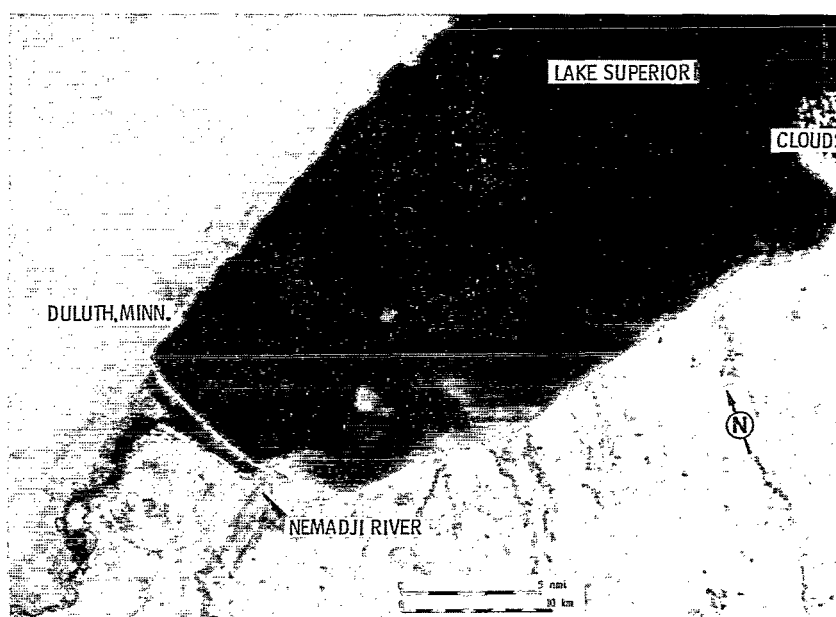


Figure 100. - Landsat image of Nemadji River-Lake Superior, February 21, 1976.

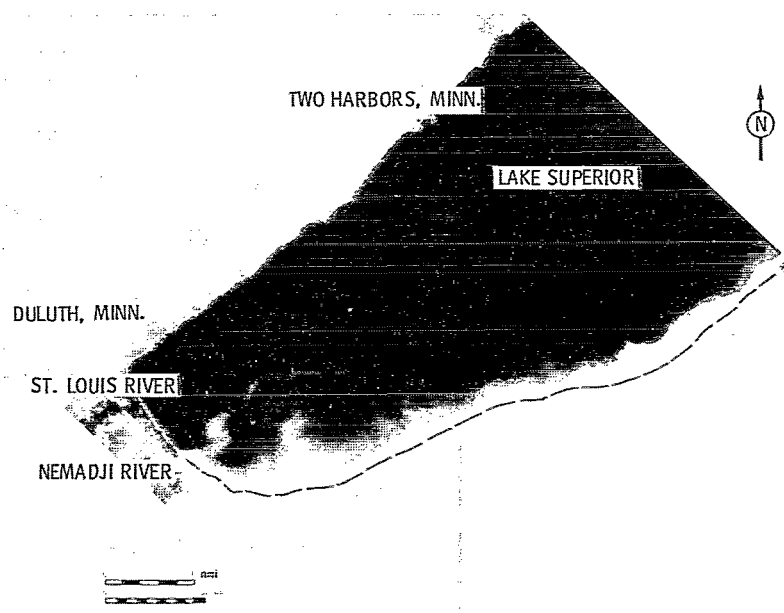


Figure 101. - Image of Nemadji River-Lake Superior, April 1, 1976. OCS scanner channel 6.

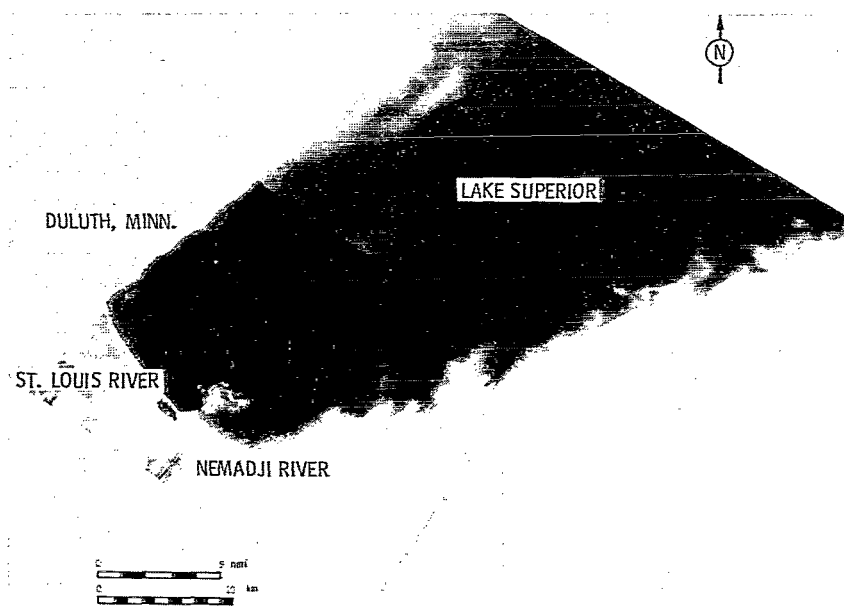


Figure 102. - Image of Nemadji River-Lake Superior, April 2, 1976. OCS scanner channel 6.

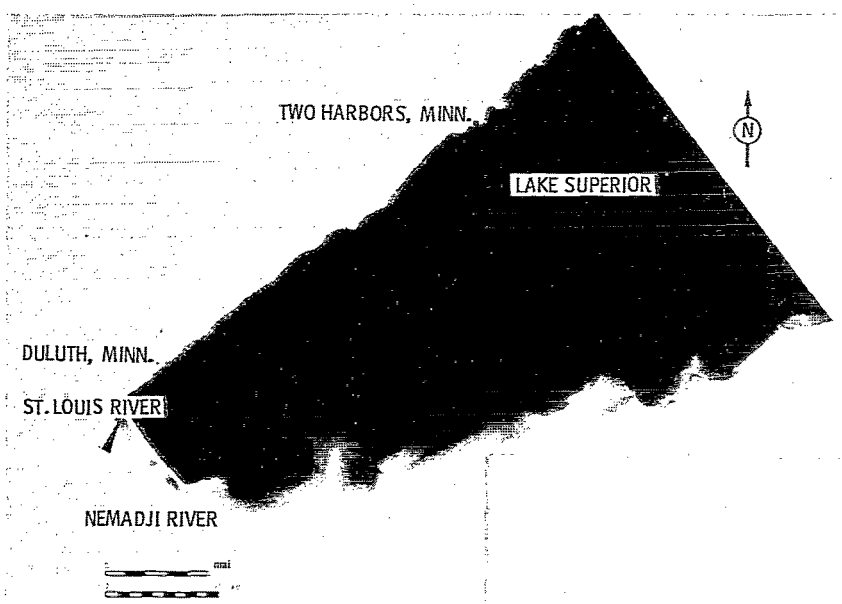


Figure 103. - Image of Nemadji River-Lake Superior, April 4, 1976. OCS scanner channel 6.

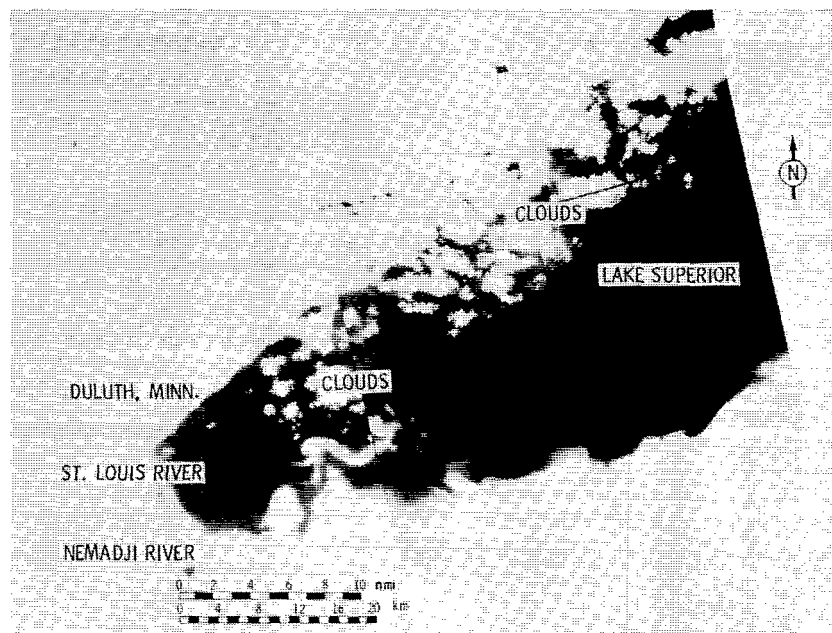


Figure 104. - Image of Nemadji River-Lake Superior, April 5, 1976. OCS scanner channel 6.

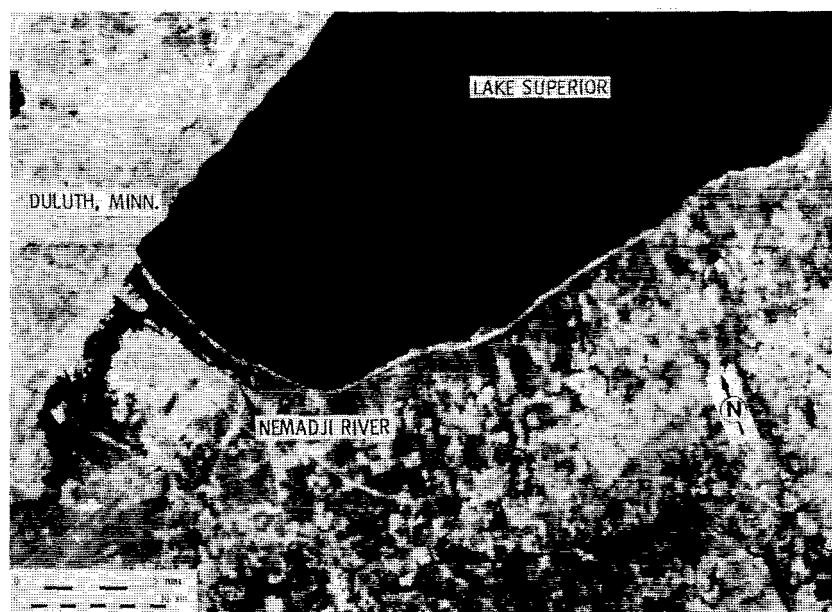


Figure 105. - Landsat image (band 5) of Nemadji River-Lake Superior, April 5, 1976.

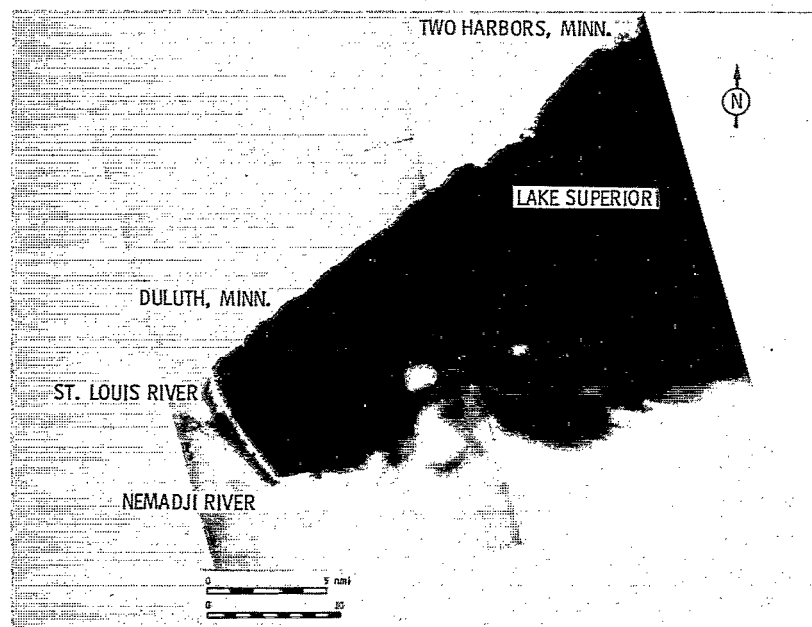


Figure 106. - Image of Nemadji River-Lake Superior, April 6, 1976.

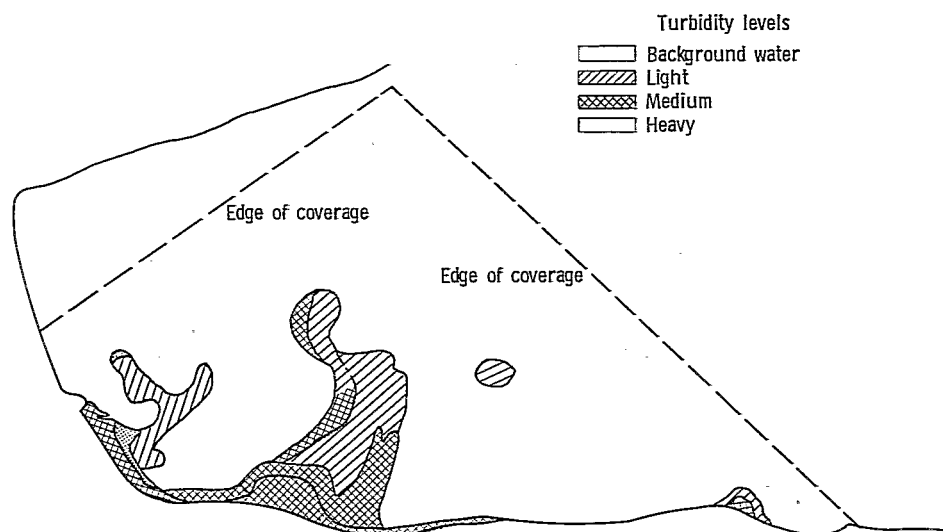


Figure 107. - Simulated imagery from April 8, 1976 (M²S channel 6).

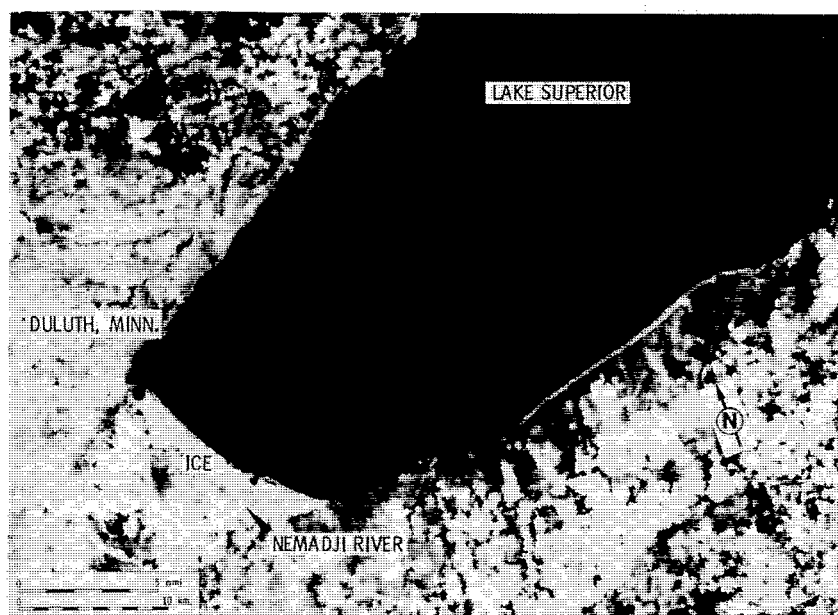


Figure 108. - Landsat image (band 5) of Nemadji River-Lake Superior, May 11, 1976.

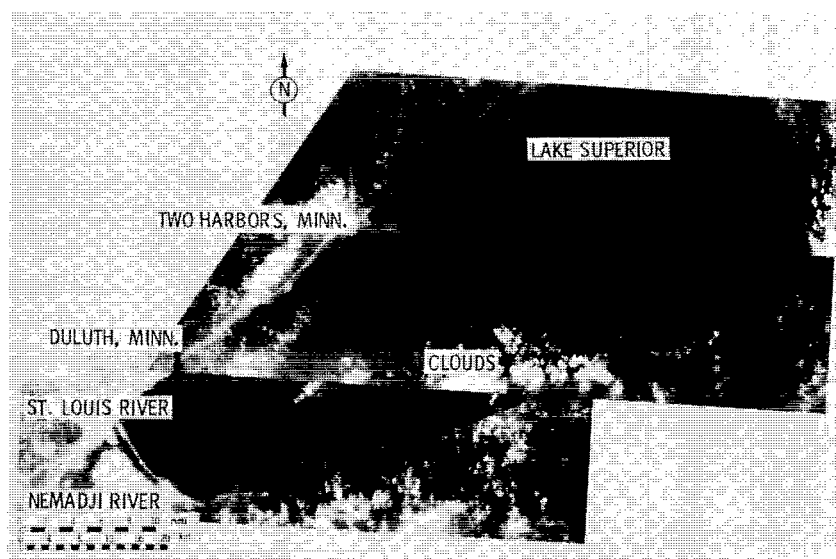


Figure 109. - Image of Nemadji River-Lake Superior, June 7, 1976. OCS scanner channel 6.

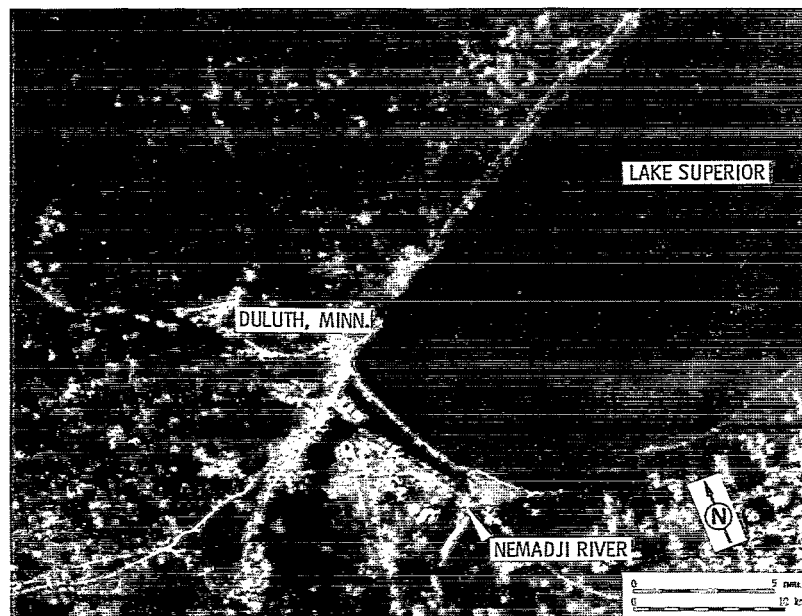


Figure 110. - Landsat image (band 5) of Nemadji River-Lake Superior, July 5, 1976.

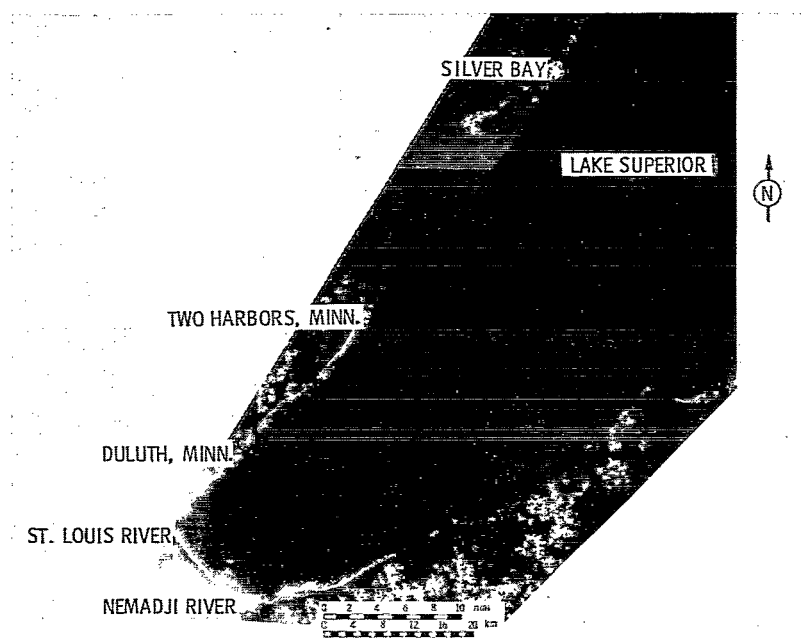


Figure 111. - Image of Nemadji River-Lake Superior, July 8, 1976. OCS scanner channel 6.

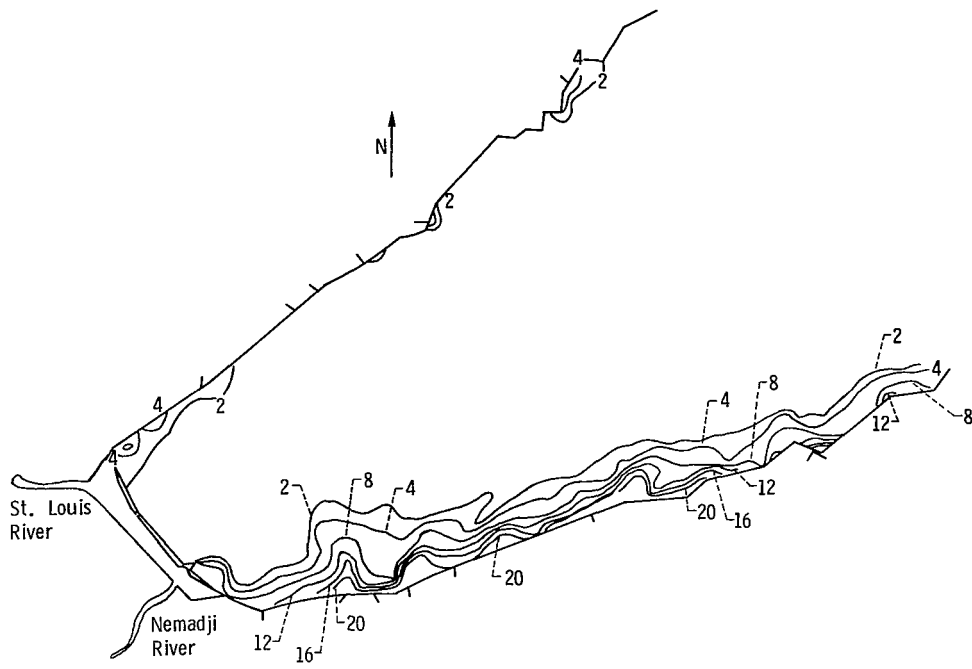


Figure 112 - Contour plot of total suspended solids (in mg/l) on April 1, 1976.

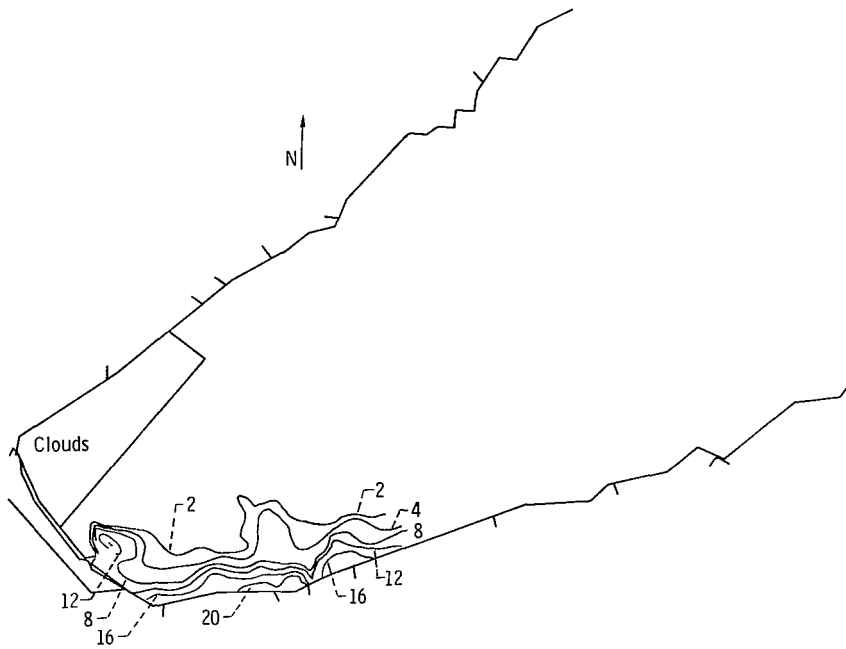


Figure 113 - Contour plot of total suspended solids (in mg/l) on April 2, 1976.

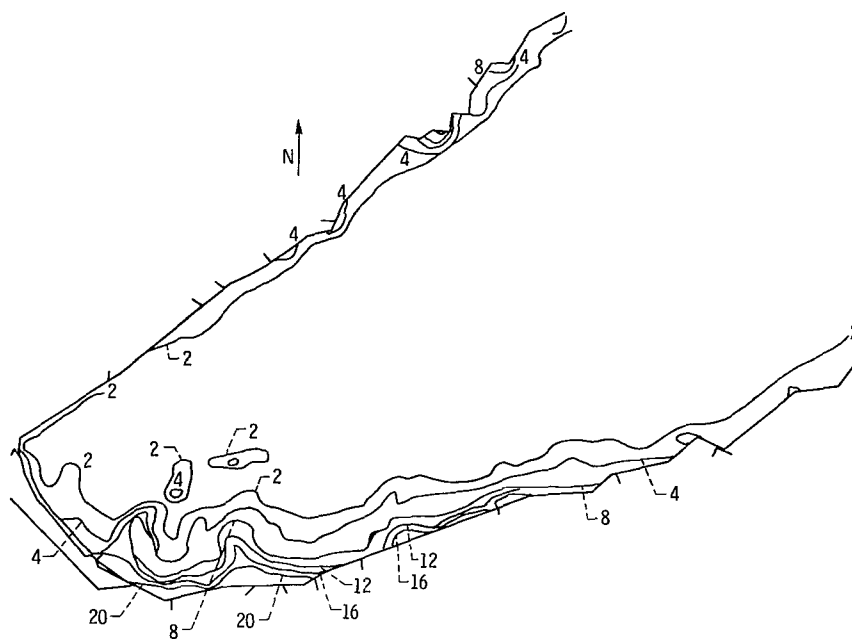


Figure 114. - Contour plot of total suspended solids (in mg/l) on April 4, 1976.

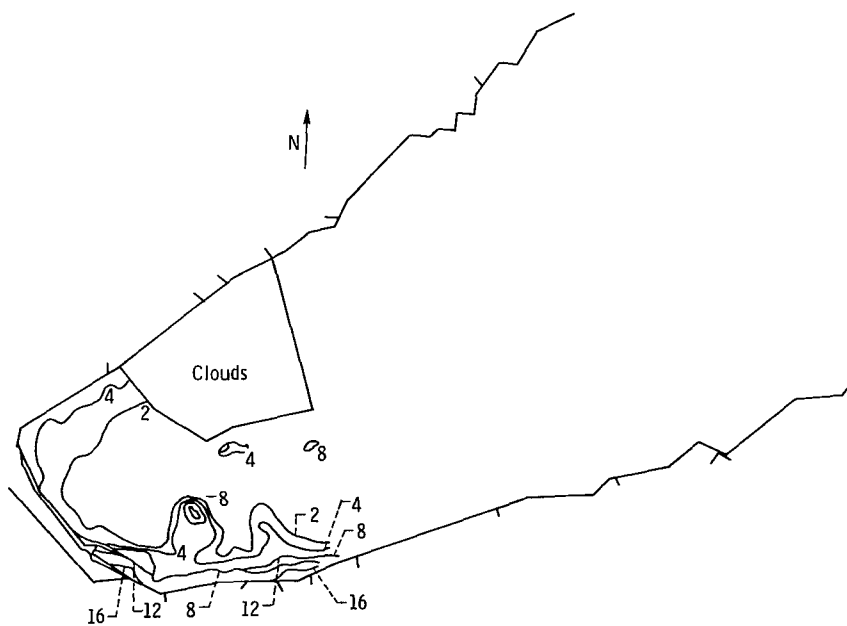


Figure 115. - Contour plot of total suspended solids (in mg/l) on April 5, 1976.

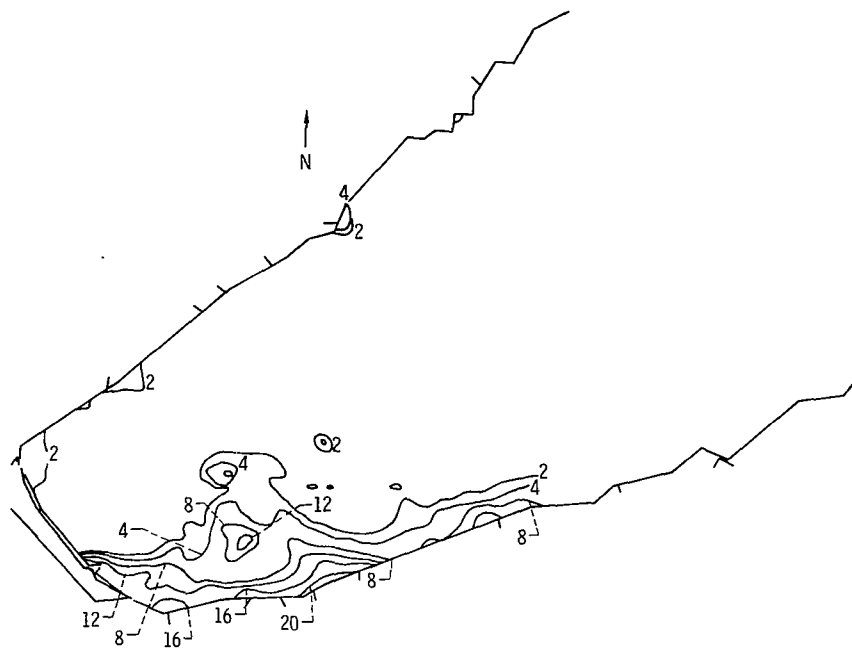


Figure 116. - Contour plot of total suspended solids (in mg/l) on April 6, 1976.

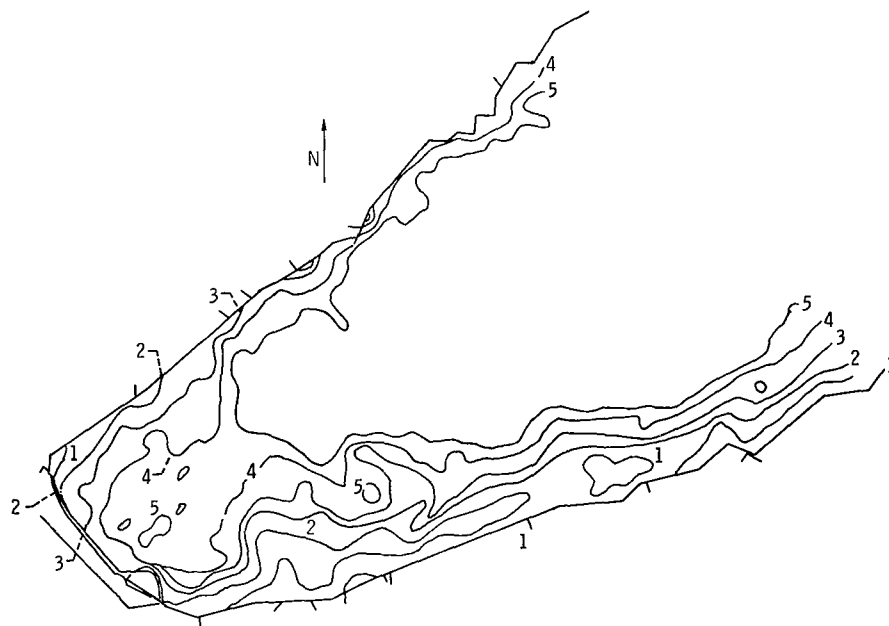


Figure 117. - Contour plot of Secchi depth (in meters) on April 1, 1976.

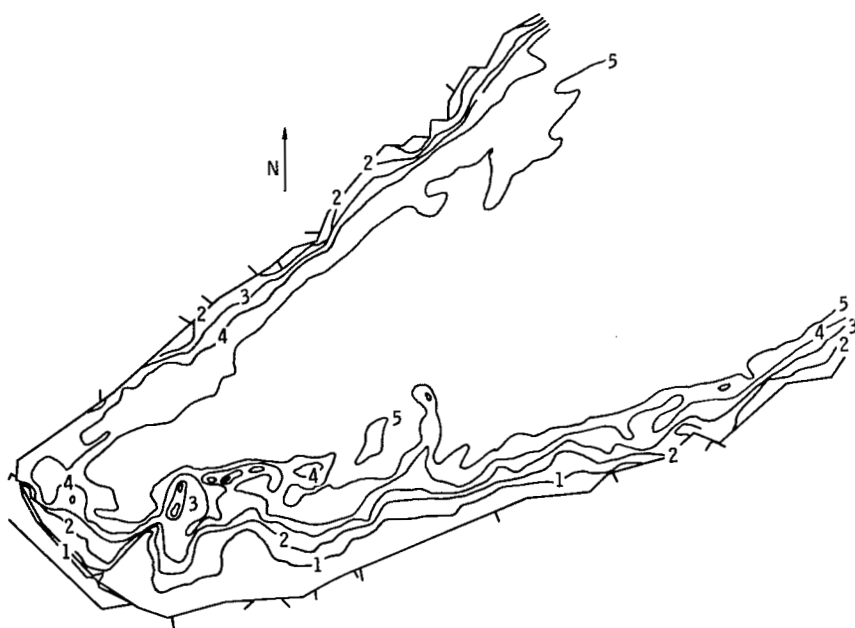


Figure 118. - Contour plot of Secchi depth (in meters) on April 4, 1976.

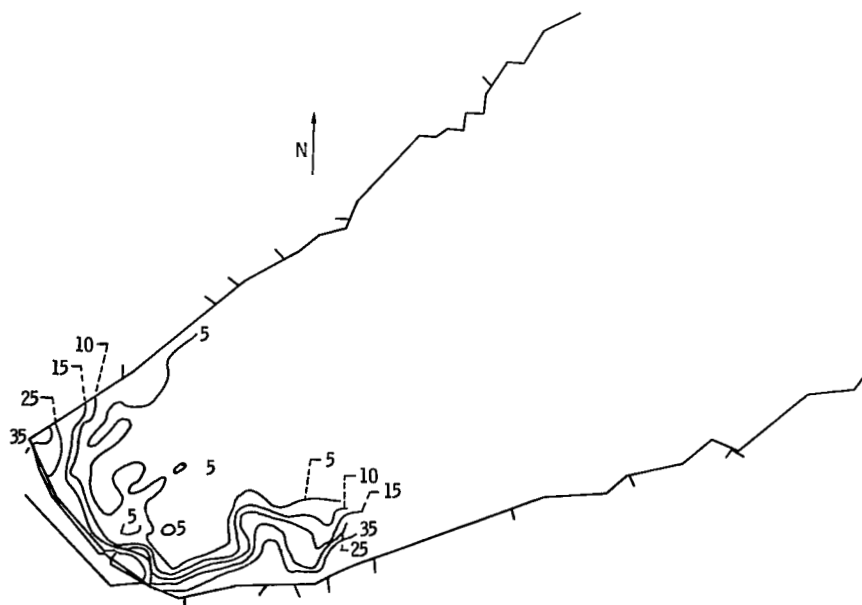


Figure 119. - Contour plot of total phosphorous (in $\mu\text{g/l}$) on April 1, 1976.

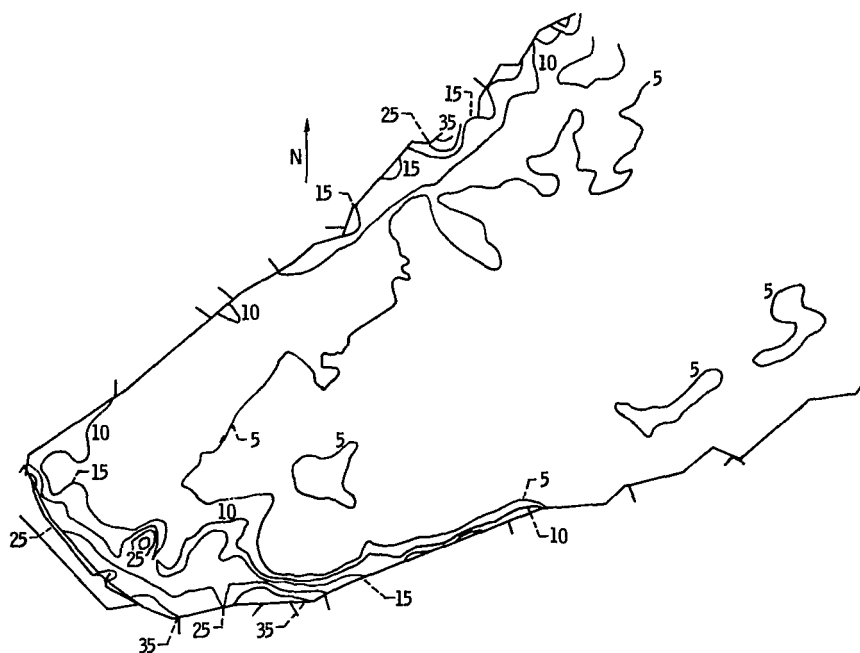


Figure 120. - Contour plot of total phosphorous (in $\mu\text{g/l}$) on April 4, 1976.

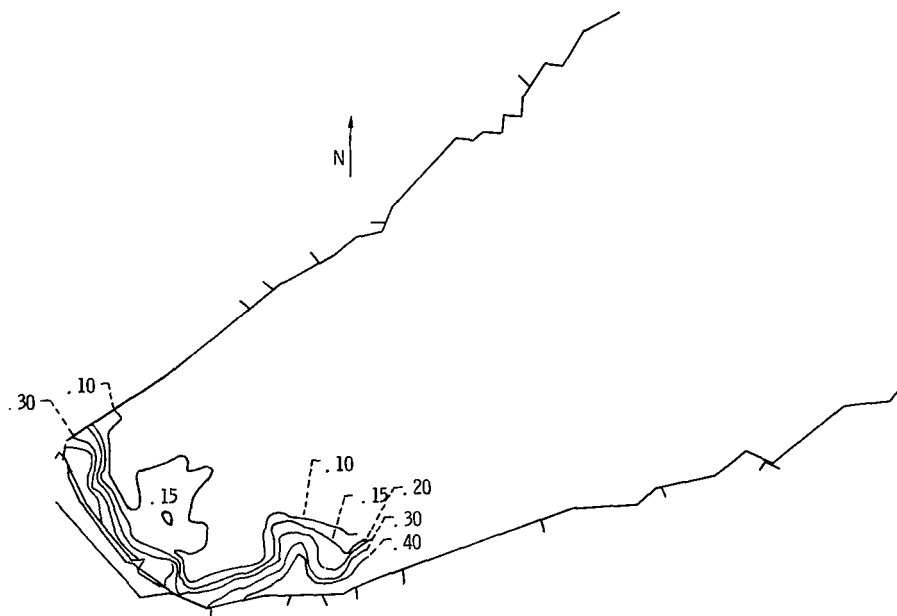


Figure 121. - Contour plot of total organic nitrogen (in mg/l) on April 1, 1976.

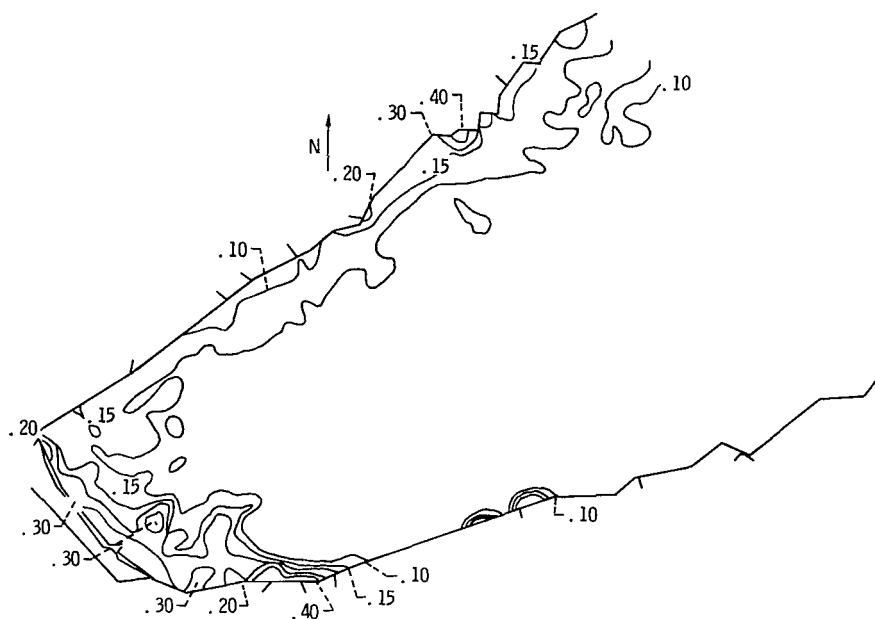


Figure 122. - Contour plot of total organic nitrogen (in mg/l) on April 4, 1976.

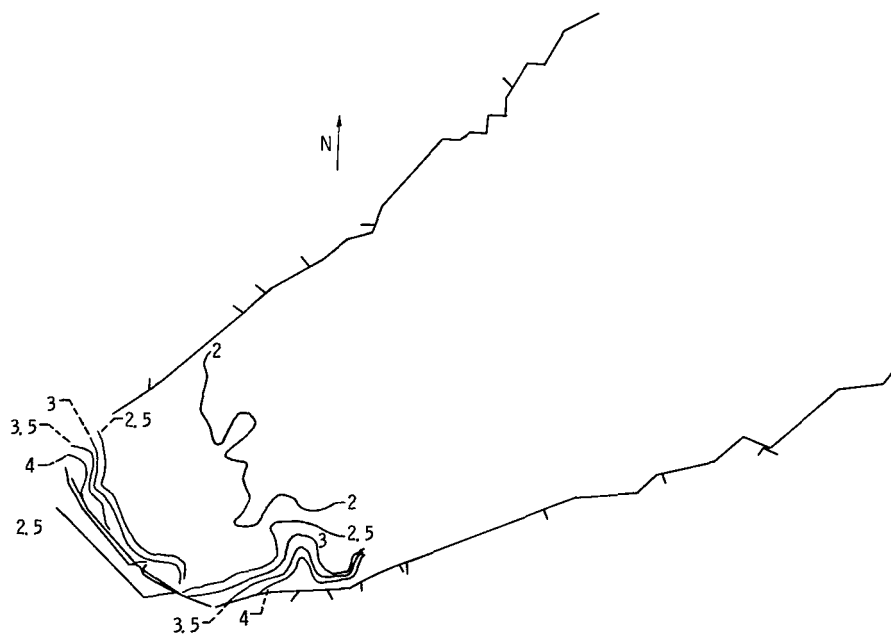


Figure 123. - Contour plot of silica (in mg/l) on April 1, 1976.

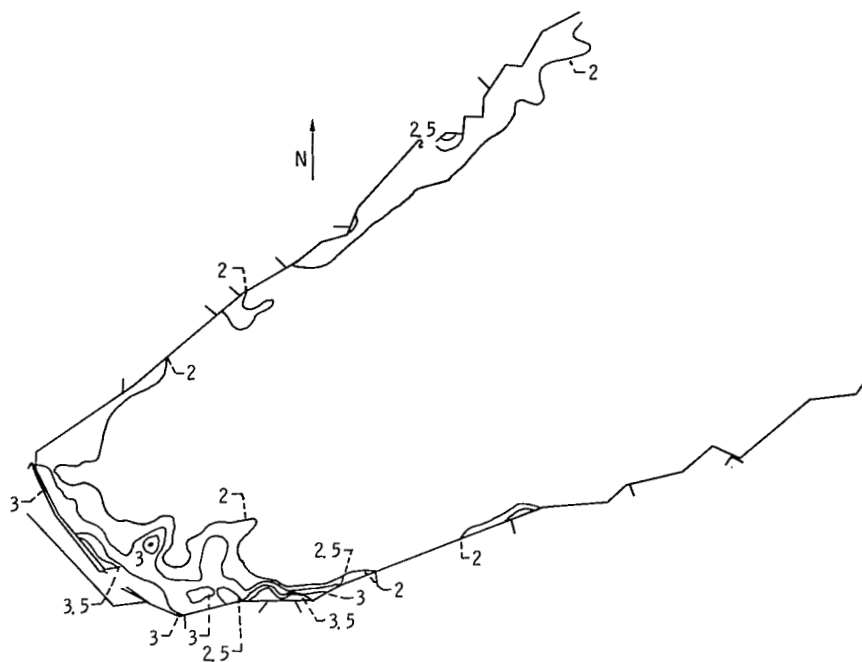


Figure 124. - Contour plot of silica (in mg/l) on April 4, 1976.

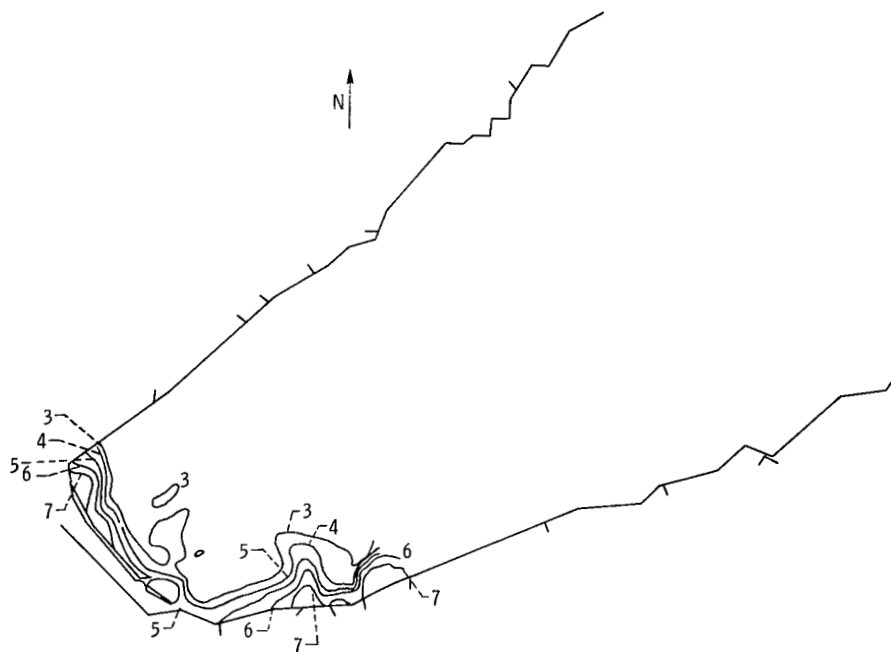


Figure 125. - Contour plot of SO_4 (in mg/l) on April 1, 1976.



Figure 126. - Contour plot of SO_4 (in mg/l) on April 4, 1976.

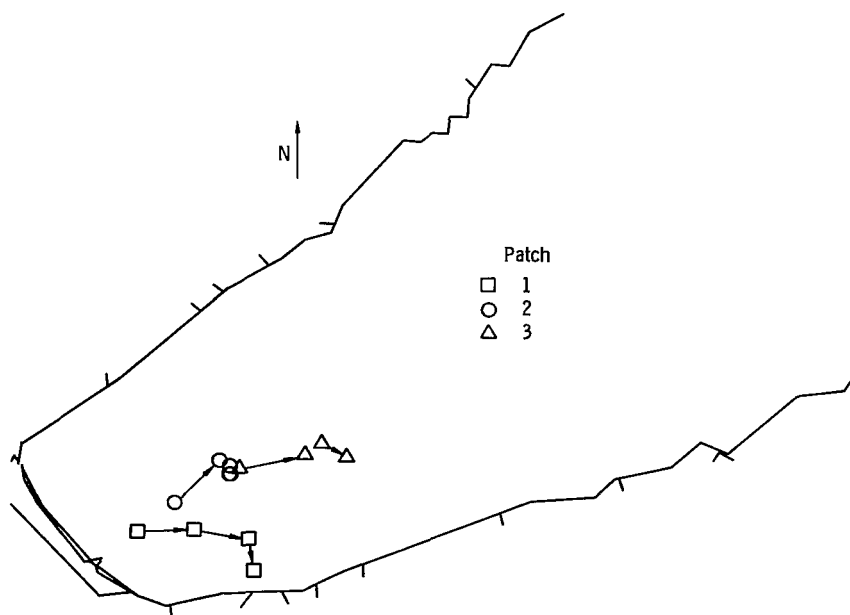


Figure 127. - Sediment patch movement beginning on April 4 and ending on April 8.

spacial concentrations of some of these parameters could be determined from the aircraft and ship data, and they were observed to follow the same general transport as the sediment, although they were not directly related to the sediment concentrations. A pocket of these effluents was also located in the southwest area of the Western Arm. The synoptic view of the remote sensing substantiated the fact that the Nemadji is not the only source of these chemicals and high concentrations exist along the northern shore even in areas of low sediment.

Because of the fortunate timing of this study, many aspects of the Nemadji River runoff and its impact into Lake Superior were available for study. The effects of peak runoff, heavy shore erosion and resuspension, and both prevalent and nonprevalent wind conditions were observed. Because these events occurred simultaneously in some cases, an evaluation of their individual impacts was difficult or impossible. Their overall role in the transport of pollutants in the Western Arm can generally be interpreted from combined remote-sensing and ship measurements.

OVERALL SUMMARY OF RESULTS

General Results

Aircraft or satellite remote sensing has proved to be a productive technique for assessing the effects of river runoff and suspended solid inputs on Great Lakes waters. Table XIV summarizes the overall remote sensing results for the coordinated aircraft and ship survey program at the five study sites. These results pertain to the sites during the Spring of 1976 and may not reflect conditions at other times.

Forty-seven overflights of the study areas have been reported, many of which were made during the spring period of maximum runoff. Single-channel multispectral scanner images have been presented for each of these overflights. On several days more than one site was covered and on one day (March 22) four of the five sites were overflowed. Twenty of the 47 overflights were made on the same dates as ship surveys and thus correlations of remote-sensing radiance data and in-the-water data were possible. At least two such same-day missions were achieved for each site. Fewer same-day missions were achieved at the Genesee, Menomonee, and Grand River sites because aircraft operations were concentrated during the spring runoff periods while the ship operations extended substantially into the summer and early fall. A number of factors prevented the coordination of more same-day surveys. These included cloud cover, which prevented or compromised the data of aircraft flights, high seas or ice conditions, which prevented ship surveys, scheduling conflicts with

other survey programs, and coordination breakdowns.

Twenty-five Landsat images of the sites have also been presented. These images augment the information obtained from the aircraft overflights. The Landsat images were especially useful in revealing the extensive resuspension and/or shore erosion along the south shore of Lake Ontario and the west shore of Lake Michigan.

Logistics of the aircraft with its scanner systems proved to be adequately responsive for covering the spring runoff events, and data were recorded at or near the spring maximum levels at four of the five sites. For the Menomonee River, where each peak discharge was small and occurred entirely within the span of a few hours, response time for aircraft flights was inadequate. The overall data-acquisition record demonstrated that there are sufficient opportunities with cloud-free sky conditions over the Great Lakes such that a dedicated remote-sensing system can meet the data requirements of timely and extensive survey programs.

Correlations and Contour Maps

Forty correlations were obtained between the scanner spectral radiance data and the surface in-the-water measurements acquired by the ship survey personnel; see table XIV for a summary of correlations. The parameters correlated for each river site varied in both type and total number, however. At all sites significant correlations were obtained for the parameter of surface suspended solids.

All other parameters that correlated with scanner radiance were related to these surface suspended solids values. This indirect method of correlation indicates that suspended solids is useful as a tracer. The objectives of determining river input dispersion and general transport mechanisms were best met by tracing suspended solids so this approach was emphasized both in surface sampling and scanner data analysis.

The scanner channel used for the direct suspended solids correlations provided data in the 600- to 720-nanometer spectral range. The use of this wavelength region restricted the observations to near-surface phenomena and provided relationships that were generally independent of water class. The coefficients of the regression equations relating suspended-solids concentrations with scanner data were generally different for each of the rivers and were also different for the same river on different days. The differences from river to river can be attributed to variations in the subsurface radiation absorption and the scattering properties of different types of particulate. These differences could not be determined because of in-

terferring effects, such as changing incident radiance due to solar altitude changes and atmospheric light attenuation and scattering, which are also the principal reasons for the day-to-day variations at a single river site. These day-to-day variations were compensated for by normalization, which made it possible to establish correlations on days when surface data were limited. The use of these methods is supported by radiative transfer model predictions, which are consistent with the empirical relationships achieved. The correlations were essentially linear up to levels of 20 to 30 mg/l of suspended solids concentration and of second order at higher concentrations.

The use of suspended solids as a tracer proved to be particularly valid for chemical parameters emanating from sources at levels well above the background values of the receiving waters. Problems were encountered in using the indirect correlations where mixing of various water sources occurred and where the relationships between suspended solids and the chemical parameters varied with different water classes. This problem was resolved for the Nemadji River data where interpretation of these data required the use of two scanner channels because of the existence of two distinctly different water classes. In this way, satisfactory correlations were obtained for a number of parameters for both water classes.

During the correlation analyses several data sets provided no significant correlation. In these cases the available data pairs were not adequate for a good test. The most serious problem encountered was what may be called nonrepresentative sampling. Nonrepresentative sampling refers specifically to the location of ship sampling sites. It does not in any way reflect on the quality of the data gathered, but rather on the characteristics of the sampling sites. In most cases the ship measurements were made at selected sampling grids. As a consequence the data were sometimes not representative of the overall water conditions in the area of the sampling sites. Also many sites were sampled on plume boundaries or other regions of rapidly changing conditions, which resulted in geographic registration errors. This problem was compounded by the fact that the aircraft and ship measurements were not made simultaneously. Many of these difficulties could have been overcome by improved aircraft and ship coordination.

Computer drawn contour maps based on the 40 correlations shown in table XIV have been presented. These maps represent the extrapolation of data from discrete ship sampling sites over the study areas. In addition to revealing transport and dispersion patterns, these maps have facilitated reliable quantitative comparisons between concentration levels at various locations on the same map as well as between locations on different maps.

River Discharge, Resuspension, and Shore Erosion

A full assessment of the effect of land use activities on lake water quality requires information on the relative roles played by river discharge, resuspension, and shore erosion. At every site examples of each of the three mechanisms were identified in the single-channel imagery. It was usually (although not always) possible to identify the river discharge plume and its spatial distribution. However, it was not generally possible to distinguish resuspension in the near-shore area from shore erosion. When mechanisms were identified, they usually were based on the suspended-solids distribution patterns revealed in the imagery in combination with wind and river discharge histories.

The remote-sensing data revealed a diversity of mechanisms existing at the various study sites. In the West Basin of Lake Erie the dominant role of the Maumee River discharge and the major role of resuspension was clearly established, while shore erosion was noted as playing a minor role. At the Genesee and Grand River sites, the importance of the river discharges is seen at some times while the effects of resuspension and shore erosion are seen as more significant at other times.

Shore erosion and/or heavy resuspension dominate the south shore of the Western Arm of Lake Superior. The runoff plume from the Nemadji River while prominent in the imagery, is not as significant a contributor to the total particulate loading at this site. The effects of the particulate discharge of the Menomonee River into Lake Michigan are seen as being insignificant relative to the extensive resuspension and shore erosion observed along the west shore of Lake Michigan. This is due to the relatively low flow of this river and to the effectiveness of the Milwaukee Harbor breakwall as a retention barrier.

At the Maumee and Nemadji sites, calculations were made of total loading based on the suspended-solids correlation and assuming an invariant distribution within the vertical water column. The ship vertical profile measurements generally show this assumption to be a reasonable one. The calculated loadings provided an estimate of the material suspended in the water column over a given area at the time of the overflight. Comparison of these loading values with published values of shore erosion and of total particulate discharges by rivers permitted a quantitative comparison of the relative importance of river inflow, resuspension, and shore erosion.

The imagery also revealed the discharges of rivers other than the five under detailed study. These were observed at the larger study areas in the West Basin of Lake Erie and the Western Arm of Lake Superior.

Sediment discharge contributions were significant from Lake St. Clair to the Detroit River flow. Another major source input was the heavy flow of particulate into Lake Ontario via the Niagara River and Welland Canal. This material appeared to originate from resuspension and shore erosion areas along the Canadian shore of eastern Lake Erie.

Transport and Dispersion of River Inputs

The scanner data at each site provided synoptic information on the spatial distribution of river discharge plumes from which information on the transport and dispersion of particulate could be inferred. The spatial extent of the observed dispersion patterns ranged from 1 or 2 to approximately 100 kilometers. The effects of the discharge of the Menomonee into the Milwaukee Harbor were localized because of the relatively low river discharge and the retention effects of the Milwaukee Harbor break-wall. At the Genesee and Grand River sites plumes were observed extending up to 5 kilometers offshore. The extent of the plumes in the direction parallel to the shore was generally greater than that offshore. However, the merging of the plume with near-shore resuspension and shore erosion made the determination of the plume boundary uncertain at times. At the Grand River, the imagery revealed the rapid change in plume direction due to wind shift. The plume from the maximum spring discharge of the Nemadji into Lake Superior was observed to extend approximately 30 kilometers into the Western Arm. Also, at this site imagery from successive days were used to follow patches of suspended material.

The most extensive transport movements were those observed in the West Basin. The data revealed suspended solids dispersion effects that extended in some cases over the entire Basin, a distance in excess of 80 kilometers. A sequential analysis of winds and scanner imagery over the spring period supports the hypothesis that the substantial amounts of particulate materials entering the Basin in the early spring are transported through to the Central Basin during repeated cycles of settling, resuspension (due to wind action in the shallow basin), drift, settling, etc., over a period of several months.

The synoptic coverage of the scanner data provided the opportunity to observe the occurrence of any international transboundary movement. None was observed in the case of the Genesee and Nemadji Rivers. In the West Basin of Lake Erie the movement of materials was generally parallel to the United States-Canadian boundary. While occasionally some crossing was observed, it was not significant in the

content of the overall basin transport. These results do not preclude, however, the possibility of transboundary movement of pollutants not associated directly with the suspended particulate; that is, those soluble materials which may eventually be distributed throughout the entire lake.

The studies revealed that the dispersion of pollutants was dependent on the local conditions. For example, it was observed that little particulate from the Menomonee River may ever reach Lake Michigan, while the relatively coarse Maumee River particulate and the fine grained particulate from the Nemadji River travels over large distances. Other factors which varied from site to site and influenced transport and dispersion included river discharge volumes, lake bottom contours, and littoral currents.

Comments on Near Real-Time Data Transmission

The process of transmitting imagery in near real-time by facsimile device was undertaken to insure greater coordination of ship and aircraft sampling. Because equipment for direct transmission was not available, data could not be sent to the ship survey teams sooner than about 6 to 8 hours after a flight. However, imagery was transmitted on at least one occasion to each of the survey personnel studying the Maumee, Grand, and Nemadji Rivers in sufficient time to have been of use in selecting sampling sites for the next day. On one occasion a transmitted image was used by OSU-CLEAR to locate a region of high suspended solids concentration near the islands in the West Basin. The next day, OSU-CLEAR recorded data, which was of critical importance in making possible a correlation that provided a suspended-solids contour map of the entire West Basin from the aircraft data. On the other hand, an image transmitted to GLERL showing the Grand River plume to be moving southward on March 22 was probably misleading, since, by the time the survey took place the next day, changing winds had shifted the plume to the north.

It is concluded that the use of remote sensing imagery for ship-survey site selection can greatly aid in the selection of sampling sites and improve the effectiveness of ship surveys. However, to insure its effectiveness, the remote-sensing data should be transmitted directly to the survey ship while it is actively sampling rather than after the ship has returned to port. In addition, the ship-survey operations and, in particular, the site selection process should be sufficiently flexible so as to make appropriate use of the remote-sensing information transmitted.

Extrapolation of Results

Forty contour maps of the various water-quality parameters were produced and represent an extrapolation of ship data collected at discrete sampling sites. This spatial extrapolation, made possible by the correlation of remote-sensing and in-the-water data, demonstrates one of the primary advantages of a combined aircraft and ship system for lake surveys. In some locations time-dependent hydrodynamic models have been developed for indicating flow patterns due to winds and river inputs. These models can be used to predict or extend in time the locations and concentrations of materials measured by remote sensing on ship surveys. Current models developed for Lake Erie (ref. 8) and Lake Superior (ref. 14) are being tested using the data from this study.

The question arises as to what extent the correlation results reported for the five study areas apply to other rivers and regions of the Great Lakes. Based on the analysis of the data, there are two responses that can be made to this question.

First, the differences in correlation results obtained for the various study sites are indicative of the diverse characteristics of the waters at locations throughout the Great lakes. This is not surprising since the composition of the suspended components in the river plumes and along the shores of the receiving waters are known to vary significantly from site to site and possibly from season to season at a given site. It is the optical properties of these varied components that determine their spectral signatures, which in turn provide the basis for the remote sensing capability. Because of the variability from site to site, one cannot assume that a correlation derived for one of the study sites is valid outside the general area over which the data were obtained. The extrapolation to other areas of the lakes can be made only after ship and aircraft surveys establish the validity of such action. Although direct correlation of Landsat data with ship measurements was not part of this study, the above comments also apply to satellite remote sensing data.

The development and cataloging of correlations and their zones of validity for the entire Great Lakes is an unfinished task. This task takes on greater significance with the advent of satellite programs such as Landsat follow-on and Nimbus 7, which offer greater spectral resolution and more frequent (five days out of six for Nimbus 7) and larger scale coverage of the Great Lakes.

The second response to the question of general extrapolation of results concerns the central role of ship

survey data in the correlation process. The extrapolation of discrete site ship data over large areas can proceed only with the simultaneous acquisition of *representative* remote-sensing and in-the-water data. The coordination of these efforts is a difficult but not insurmountable task.

Lewis Research Center,
National Aeronautics and Space Administration,
Cleveland, Ohio, November 16, 1979,
146-20.

REFERENCES

1. Plan of Study for U.S. Task D Study on Great Lakes Pollution From Land Use Activities. Great Lakes Basin Commission, Ann Arbor, Mich., 1975.
2. Svehla, R.; et. al.: Remote Sensing Study of Maumee River Effects on Lake Erie. NASA TM X-71780, 1975.
3. Herdendorf, C.E.: Effects of Maumee River Input on Lake Erie Water Quality. Center for Lake Erie Area Research, Ohio State University, July 1975.
4. Rogers, R.H.; et al.: Application of Landsat to the Surveillance and Control of Eutrophication in Saginaw Bay. International Symposium on Remote Sensing of Environment, 10th. Vol. I. Environmental Research Institute of Michigan, Univ. Michigan, 1975, pp. 437-446.
5. Stortz, Kirby; and Sydor, Michael: Remote Sensing of Western Lake Superior. International Symposium on Remote Sensing of Environment, 9th, Vol. II. Environmental Research Institute of Michigan, Univ. Michigan, 1974, pp. 933-937.
6. Johnson, R. W.: Quantitative Sediment Mapping From Remotely Sensed Multispectral Data. Remote Sensing of Earth Resources, Vol. 4. F. Shahrokhi, ed., University of Tennessee, 1975, pp. 565-576.
7. Monteith, T. J.; and Sonzogni, W. C.: U.S. Great Lakes Shoreline Erosion Loadings. Great Lakes Basin Commission, Ann Arbor, Michigan, Dec. 1976.
8. Sheng, Y. P.; and Lick, W.: The Transport and Resuspension of Sediments in a Shallow Lake. J. Geophys. Res., vol. 84, no. 4, Apr. 1979, pp. 1809-1826.
9. Shelley, Philip E.: Sediment Measurement in Estuarine and Coastal Areas. NASA CR-2769, 1976.
10. NASA Langley Research Center, January 1977, 1976 Environmental Quality Program Research Review, Environmental Quality, pp. 58-62.
11. Bennett, Peter; and Sydor, Michael: Use of ERTS in Measurements of Water Quality in Lake Superior and the Duluth Superior Harbor. Remote Sensing of Earth Resources, Vol. 3. F. Shahrokhi, ed., University of Tennessee, 1974, pp. 85-92.
12. Sherz, J. P.; and Van Domelen, J. F.: Water Quality Indicators Obtainable from Aircraft and Landsat Images and Their Use in Classifying Lakes. International Symposium on Remote Sensing of Environment, 10th, Vol. I. Environmental Research Institute of Michigan, Univ. Michigan, 1975, pp. 447-460.
13. Sydor, Michael: Effects of Nemadji Runoff on Lake Superior. Environmental Protection Agency, Chicago, Ill., Dec. 1977.

TABLE I. - SUMMARY OF AIRCRAFT AND SHIP ACTIVITY

Site	Period of aircraft flights	Period of ship surveys	Planned site coverage	Number of aircraft flights	Number of ship survey days	Number of same-day aircraft and ship coverage
Maumee	2/17 - 6/5	2/18 - 6/23	17	16	^a 15	8
Genesee	2/24 - 9/24	3/31 - 9/24	4	6	7	2
Menomonee	2/20 - 6/7	2/13 - 9/9	4	7	7	2
Grand	2/23 - 4/2	2/25 - 7/2	4	9	9	3
Nemadji	4/1 - 7/8	3/31 - 5/21	<u>4</u>	<u>9</u>	<u>10</u>	<u>5</u>
			33	47	48	20

^aTotal cruises reported; most were multiple-day cruises.

TABLE II. - SHIP SURVEY IN-THE-WATER MEASUREMENTS

Field parameters:

Temperature
Dissolved oxygen
Specific conductance
pH
Secchi disk transparency
Transmissibility
Solar illumination

Physical parameters:

Suspended solids
Turbidity

Nutrients:

Total phosphorus
Soluble reactive phosphorus
Ammonia nitrogen
Nitrate nitrogen
Organic nitrogen
Dissolved silica

Salts:

Chloride
Alkalinity
Calcium-magnesium
Sulfate

Organics:

Chlorophyll a
Organic carbon
Pesticide scan (infrequent)
PCB's (infrequent)

Metals (all infrequent):

Cadmium
Chromium
Copper
Mercury
Zinc
Arsenic
Lead
Nickel

TABLE III. - SPECIFICATIONS OF MULTISPECTRAL SCANNERS USED
IN AIRCRAFT REMOTE-SENSING SURVEYS

(a) Ocean color scanner (OCS); bandwidth, 40 nm

Channel number	Center wavelength, λ_C , nm	OCS on F-106 or Lear Jet at 12.5 km (41 000 ft)
1	428	Ground speed, km/hr (knot) 834 (450) Scan rate, scans/sec 4.1 Sample rate, samples/90° scan 350 Ground resolution, m (ft) 60 by 60 (300 by 300)
2	466	
3	508	
4	549	
5	592	
6	632	
7	674	
8	714	
9	756	
10	794	

(b) Modular multiband scanner (M²S)

Channel number	Center wavelength, λ_C , nm	Bandwidth, $\Delta\lambda$, nm	M ² S on C-47 aircraft at 3.05 km (10 000 ft)
1	410	60	Ground speed, km/hr (knots) 232 (125) Scan rate, scans/sec 10 Sample rate, samples/110° scan 802 Ground resolution, m (ft) 7.6 by 7.6 (25 by 25)
2	465	50	
3	515	50	
4	560	40	
5	600	40	
6	640	40	
7	680	40	
8	720	90	
9	815	90	
10	1 015	90	
11	11 000	2500	
(thermal)			

TABLE IV. - SUMMARY OF AIRCRAFT AND SHIP

ACTIVITY IN THE WEST BASIN OF LAKE ERIE

Date (all 1976)	NASA flight number	Clear cruise number	Number of ship sampling sites	Flow, m ³ /sec	
				Maumee River	Detroit River
2/18	--	1	--	1900	6113
2/23	48	-----	--	1980	6764
2/25	51	2	10	1811	6537
3/8	52	3	25	991	6452
3/11	53	-----	--	396	6000
3/15	54	-----	--	198	5886
3/22	57	-----	--	133	5773
3/23	58 }	4	{ 2	152	5632
3/25	60 }			108	5886
4/3	62	-----	--	100	5886
4/5	64	-----	--	84	6000
4/12	68	5, 6	17	42	6000
4/13	69		22	37	5886
4/21	--	7, 8	--	57	5745
4/29	72	9, 10	24	190	6283
5/8	74	11, 12	8	104	6254
5/20	--	13	--	85	6226
6/5	84	14	--	113	6113
6/7	88		4	79	6113

TABLE V. - HISTORICAL WIND DATA AT TOLEDO, OHIO^a

Day	Resultant direction, deg	Average wind speed		Resultant direction, deg	Average wind speed		Resultant direction, deg	Average wind speed		Resultant direction, deg	Average wind speed		Resultant direction, deg	Average wind speed					
		m/sec	mph		m/sec	mph		m/sec	mph		m/sec	mph		m/sec	mph				
February				March				April				May				June			
1	270	6.6	14.7	60	7.2	16.0	260	5.2	11.7	210	2.7	6.0	50	3.8	8.5				
2	260	5.2	11.7	70	5.1	11.4	300	4.4	9.8	230	6.4	14.4	60	4.4	9.9				
3	190	2.9	6.5	280	4.0	8.9	100	4.4	9.8	270	6.8	15.2	50	5.0	11.1				
4	280	4.8	10.8	100	4.7	10.5	10	5.3	11.9	230	4.8	10.8	80	4.4	9.8				
5	50	5.4	12.1	260	9.3	20.7	260	4.6	10.4	220	7.8	17.4	60	2.4	5.3				
6	290	5.3	11.8	260	7.8	17.5	290	4.0	8.9	50	5.1	11.5	40	1.4	3.2				
7	230	6.3	14.2	280	7.0	15.7	350	3.9	8.8	340	5.9	13.1	300	3.1	6.9				
8	280	6.9	15.4	360	2.8	6.3	10	4.4	9.8	270	3.3	7.3	290	3.0	6.8				
9	180	4.1	9.2	80	3.5	7.9	310	2.3	5.2	240	5.5	12.4	240	2.1	4.6				
10	210	6.4	14.4	250	4.3	9.6	240	4.4	9.9	230	4.7	10.5	240	3.5	7.9				
11	270	6.2	13.8	70	4.7	10.5	360	6.2	13.8	310	5.5	12.4	280	4.5	10.1				
12	200	5.3	11.9	180	6.7	15.0	290	2.8	6.2	300	2.5	5.6	70	4.7	10.5				
13	300	5.3	11.8	270	8.0	18.0	260	2.9	6.5	130	3.2	7.2	210	3.4	7.5				
14	100	3.5	7.9	240	5.5	12.2	210	3.7	8.2	210	3.2	7.1	220	4.3	9.6				
15	210	6.0	13.4	40	4.1	9.2	220	5.2	11.7	70	4.2	9.5	210	5.9	13.2				
16	100	3.7	8.2	320	5.8	12.9	220	5.5	12.2	170	2.3	5.2	250	4.6	10.4				
17	250	5.6	12.5	280	6.2	13.8	190	4.4	9.9	300	5.1	11.4	50	1.7	3.7				
18	260	7.0	15.7	180	4.0	8.9	210	5.0	11.2	330	6.3	14.0	170	3.8	8.6				
19	260	4.7	10.5	210	6.3	14.2	270	4.3	9.6	300	5.8	12.9	310	5.0	11.1				
20	180	3.4	7.6	200	7.6	17.1	60	5.1	11.4	260	5.1	11.5	40	3.8	8.5				
21	110	5.5	12.4	280	7.8	17.5	170	4.2	9.5	310	4.7	10.5	350	2.4	5.3				
22	320	6.5	14.5	230	2.0	4.5	270	5.9	13.2	360	3.5	7.9	170	3.2	7.1				
23	240	4.9	10.9	220	4.2	9.5	80	3.5	7.8	50	2.9	6.5	160	2.4	5.3				
24	210	6.3	14.1	210	6.2	13.8	70	6.5	14.5	20	3.8	8.6	180	5.5	12.4				
25	210	5.7	12.7	240	5.1	11.4	30	7.3	16.4	30	3.0	6.6	260	4.8	10.8				
26	240	5.3	11.8	180	6.3	14.0	340	5.1	11.4	10	2.7	6.0	230	3.5	7.9				
27	220	4.9	10.9	230	7.5	16.7	310	4.7	10.6	70	2.6	5.9	230	3.2	7.1				
28	290	4.4	9.8	90	3.3	7.3	280	3.8	8.6	140	3.0	6.8	230	3.4	7.5				
29	260	5.0	11.2	90	4.4	9.9	300	3.9	8.8	90	4.3	9.6	300	4.4	9.8				
30	---	---	---	200	7.8	17.4	230	2.3	5.2	110	2.9	6.5	270	5.7	12.8				
31	---	---	---	250	4.1	9.1	---	---	---	270	2.9	6.5	---	---	---				

^aData source: Monthly local climatological data summary, National Weather Service Office at Toledo Express Airport, Toledo, Ohio.

TABLE VI. - SUMMARY OF CORRELATION RESULTS OF THE ERIE WEST BASIN STATISTICAL
ANALYSIS RELATING SUSPENDED SOLIDS WITH UPWELLING RADIANCE

Date	Variables		Equation	Measured range dependent variable	Correlation range	Correlation coefficient	Standard error of estimate
	Dependent	Independent					
3-8-76	Suspended solids, mg/l	Channel 8, counts	$S.S. = -15.41 + 1.75 x + 0.005 x^2$	4.1 - 286	0 - 200	1.00	4.4
	Dissolved oxygen, ppm	Suspended solids, mg/l	$D.O. = 13.38 - 0.01 S.S.$	11 - 14	11 - 14	.92	.25
	Secchi depth, m	Suspended solids, mg/l	$S.D. = 0.70 - 0.0038 S.S.$	0.05 - 1.1	0 - 0.7	.77	.18
	Total phosphorous, ppb	Suspended solids, mg/l	$T.P. = 27.13 + 1.60 S.S.$	15 - 980	0 - 237	.96	17.6
	Total phosphorous, ppb	Suspended solids, mg/l	$T.P. = -708 + 7.0 S.S.$	15 - 980	237 - 980	----	-----
	Turbidity, JTU	Suspended solids, mg/l	$Turb = 6.9 + 0.66 S.S. + 0.00078 (S.S.)^2$	0 - 286	0 - 286	.99	5.5
	Inorganic solids, mg/l	Suspended solids, mg/l	$I.S. = -2.155 + 0.886 S.S.$	0 - 240	0 - 240	1.00	1.5
3-23-76	Suspended solids, mg/l	Channel 8, counts	$S.S. = -9.48 + 0.321 x + 0.0019 x^2$	3 - 70	0 - 100	.99	5.3
4-12-76	Suspended solids, mg/l	Channel 8, counts	$S.S. = -7.20 + 0.185 x - 0.00054 x^2$	6 - 70	0 - 100	.99	5.3
4-13-76	Suspended solids, mg/l	Channel 8, counts	$S.S. = -15.5 + 0.222 x + 0.00422 x^2$	3 - 40	0 - 100	.99	5.3
5-12-76	Suspended solids, mg/l	Channel 8, counts	$S.S. = -4.25 + 0.143 x + 0.00027 x^2$	3 - 9.6	0 - 50	.99	5.3

TABLE VII. - DISTRIBUTION OF SECONDARY PARAMETERS
RELATIVE TO TOTAL SUSPENDED SOLIDS
FOR THE ERIE WEST BASIN^a

Total suspended solids, mg/l	Total phosphorus, ppb	Dissolved oxygen, ppm	Secchi depth, m	Turbidity, JTU	Inorganic suspended solids, mg/l
10	43	13.3	0.66	13.6	6.7
20	59	13.2	.62	20.4	15.6
30	75	13.1	.59	27.4	24.4
50	107	12.9	.51	41.9	42.1
75	147	12.6	.42	60.8	64.3
100	187	12.4	.32	80.7	86.4
125	227	13.1	.23	101.6	108.6
150	342	11.9	.13	123.5	130.7
175	517	11.6	.04	146.3	152.9
200	692	11.4	----	170.1	175.0

^aSee fig. 3.

TABLE VIII. - ESTIMATE OF THE TOTAL SUSPENDED SOLIDS
LOADING OF THE ERIE WEST BASIN

Month	Day	Maumee River discharge monthly total, metric tons	Calculated basin load on given date, metric tons	U. S. shore erosion input estimated monthly total, metric tons
January	----	2.8×10^4	-----	1.5×10^4
February	----	110	-----	3.0
March	8th	34	70×10^4	4.5
	12th	-----	71	-----
April	----	1.2	-----	4.5
	12th	-----	40	-----
	13th	-----	53	-----
May	----	1.2	-----	3.0
	12th	-----	15	-----
June	----	<u>.70</u>	-----	<u>1.5</u>
6-month total		149.9		18.0

TABLE IX. - HISTORICAL WIND DATA AT

MILWAUKEE, WISCONSIN^a

Date	Resultant direction, deg	Average wind speed		Date	Resultant direction, deg	Average wind speed	
		m/sec	mph			m/sec	mph
February				May			
20	200	3.2	7.1	5	240	9.7	21.6
21	20	10.4	23.3	6	20	7.6	17.1
22	320	5.3	11.9	7	10	4.8	10.8
23	220	6.9	15.4	8	240	5.7	12.8
24	220	4.7	10.5	25	20	4.6	10.2
25	240	4.6	10.4	26	90	2.5	5.5
26	300	4.1	9.2	27	130	2.8	6.2
March				28	80	4.4	9.8
12	190	8.2	18.3	29	50	2.5	5.6
13	290	6.7	15.0	30	40	2.1	4.8
14	260	7.9	17.7	31	20	3.2	7.2
15	360	3.9	8.8	June			
16	300	6.9	15.5	1	360	6.0	13.4
17	270	4.8	10.8	2	10	4.5	10.1
18	210	7.3	16.3	4	30	3.9	8.8
19	210	7.5	16.8	5	40	2.6	5.8
20	220	10.2	22.9	6	210	2.2	5.0
21	300	7.6	17.1	7	270	3.5	7.9
22	250	3.4	7.6				
30	220	8.6	19.3				
31	280	5.5	12.2				
April							
1	310	5.9	13.2				
2	130	3.3	7.3				
5	250	4.9	10.9				
6	250	3.5	7.8				
7	20	5.9	13.2				
8	50	4.1	9.1				
25	20	11.8	26.3				
26	20	6.4	14.4				
27	20	4.3	9.6				
28	90	3.3	7.3				
29	160	3.8	8.6				

^aData source: Monthly local climatological data summary,
National Weather Service Office at General Mitchell
Field, Milwaukee, Wisconsin.

TABLE X. - SUMMARY OF RESULTS OF THE STATISTICAL ANALYSIS

FOR THE MENOMONEE RIVER

Date	Parameter	Total experimental data range (all stations)	Experimental data range used in correlation	Equation ^a for parameter	Standard error of estimate	Best ^b channel
2/25	Suspended solids	6 - 18 mg/l	6 - 15 mg/l	$0.213 + 0.1154x$	0.93	8
	Chlorides	8 - 140 mg/l	8 - 50 mg/l	$-34.50 + 0.668x$	8.3	7
				$-26.08 + 5.52 SS$	6.9	
	Total phosphorus	10 - 210 μ g/l	10 - 85 μ g/l	$-59.49 + 1.130x$	17.0	
	Particulate phosphorus	5 - 120 μ g/l	5 - 49 μ g/l	$-49.04 + 9.64 SS$	11.5	
				$-33.45 + 0.660x$	10.9	
				$-27.59 + 5.63 SS$	7.8	
	NO ₂ + NO ₃ nitrogen	0.25 - 1.76 mg/l	0.25 - 0.68 mg/l	$-0.1478 + 0.00636x$.094	
				$-0.0989 + 0.0556 SS$.057	
	NH ₃ nitrogen	0.02 - 0.44 mg/l	0.02 - 0.44 mg/l	$-0.4069 + 0.00676x$.10	
4/8				$-0.3004 + 0.0539 SS$.11	8
	Total solids	170 - 580 mg/l	170 - 305 mg/l	$35.45 + 2.10x$	26.9	
				$59.59 + 17.62 SS$	20.4	
	Dissolved oxygen	11.9 - 13.1 mg/l	11.9 - 13.1 mg/l	$13.83 - 0.0157x$.35	
				$14.10 - 0.1585 SS$.23	
	Suspended solids	0 - 17 mg/l	0 - 15 mg/l	$-12.24 + 0.304x$.70	5
	Particulate phosphorus	7 - 122 μ g/l	7 - 37 μ g/l	$-0.947 + 0.631x$	5.5	7
				$12.80 + 1.333 SS$	6.2	

^aWhere x equals counts and SS equals concentration of suspended solids in mg/l.^bFebruary 25 corresponds to OCS and April 8 corresponds to M²S.

TABLE XI. - DISTRIBUTION OF SECONDARY PARAMETERS RELATIVE TO TOTAL

SUSPENDED SOLIDS FOR THE MENOMONEE RIVER

Date	Suspended solids, mg/l	Chloride, mg/l	Total phosphorus, μ g/l	Particulate phosphorus, μ g/l	NO ₂ + NO ₃ nitrogen, mg/l	NH ₃ nitrogen, mg/l	Total solids, mg/l	Dissolved oxygen, mg/l
2/25	4	--	---	--	0.12	---	130	13.5
	5	2	---	1	.18	---	148	13.3
	6	7	9	6	.23	0.02	165	13.1
	7	13	18	12	.29	.08	183	13.0
	9	24	38	23	.40	.18	218	12.7
	13	46	76	46	.62	.40	289	12.0
	19	79	134	79	.96	.72	394	11.1
4/8	1	(a)	(a)	14	(a)	(a)	(a)	(a)
	3			17				
	6			21				
	9			25				
	12			29				
	18			37				
	24			45				

^aNo correlation.

TABLE XII. - HISTORICAL WIND DATA AT MUSKEGON, MICHIGAN^a

Date	Resultant direction, deg	Average wind speed		Resultant direction, deg	Average wind speed		Resultant direction, deg	Average wind speed	
		m/sec	mph		m/sec	mph		m/sec	mph
	February			March			April		
1	320	10.7	23.9	80	7.0	15.7	320	5.1	11.5
2	300	5.1	11.4	80	6.7	15.0	290	3.2	7.2
3	222	6.3	14.1	30	4.2	9.5	90	5.4	12.1
4	320	5.4	12.1	70	5.2	11.7	360	5.0	11.2
5	60	3.7	8.2	240	5.8	21.9	230	3.8	8.6
6	300	5.3	11.8	260	8.6	19.3	270	2.9	6.6
7	250	5.7	21.7	300	7.6	17.0	340	5.1	11.5
8	300	6.3	14.2	270	2.5	5.5	340	5.0	11.2
9	180	6.3	14.2	170	1.3	3.0	260	2.7	6.0
10	230	6.1	13.7	320	2.9	6.5	230	5.6	12.5
11	280	6.3	14.1	120	4.3	9.6	10	6.7	15.0
12	200	6.6	19.3	160	7.4	16.5	220	2.8	6.2
13	310	5.0	11.1	320	8.2	18.4	210	3.4	7.6
14	150	3.3	7.3	250	7.4	16.5	200	6.4	14.4
15	210	7.3	16.3	320	4.0	8.9	200	6.5	14.5
16	70	3.8	8.5	320	6.6	14.8	200	8.0	18.0
17	340	4.0	8.9	300	6.6	14.7	190	8.4	18.7
18	220	7.3	16.3	190	8.0	18.0	200	8.2	18.4
19	270	5.1	11.5	200	8.4	18.8	270	4.4	9.8
20	220	2.3	5.2	190	5.6	21.4	100	4.5	10.1
21	30	6.3	14.1	310	6.8	15.2	160	7.1	15.8
22	333	6.2	13.8	180	3.8	8.6	280	6.3	14.0
23	200	5.9	13.1	200	7.5	16.7	80	4.4	9.8
24	200	6.5	14.5	200	10.7	24.0	90	8.8	19.6
25	210	6.3	14.0	270	4.6	10.4	50	7.7	17.3
26	230	2.9	6.5	190	8.9	19.8	350	6.2	13.8
27	220	4.2	9.4	310	6.2	13.8	340	5.5	12.4
28	310	3.2	7.2	120	3.8	8.5	310	5.0	11.1
29	320	4.1	9.1	120	6.0	13.4	260	3.2	7.2
30	---	---	---	190	7.5	16.7	210	4.7	10.5
31	---	---	---	240	5.1	11.5	---	---	---

^aData source: Monthly local climatological data summaries, National Weather Service Office at Muskegon County Airport, Muskegon, Michigan.

TABLE XIII. - SUMMARY OF RESULTS OF STATISTICAL ANALYSIS

FOR WESTERN LAKE SUPERIOR

Date	Parameter	Measured range	Correlation range	Scanner channel used	Correlation coefficient	Standard error of estimate
4/1/76	Suspended solids, mg/l	0.7 - 14.7	0 - 20.0	8	0.99	0.68
	SiO ₂ , mg/l	1.8 - 3.8	2.0 - 4.0	4, 8	.87	.44
	SO ₄ , mg/l	2.7 - 6.5	3.0 - 7.0	4, 8	.98	.31
	Total phosphorous, µg/l	4.4 - 48.3	5.0 - 35.0	4, 8	.98	3.36
	Total organic nitrogen, mg/l	0.1 - 0.4	0 - 0.4	4, 8	.97	.04
	Secchi depth, m	0.7 - 4.8	0 - 5.0	8	.89	.95
4/4/76	Suspended solids, mg/l	1.2 - 49.2	0 - 20.0	8	.99	0.61
	SiO ₂ , mg/l	1.7 - 5.1	2.0 - 4.0	4, 8	.92	.32
	SO ₄ , mg/l	2.8 - 7.8	3.0 - 7.0	4, 8	.92	.44
	Total phosphorus, µg/l	5.0 - 97.0	5.0 - 35.0	4, 8	.97	4.34
	Total organic nitrogen, mg/l	0.1 - 0.6	0 - 0.4	4, 8	.97	.03
	Secchi depth, m	0.3 - 4.0	0 - 5.0	8	.98	.23
4/5/76	Suspended solids, mg/l	0.9 - 93.0	0 - 20.0	10	0.96	1.54
4/6/76	Suspended ^a solids, mg/l	0.7 - 24.0	0 - 20.0	8	0.93	1.69

^aDerived from turbidity measurements.

TABLE XIV. - OVERALL SUMMARY OF

River/study site	Number of aircraft flights reported	Landsat images presented	Number of same-day aircraft and ship coverage	Coverage during major runoff events	Correlations, contour maps reported		Relative importance of river discharge, resuspension, or shore erosion	Transport and dispersion noted
					Water quality parameter	Number reported		
Maumee/ West Basin of Lake Erie	16	5	8	Yes	Tot. susp. solids	5	Major roles of runoff and re-suspension noted	Yes
					Tot. phos.	1		
					Turbidity	1		
					Inorganic solids	1		
					Secchi depth	1		
					Dissolved O ₂	1		
Genesee/ Lake Ontario	6	6	2	Yes	Tot. susp. solids	1	All three mechanisms significant	Yes
					Chlorophyll <u>a</u>	1		
Menomonee/ Lake Michigan	7	6	2	No	Tot. susp. solids	2	Major effects of resuspension and shore erosion noted along western shore	No, runoff particulates retained by breakwall
					Chlorides	1		
					Tot. phos.	1		
					NO ₂ + NO ₃ nitrogen	1		
					Tot. solids	1		
					Dissolved O ₂	1		
Grand/ Lake Michigan	9	4	3	Yes	Tot. susp. solids	3	Examples of all three mechanisms seen; re-suspension effects significant	Yes, dispersion out to 10 km offshore noted
					Plots of 8 water param as function of susp. solids for 3 days ^b			
Nemadji/ Lake Superior	9	4	5	Yes	Tot. susp. solids	4	Dominant role of south shore erosion noted	Yes, dispersion and transport of Nemadji discharge traced in western arm
					SiO ₂	2		
					SO ₄	2		
					Tot. phos.	2		
					Tot. org. N	2		
					Secchi depth	2		

^aValid during study period only.^bCalcium, total Kjeldahl nitrogen, magnesium, chlorophylla, Secchi depth, silica, turbidity, and total phosphorus.

REMOTE-SENSING RESULTS^a

Effects of ice on transport noted	Effects of winds noted	Particulate transport across international boundary noted	Total suspended solids loading calculated	Data used in existing modeling work	Discrimination of multiple runoff sources accomplished	Use of telefacsimile imagery by ships	Other
Yes	Yes	None significant	Yes (5 days)	Yes	Yes (Maumee, Detroit Rivers)	Usefulness demonstrated on one occasion	Lake St. Clair noted as source for suspended material for Detroit River
No ice present	Yes	None (transport of Lake Erie Northern Shore particulate to Lake Ontario Southern Shore observed)	No	No	No	Not tested adequately	Significant contribution from Niagara River and Welland Canal to South Shore loading
No ice present	Yes	N/A	No	No	No	Not tested adequately	Role of Milwaukee Harbor as settling basin noted
Yes	Yes	N/A	No	No	No	Demonstrated, but 24-hour response not adequate	-----
Yes	Yes	None	Yes (3 days)	Yes	Yes (Nemadji, St. Louis Rivers)	Data transferred on four occasions	High nutrient levels from St. Louis River

1. Report No. NASA TP-1694	2. Government Accession No.	3. Recipient's Catalog No.
4. Title and Subtitle COORDINATED AIRCRAFT AND SHIP SURVEYS FOR DETERMINING IMPACT OF RIVER INPUTS ON GREAT LAKES WATERS - REMOTE SENSING RESULTS	5. Report Date July 1980	6. Performing Organization Code
7. Author(s) Charles A. Raquet, Jack A. Salzman, Thom A. Coney, Roger A. Svehla, Donald F. Shook, and Richard T. Gedney	8. Performing Organization Report No. E-172	10. Work Unit No. 146-20
9. Performing Organization Name and Address National Aeronautics and Space Administration Lewis Research Center Cleveland, Ohio 44135	11. Contract or Grant No.	13. Type of Report and Period Covered Technical Paper
12. Sponsoring Agency Name and Address National Aeronautics and Space Administration Washington, D. C. 20546	14. Sponsoring Agency Code	
15. Supplementary Notes		
16. Abstract <p>The remote sensing results of a coordinated program of aircraft and ship surveys for determining the impact of river effluents on Great Lakes waters are presented. Aircraft multi-spectral scanner data were acquired throughout the spring and early summer of 1976 at five locations: the West Basin of Lake Erie, Genesee River - Lake Ontario, Menomonee River - Lake Michigan, Grand River - Lake Michigan, and Nemadji River - Lake Superior. Forty-seven images of the various study sites are presented. Twenty of these overflights were coincident with ship surveys. Multispectral scanner data and ship surface sample data are correlated resulting in 40 contour plots showing large-scale distributions of parameters such as total suspended solids, turbidity, Secchi depth, nutrients, salts, and dissolved oxygen. The imagery and data analysis are used to determine the transport and dispersion of materials from the river discharges, especially during spring runoff events, and to evaluate the relative effects of river input, resuspension, and shore erosion. Twenty-five Landsat satellite images of the study sites are also included in the analysis. Examples of the use of remote sensing data in quantitatively estimating total particulate loading, in determining water types, in assessing transport across international boundaries, and in supporting numerical current modeling are included. The importance of coordination of aircraft and ship lake surveys is discussed, including the use of telefacsimile for the transmission of imagery.</p>		
17. Key Words (Suggested by Author(s)) Pollution; Water; Great Lakes; Inland waters; Water flow	18. Distribution Statement Unclassified - unlimited STAR Category 45	
19. Security Classif. (of this report) Unclassified	20. Security Classif. (of this page) Unclassified	21. No. of Pages 103
		22. Price* A06

National Aeronautics and
Space Administration

Washington, D.C.
20546

Official Business

Penalty for Private Use, \$300

THIRD-CLASS BULK RATE

Postage and Fees Paid
National Aeronautics and
Space Administration
NASA-451



5 1 10,E, 070380 S00903DS
DEPT OF THE AIR FORCE
AF WEAPONS LABORATORY
ATTN: TECHNICAL LIBRARY (SUL)
KIRTLAND AFB NM 87117

NASA

POSTMASTER: If Undeliverable (Section 158
Postal Manual) Do Not Return
